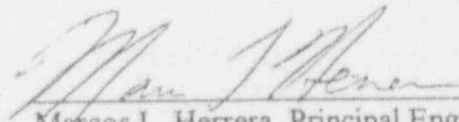


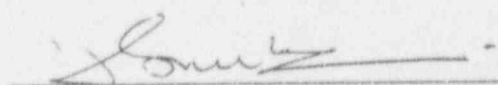
**Evaluation and Screening Criteria
for the
Peach Bottom Unit-3 Shroud Indications**

December 3, 1993

Prepared by:

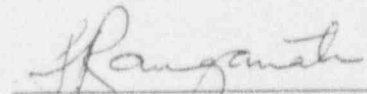


Marcos L. Herrera, Principal Engineer
Structural Mechanics Projects



Dr. Hardayal Mehta, Principal Engineer
Structural Mechanics Projects

Approved By:



Dr. Sampath Ranganath, Manager
Structural Mechanics Projects

**GE Nuclear Energy
San Jose, CA**

**IMPORTANT NOTICE REGARDING
CONTENTS OF THIS REPORT**

Please Read Carefully

The only undertakings of the General Electric Company (GE) respecting information in this document are contained in the contract between Philadelphia Electric Co. and GE, and nothing contained in this document shall be construed as changing the contract. The use of this information by anyone other than PECO, or for any purpose other than that for which it is intended under such contract is not authorized; and with respect to any unauthorized use, GE makes no representation or warranty, and assumes no liability as to the completeness, accuracy, or usefulness of the information contained in this document, or that its use may not infringe privately owned rights.

Table of Contents

EXECUTIVE SUMMARY	iv
1.0 INTRODUCTION.....	1
1.1 Background.....	3
1.2 Screening Criteria.....	3
1.3 References.....	6
2.0 FABRICATION HISTORY.....	11
3.0 CHEMISTRY AND FLUENCE CONSIDERATIONS.....	23
3.1 Water Chemistry History.....	23
3.2 Fluence Considerations.....	25
3.3 References.....	26
4.0 IN-VESSEL VISUAL INSPECTION.....	36
5.0 FLAW EVALUATION.....	39
5.1 Structural Analysis.....	39
5.2 Allowable Through-Wall Flaws.....	43
5.3 Screening Criteria.....	46
5.4 Summary of Screening Criteria.....	48
5.5 Application of Screening Criteria.....	49
5.6 References.....	50
6.0 SUMMARY AND CONCLUSIONS.....	57
APPENDIX A	DETERMINATION OF THE EFFECTIVE FLAW LENGTH
APPENDIX B	BASIS FOR CRACK GROWTH RATE



EXECUTIVE SUMMARY

Indications have been observed in the Peach Bottom Unit 3 core shroud. Indications were seen during in-vessel visual inspection (IVVI) of the various shroud welds as recommended by GE SIL 572, Rev. 1. Results showed that both circumferential and axial indications were present at the H3 and H4 welds. H3 corresponds to the weld between the top guide support ring and core shroud cylinder, and the H4 weld is located at approximately the mid-height of the fuel. In addition, circumferential indications were observed in the shroud plate associated with a vertical weld. The lengths of the indications associated with the vertical welds were short ($\cong 2.5$ " max.) compared to those associated with the horizontal welds.

This evaluation was performed to disposition the indications by demonstrating that the structural integrity of the shroud is maintained for the next fuel cycle (two year cycle with power rerate conditions). In addition, the report documents material, water chemistry and fluence information which are additional variables which may have contributed to the shroud condition.

The primary focus of this report is to demonstrate that even with several conservatisms in the evaluation, the structural integrity of the shroud is maintained during a limiting event. This was performed by developing conservative screening criteria, assuming throughwall indications, which can determine the acceptability of the flaws based solely on the IVVI results. The assumption of through-wall indications removes any uncertainty regarding sizing and the need to further characterize the indications. By meeting the screening criteria, the ASME Code Section XI safety margins are satisfied.

The screening criteria use both linear elastic fracture mechanics (LEFM) and limit load concepts to determine acceptable through-wall indication lengths. The limiting flaw length based on either LEFM or limit load was used for the screening criteria.

The screening criteria also use the ASME Code Section XI criteria for combining flaws based on the proximity of indications. In addition, a second method for including the interaction between neighboring indication tips was considered for the LEFM allowable flaw size calculation. The resulting effective flaw lengths were compared against the screening criteria to determine if the structural integrity of the shroud was maintained.

Based on the results of the application of the screening criteria to the observed indications, it is concluded that the structural integrity of the shroud is maintained for the next fuel cycle. All effective indication lengths were shown to be less than the allowable flaw size.

1.0 INTRODUCTION

The objective of this report is to document the conditions found on the Peach Bottom Unit-3 shroud, and evaluate these conditions based on GE SIL 572, Rev. 1 (Reference 1-1) recommendations, in order to validate the structural margins of the shroud.

Recently, in-vessel visual inspection (IVVI) of the Peach Bottom Unit-3 shroud revealed indications in the inside surface heat affected zones (HAZ) at weld locations H3 and H4. Figure 1-1 is a schematic illustrating the general locations of the shroud welds in Unit-3. Figures 1-2 and 1-3 are the shroud maps which show the locations where indications were found. Figure 1-4 is a plan view which indicates the locations referred to in Figures 1-2 and 1-3. Figure 1-2 shows the inside surface shroud map and Figure 1-3 shows the outside surface shroud map. Horizontal and vertical indications were seen associated with the H3 and H4 welds. Circumferential indications were also observed associated with one of the vertical welds (V3). However, these indications were relatively short compared to those associated with the horizontal welds.

In addition to the H3 and H4 welds, IVVI of the H1, H2, H5, H6, H7 and H8 welds was performed on the outside surface. Only a few short indications were observed on the outside surface of H1 and H4. It should also be noted that the area adjacent to the H9 weld was visually inspected as part of the access hole cover inspection (AHC) at this outage. The inspection did not reveal any indications. Additional detail of the IVVI results is presented in Section 4.0.

GE SIL 572, Rev. 1, provides the following recommendations based on the observed indications and evaluations performed to date:

Plant Fabrication and Operational History

Review plants fabrication and operational histories for the core shroud, including the materials of construction.

Non-Destructive Examination Actions

Visual examinations of accessible areas should be performed on the shroud ID and OD surface at the next scheduled refueling outage for all plants with Type 304 stainless steel shrouds with six or more years of power operation, and for all plants with L-grade

stainless steel shrouds with eight or more years of power operation. These examinations should be performed with an enhanced VT-1 system or a qualified UT examination from the outer surface.

If indications are not observed, examination should be performed at every second refueling outage. If indications are observed, the shroud should be examined and lengths measured during each refueling outage. The SIL also provides a recommended examination process.

Destructive Testing

A boat or core sample may be necessary depending on the results of the examination.

Structural Margin Analysis

Perform a structural margin analysis using the results from the NDE, and, if performed, the destructive analysis. If numerous indications are observed, the need for corrective action can be assessed using cumulative flaw length structural margin criteria.

Corrective Action

Based on the results of the structural margin evaluation, determine if continued operation is justified for another cycle without repair. If cracking is found and sufficient structural margin remains, examine the shroud during each subsequent refueling outage.

This report provides the pertinent information required to demonstrate that continued operation of Peach Bottom Unit-3 is justified based on the SIL recommendations noted above. Specifically, the report presents the following information:

- Fabrication history of the shroud.
- Water Chemistry and Fluence Considerations
- In-Vessel Visual Inspection
- Structural Margin Analysis
- Screening Criteria for Application to IVVI results.

It is noted that the loads used in this evaluation correspond to those for power rerate. A two-year operating cycle was used in the determination of crack growth.

1.1 Background

Indications have been observed in the shrouds of three plants to date (including Peach Bottom Unit-3). Cracking was observed in a BWR/4 located outside the United States in 1990. The cracking was confined to the heat affected zone (HAZ) of a circumferential weld.

In 1993, the second occurrence of cracking in a shroud was reported. Cracking was observed on the inside surface (ID) of the top guide support ring near the H3 weld. The cracking was approximately 360° around the circumference, in the weld heat affected zone (HAZ), in a material with carbon content of 0.06%. The fluence was estimated as 1.8×10^{20} nvt ($E > 1 \text{ Mev}$).

In addition to the H3 weld HAZ cracking, indications were visually observed at the H1, H2, H4, H5 (shroud cylinder) and, H6a weld HAZ (at core plate support ring). Indications were seen mostly on the inner surface at H3, H4 and H5. Indications were seen on the outer surface at the H1, H2 and H6 welds.

1.2 Screening Criteria

IVVI provides the length characterization of any present indications. Given that non-destructive examination (NDE) of every visually detected indication could be difficult and time consuming, a method of screening indications for subsequent evaluation is required. This report presents such a screening criterion.

The guiding parameter used for the selection of the indications for further evaluation is the allowable through-wall flaw size, which already includes the safety factors. If all of the visually detected indications are assumed to be through-wall, then the longest flaws, or combination of flaws, would have the limiting margin against the allowable through-wall flaw size. In reality, the indications are likely not through-wall, and therefore, the criteria and methods presented in this report are conservative.

The result of this procedure will be the determination of the effective flaw lengths which will be used to compare against the allowable flaw size and selection of indications for more detailed evaluation. The determination of effective flaw length is based on ASME Code, Section XI, Subarticle IWA-3300 (1986 Edition) proximity criteria. These criteria

provide the basis for the combination of neighboring indications depending on various geometric dimensions. Crack growth over a subsequent two year operating and power rerate cycle is factored into the criteria. This is conservative since power rerate will not be in effect during the next fuel cycle.

The proximity rules described here also conservatively assume that there is interaction between two perpendicular flaws. It is assumed that circumferential and axial indications could increase the effective flaw length depending on the unflawed distance between them. This effective circumferential flaw length must be compared against the allowable circumferential flaw length. The axial flaw would be compared against the allowable axial flaw length.

Flaws are considered in the same plane if the perpendicular distance between the planes is 4" or less. Any flaws which lie at an angle to the horizontal plane should be separated into a circumferential and axial component. These components can then be used separately in the determination of effective flaw lengths.

The selection of indications for further investigation can be performed by evaluating the resulting effective flaw lengths. **Indications with effective flaw lengths greater than the allowable flaw sizes would require further characterization by NDE or more detailed analysis.** The procedure described here is conservative since all of the indications are assumed through-wall and are being compared against the allowable through-wall flaw size.

The report covers the limiting stresses for all the shroud welds (H1 through H8 welds). Therefore, the screening criteria developed here cover all shroud weld indications. A list of conservatisms used in this evaluation is summarized in Table 1-1.

Table 1-1 Conservatisms Included In Screening Evaluation

1. All surface indications were assumed to be through-wall for analysis.
2. The screening criteria limit one-fourth of allowable circumferential flaws to any arbitrary 90° sector.
3. All indications are assumed to be grouped together for the limit load calculation and no credit is taken for the spacing between indications.
4. ASME Code primary pressure boundary safety margins were applied even though the shroud is not a primary pressure boundary.
5. ASME Code, Section XI proximity rules were applied.
6. An additional proximity rule which accounts for fracture mechanics interaction between adjacent flaws was used (See Appendix A).
7. The highest stress computed for any single location was used for all locations.
8. Both LEFM and limit load analysis were applied, even though LEFM underestimates allowable flaw size for austenitic materials and is not required per ASME Code Section XI procedures.
9. Fracture toughness measured for similar materials having a higher fluence was used.
10. The bounding crack growth estimated for the next fuel cycle was included in flaw lengths used for evaluation (See Appendix B).
11. A proximity rule to account for perpendicular flaws was applied, although not required by Section XI.
12. Power rerate conditions were used although it will not be in effect during the next fuel cycle.



1.3 References

1. GE Services Information Letter (SIL) 572, Rev. 1, October, 1993

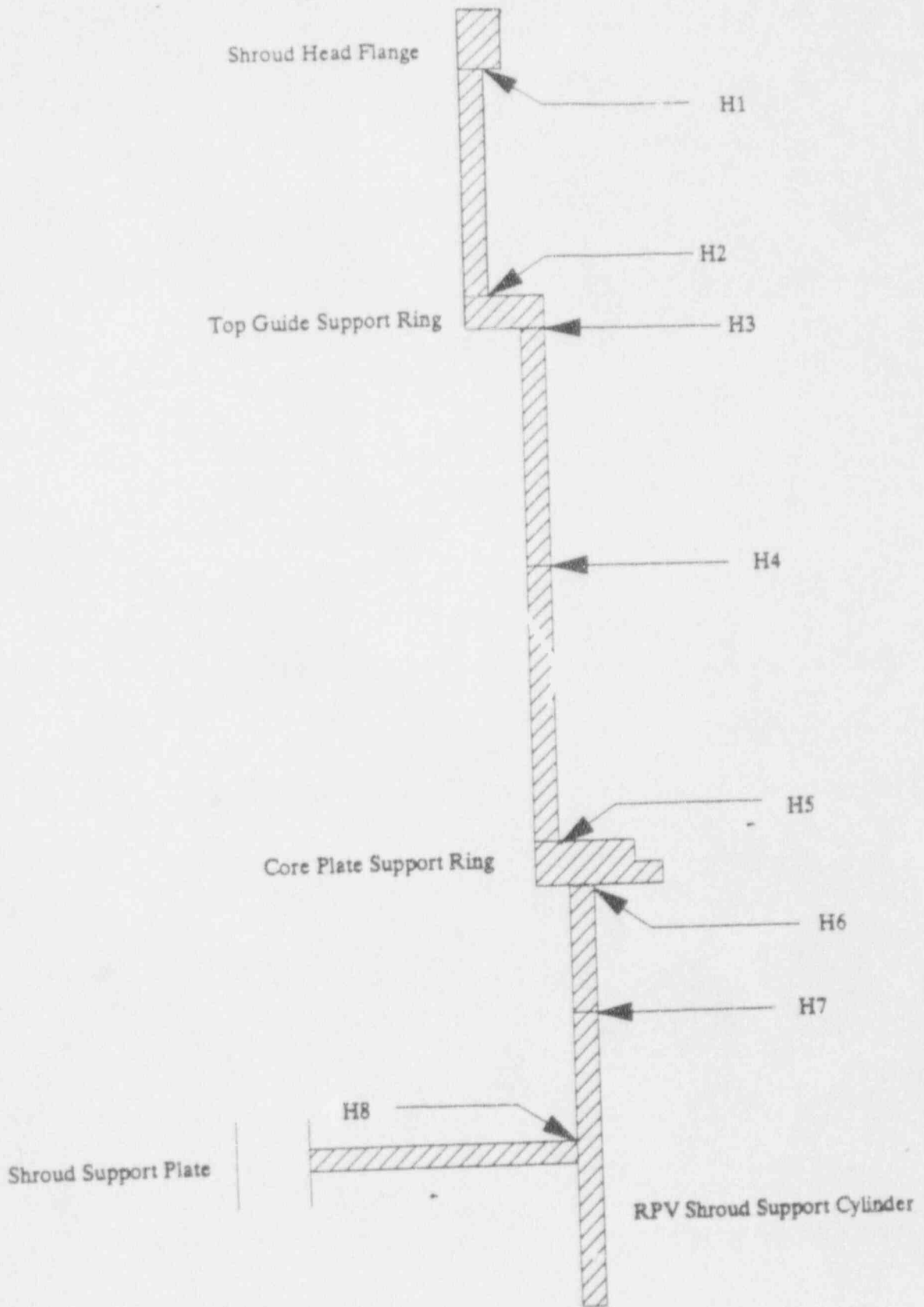
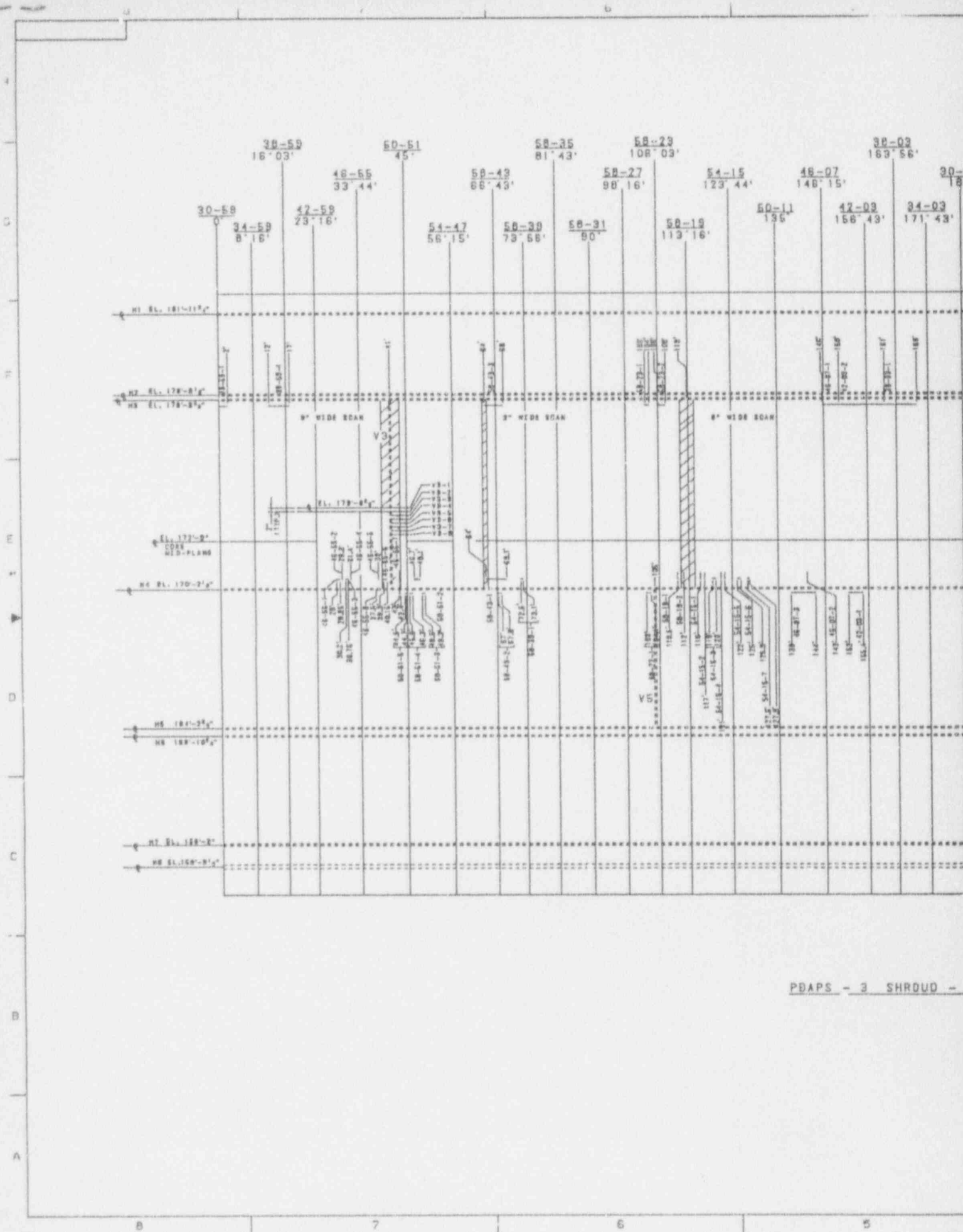
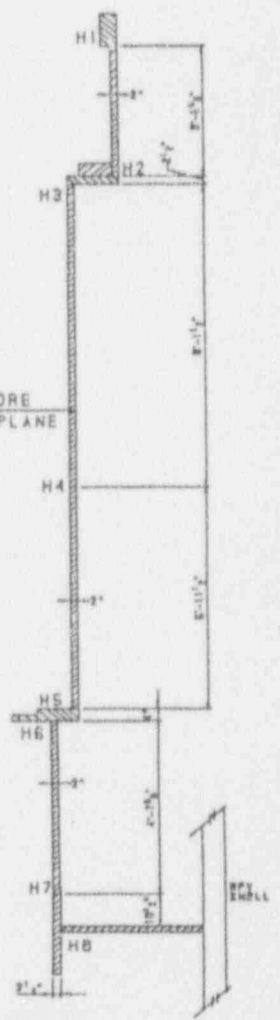
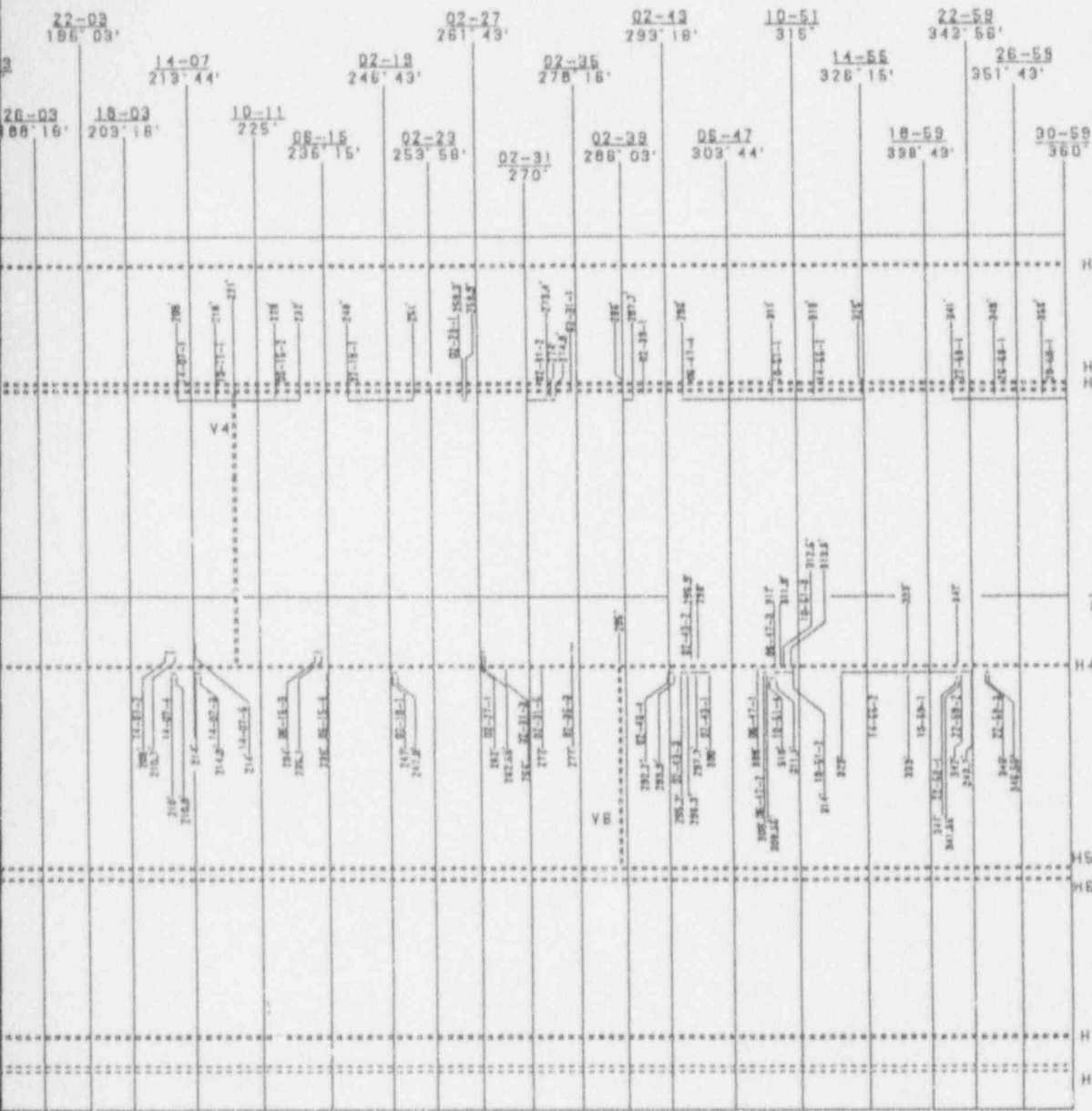


Figure 1-1



PBAPS - 3 SHROUD -



ANSTEC
APERTURE
CARD

Also Available on
Aperture Card

DIMENSIONAL INFORMATION:
1 DEGREE = 1.7725" AT H3 AND
H4 WELD LOCATION

LEGEND:
— AS-FOUND INDICATIONS

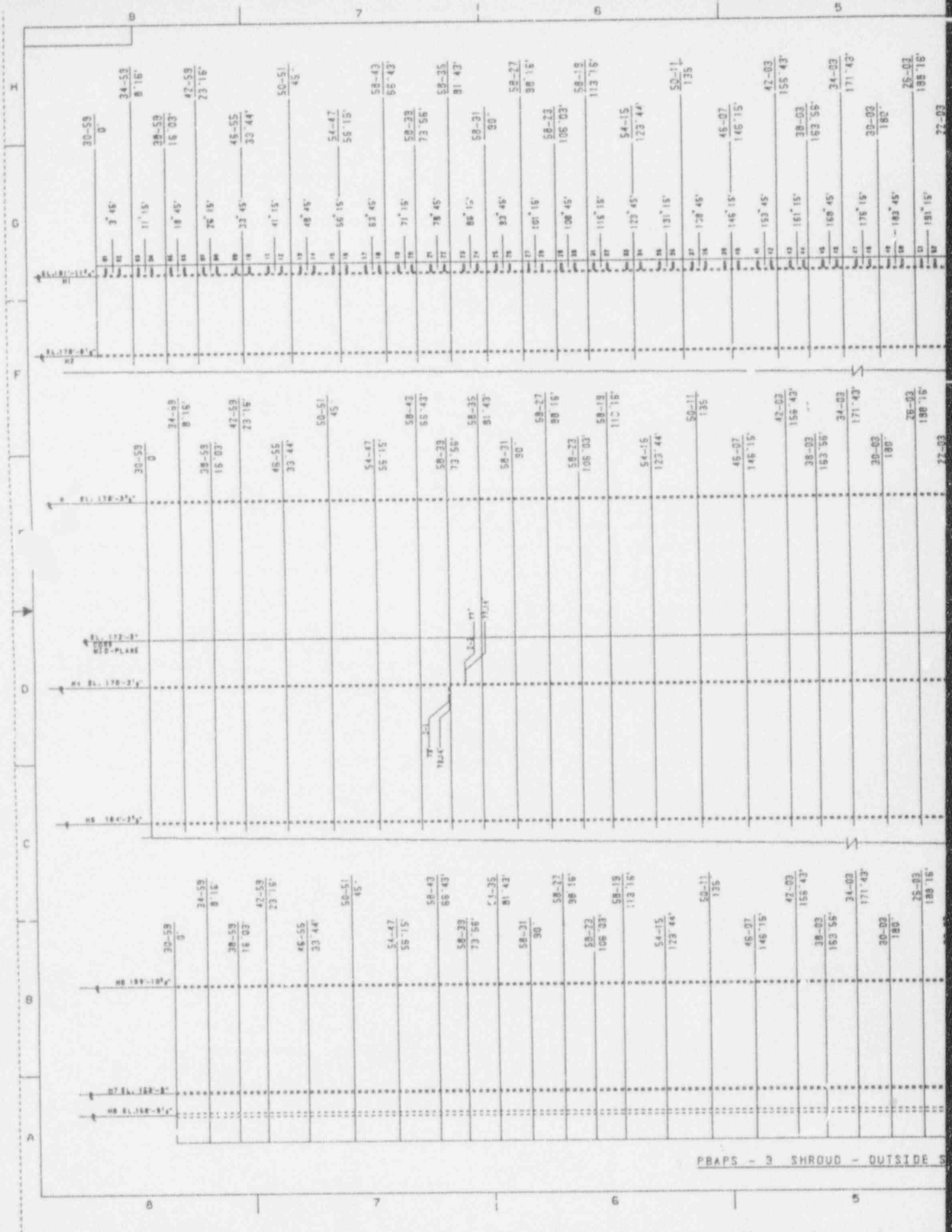
NOTE:
1. EXAMINER'S ST-1 EXAMINATION PERFORMED ON
100% OF WELDS H-3 AND H-4 (INSIDE SURFACES)

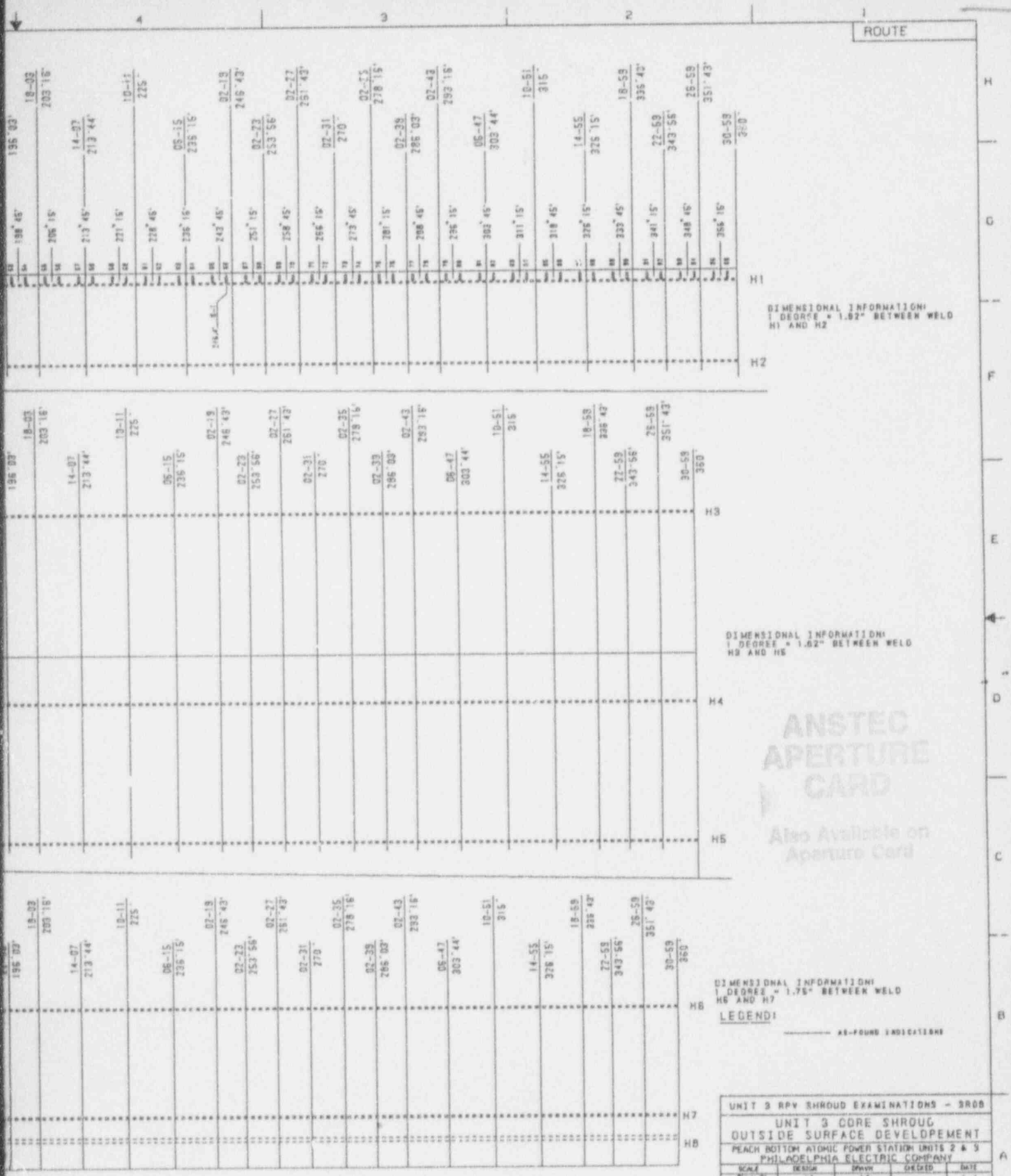
INSIDE SURFACE DEVELOPMENT

FOR INFO ONLY

UNIT 3 RPV SHROUD EXAMINATIONS - 3008				
UNIT 3 CORE SHROUD				
INSIDE SURFACE DEVELOPMENT				
PEACH BOTTOM ATOMIC POWER STATION UNITS 2 & 3				
PHILADELPHIA ELECTRIC COMPANY				
DATE	DESIGN	DRAWN	CHECKED	DATE
11-1-78	LA	LA	LA	11-1-78
APPROVED		APPROVED		
JOB NO	DRAWING NUMBER	SHEET NUMBER	REV	
6280	FIGURE 1-2			

9403230107-01





DIMENSIONAL INFORMATION:
1 DEGREE = 1.02" BETWEEN WELD
H1 AND H2

DIMENSIONAL INFORMATION:
1 DEGREE = 1.02" BETWEEN WELD
H2 AND H3

DIMENSIONAL INFORMATION:
1 DEGREE = 1.75" BETWEEN WELD
H6 AND H7

LEGEND:

----- AS-FOUND INDICATIONS

**ANSTEC
APERTURE
CARD**

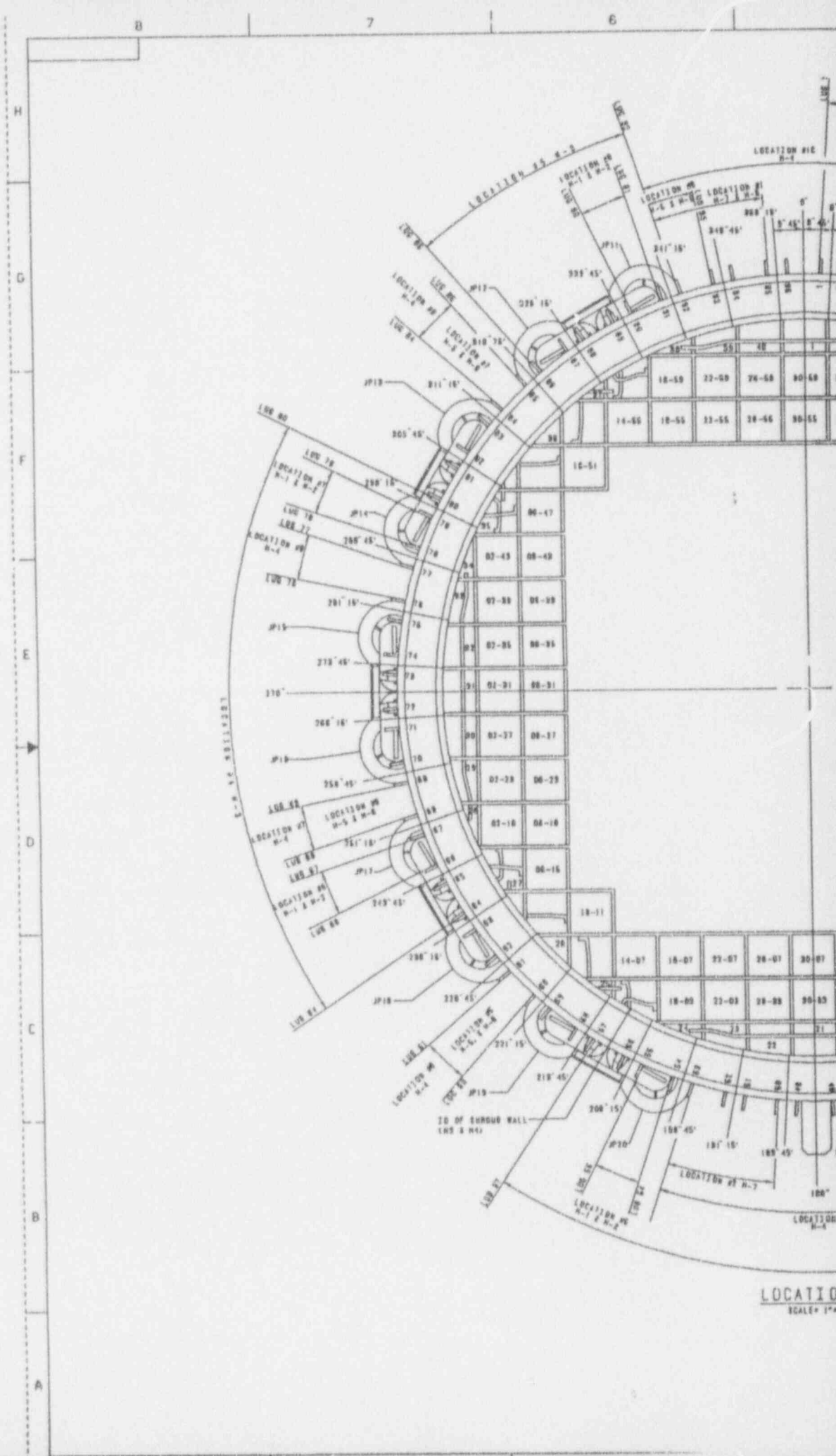
Also Available on
Aperture Card

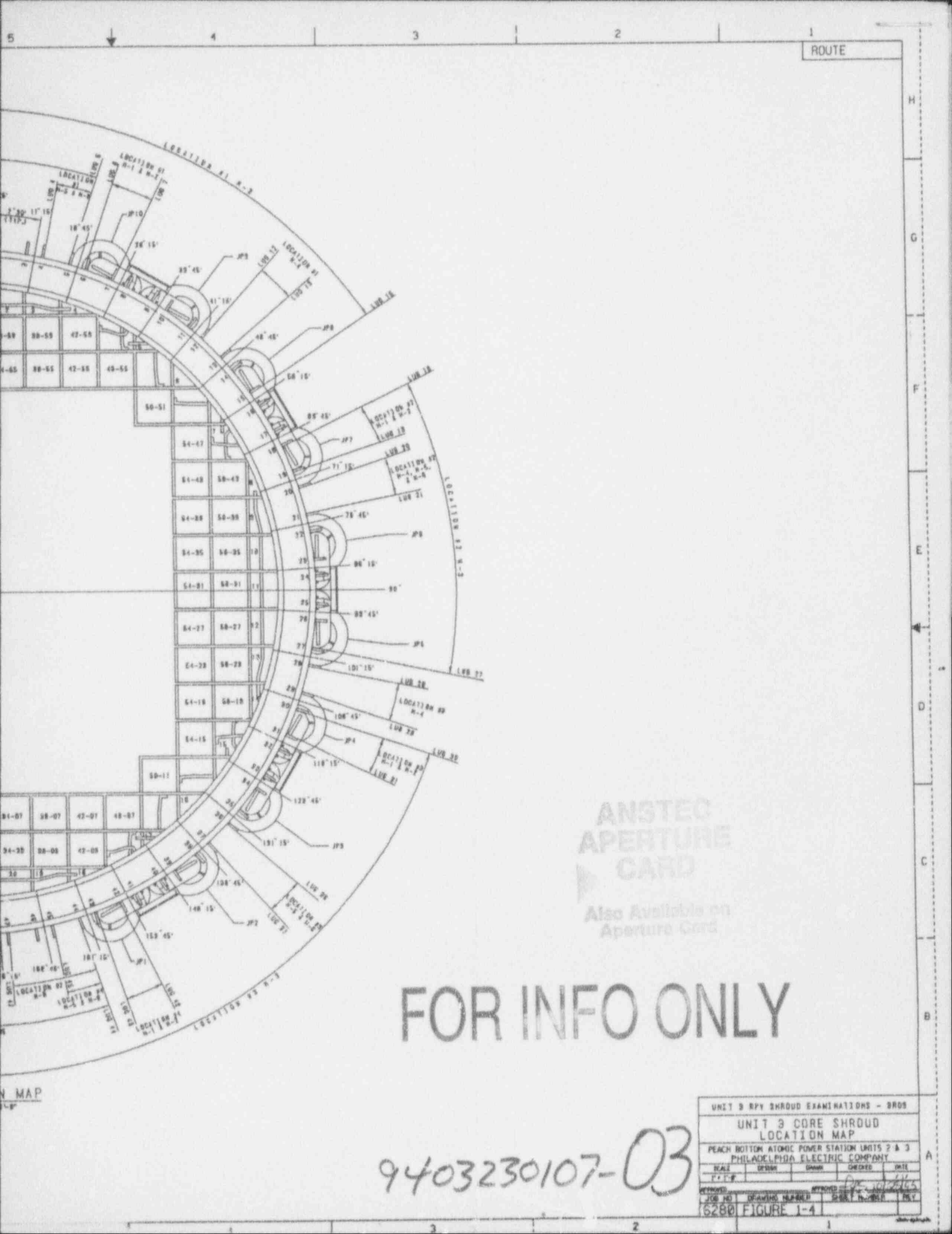
UNIT 3 RPV SHROUD EXAMINATIONS - 3R08				
UNIT 3 CORE SHROUD OUTSIDE SURFACE DEVELOPMENT				
PEACH BOTTOM ATOMIC POWER STATION UNITS 2 & 3 PHILADELPHIA ELECTRIC COMPANY				
SCALE	DESIGN	DRAWN	CHECKED	DATE
1/4" = 1'	LA	LA		1/1
APPROVED	APPROVED			
JOB NO. 6280	DRAWING NUMBER FIGURE 1-3	SHEET NUMBER 1	REV	

FOR INFO ONLY

9403230107-02

SURFACE DEVELOPMENT





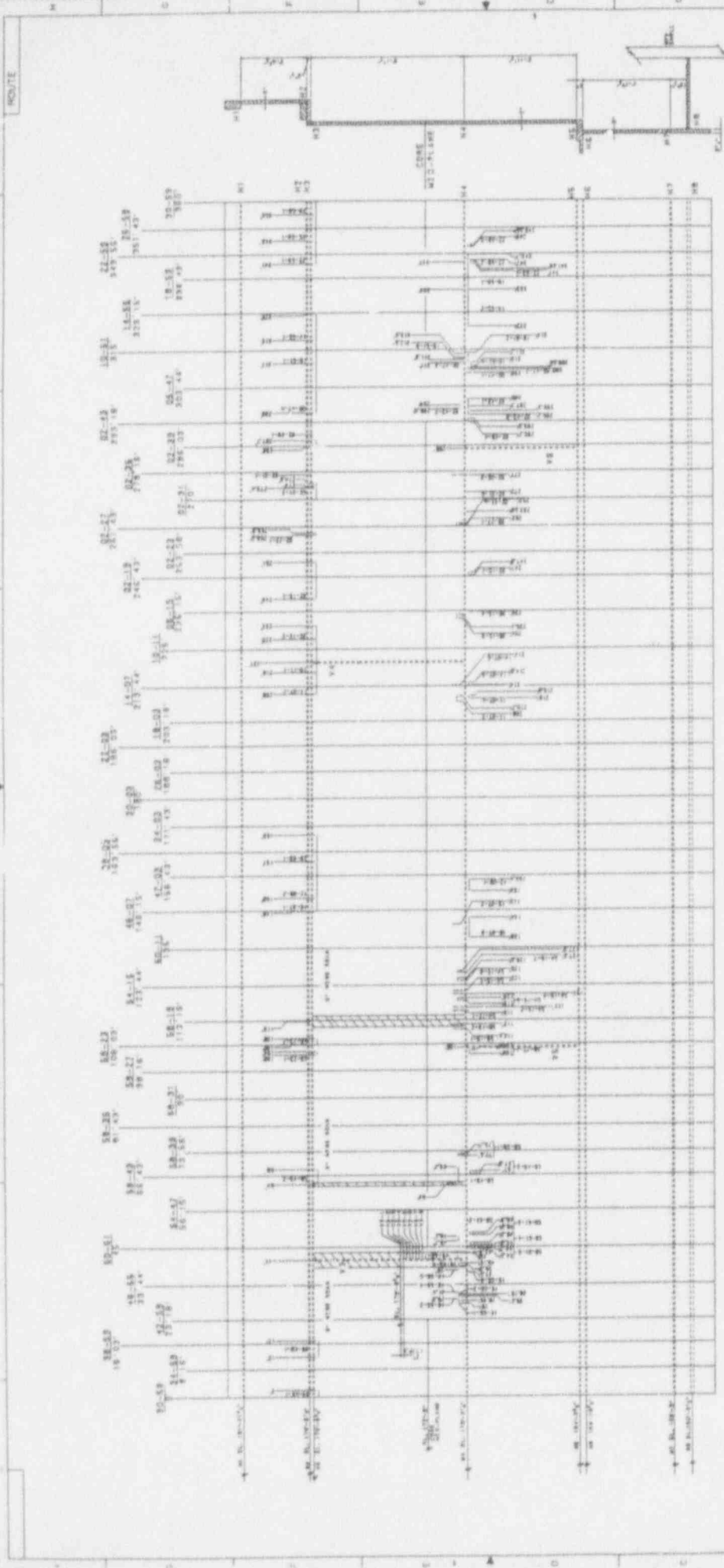
ROUTE

ANSTEC
APERTURE
CARD
Also Available on
Aperture Card

FOR INFO ONLY

9403230107-03

UNIT 3 RPY SHROUD EXAMINATIONS - SRO5				
UNIT 3 CORE SHROUD LOCATION MAP				
PEACH BOTTOM ATOMIC POWER STATION UNITS 2 & 3 PHILADELPHIA ELECTRIC COMPANY				
SCALE	DESIGN	DRAWN	CHECKED	DATE
1" = 10'				
APPROVED	APPROVED			
DWG NO.	DRAWING NUMBER	DWG. NUMBER	REV.	
6280	FIGURE 1-4			



DIMENSIONAL INFORMATION:
 ALL DIMENSIONS ARE IN MILLIMETERS
 UNLESS OTHERWISE SPECIFIED

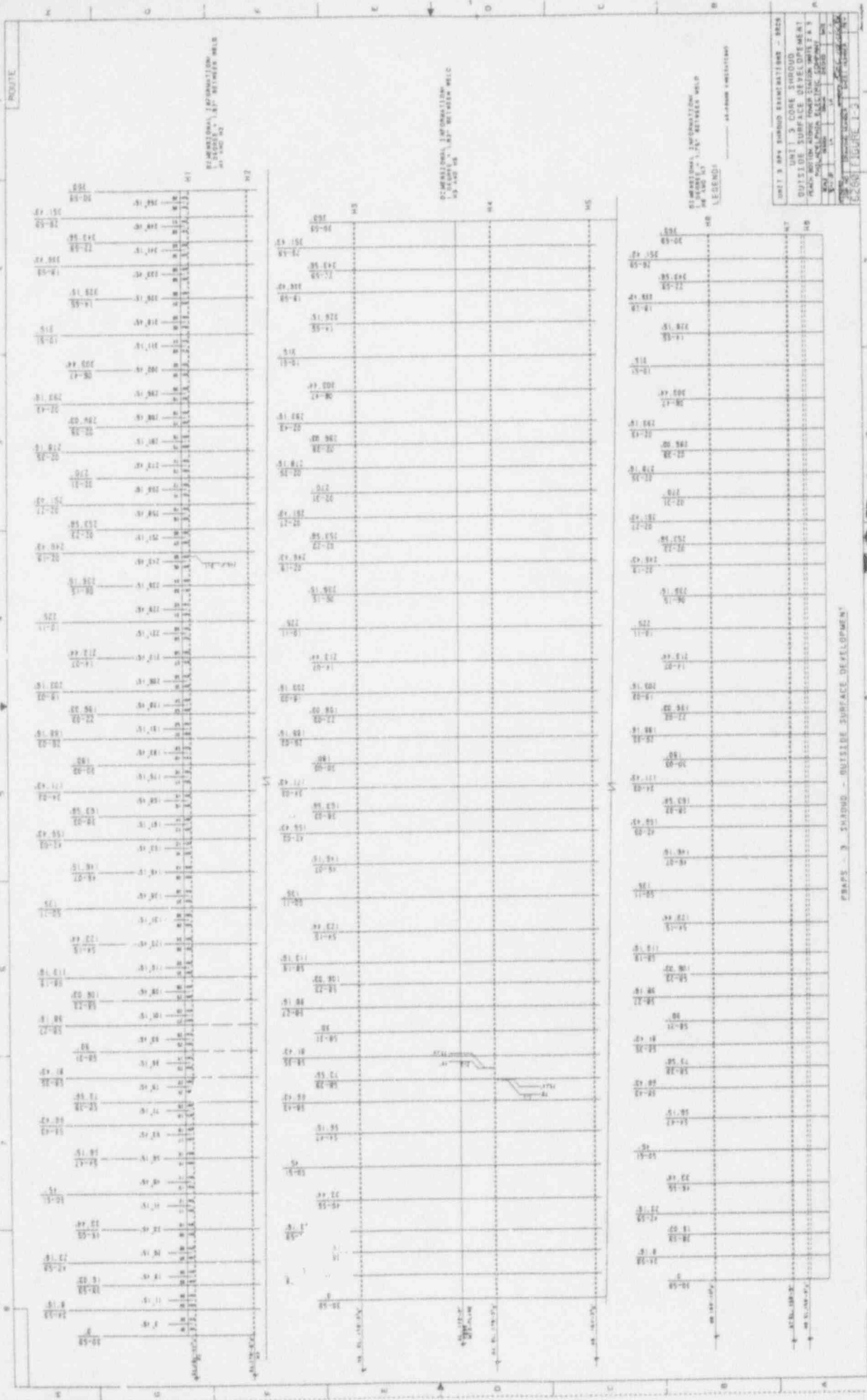
LEGEND:
 --- 10-MILLIMETER DIMENSION

SCALE:
 1:1000 (AS SHOWN)

UNIT 3 PIPE SURFACE DEVELOPMENT - 2020
UNIT 3 CORE THROUGH
INSIDE SURFACE DEVELOPMENT
PERIOD ACTION: INSIDE SURFACE DEVELOPMENT
DATE: 10/10/2019
TIME: 10:10:10
USER: [unreadable]
PROJECT: [unreadable]
FIGURE: 1-2

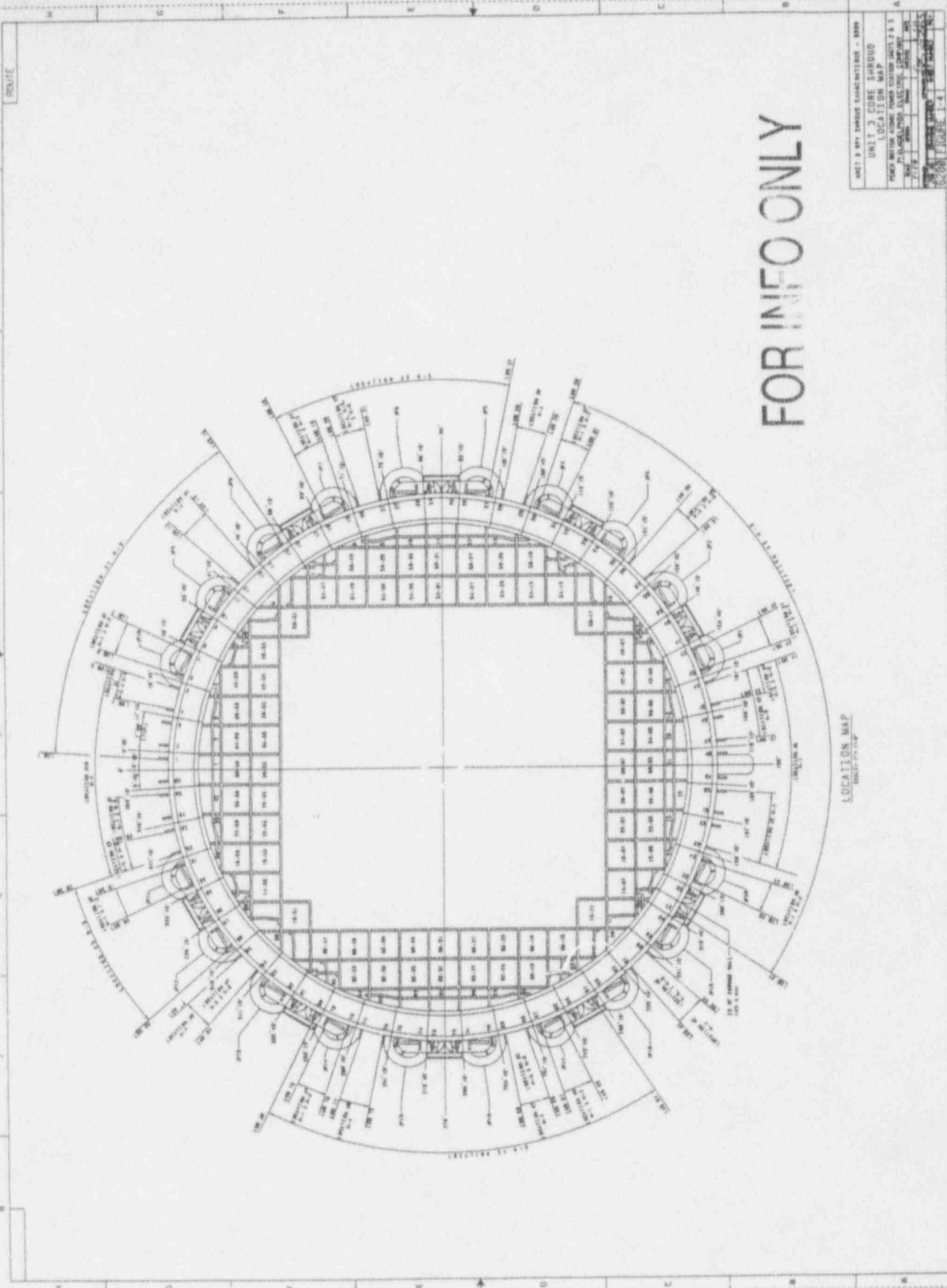
FIGURE 1-2 - INSIDE SURFACE DEVELOPMENT

FOR INFO ONLY



FOR INFO ONLY

FRAPS - 3 - SHEDS - OUTSIDE SURFACE DEVELOPMENT



FOR INFO ONLY

LOCATION MAP
SCALE 1" = 10'

UNIT 3 CORE SHEDDING LOCATION MAP	
PROJECT NO.	100-100-100
DATE	10/1/58
SCALE	1" = 10'
DRAWN BY	J. J. BROWN
CHECKED BY	J. J. BROWN
APPROVED BY	J. J. BROWN
DATE	10/1/58
FIGURE NO.	1-4

2.0 FABRICATION HISTORY

This section describes the fabrication history of the Peach Bottom Unit-3 shroud. Of key interest is the material composition and any activities which could have possibly contributed to the increase of intergranular stress corrosion cracking (IGSCC) susceptibility. Quality assurance records received from the vessel vendor (Rotterdam) were examined in detail to determine the appropriate information.

Table 2-1 shows the material data for the Unit-3 shroud. The part numbers are identified in the schematic shown as part of Table 2-1. Also shown in the table is the number of pieces for each part, material designation, heat numbers, and carbon content.

Figure 2-1 shows the assembly of the shroud. All welds are identified including vertical and horizontal welds. Figure 2-2 through 2-9 show the details of the shroud welds as labeled in Figure 2-1.

The upper, central and lower rings (part numbers 1, 3 and 6) are austenitic stainless steel seamless rolled forging. The material is ASTM A182 - F304. The heat treatment of these rings consisted of heating to 1100°C, holding for 6 hours, followed by water quenching to below 100°C. The carbon content of the rings ranges from 0.03% to 0.035% max. Hardness measurements upon completion of solution heat treatment and rough machining of the rings ranged from Brinell Hardness of 137 to 153.

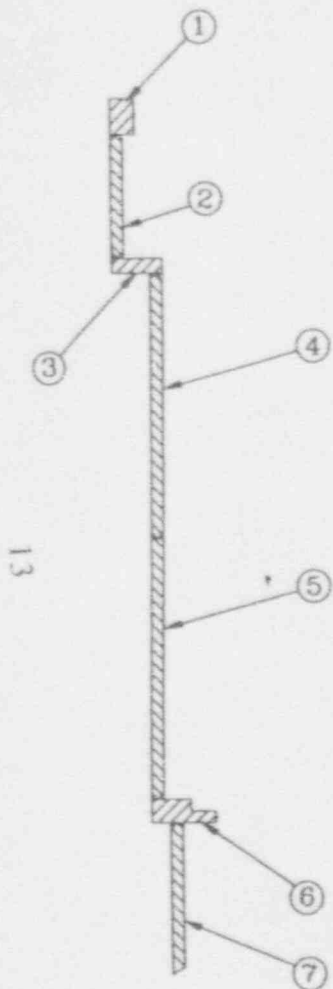
Each cylinder is made of 2 plate segments formed and welded to drawing requirements. Plate material is austenitic stainless steel made to ASTM A240, Type 304 specifications. The carbon content of the plate material ranges from 0.057% to 0.062% max. The hardness of the plate material ranges from Brinell Hardness of 137 to 155.

All welding was performed by submerged arc-welding except H7. The procedure and welder qualification was performed to ASME Section IX requirements. The filler metal met ASTM A-371 Type ER-308 requirements with required carbon content of 0.08% max. The welded joints did not use backing strips but utilized 3 to 4 hand weld passes. Weld prep surfaces of the base metal were prepared by machining. The backside of the groove welding was prepared by grinding or gouging followed by liquid penetrant inspection. Final surfaces of the welds were inspected by liquid penetrant examination.

The H7 weld was performed using metal inert gas with Alloy 82 wire. In addition, 100% ultrasonic examination of weld H7 was performed.

Based on GE Quality Assurance records received from Rotterdam, no abnormal fabrication history was found. General practice during assembly and shipment of the of the shroud, bracing, temporary welds, and supports are used to help in meeting the joining of the various components and to meet geometric tolerances. Although there is no record documentation of these practices, it is likely that they were present during fabrication. These actions result in a local effect on material behavior and stress. For example, the welding of temporary pads would result in a local area of weld residual stress and perhaps some grinding (cold work). If these local effects contribute to SCC, it is likely that the cracking would be of lesser concern than cracks near the horizontal welds.

Peach Bottom 3 Shroud Data

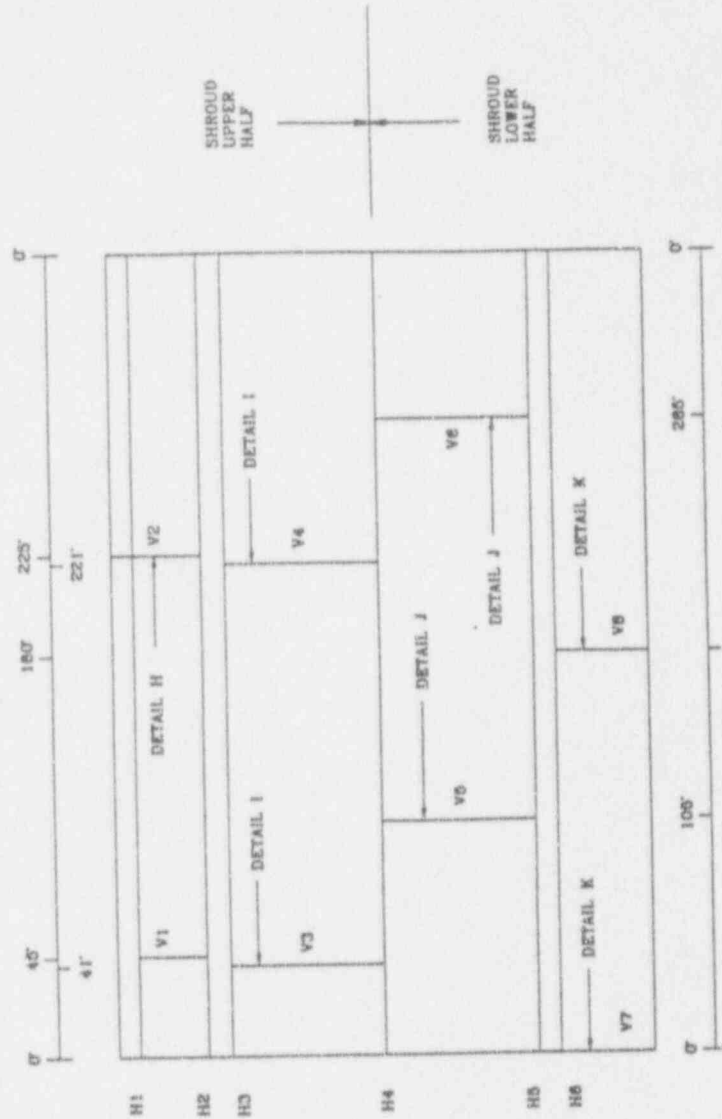


Part Number	Part Name	Quantity	Material	Heat / Certificate Number	Carbon Content - %	Comments on Material / Process
1	Upper Ring	1 Piece	A182 - F304	F1343-66.168	0.035	
2	Upper Cylinder	2 Pieces	A240 Type 304	3582-E9967	0.082	
3	Central Ring	1 Piece	A182 - F304	F1399-65.587	0.030	
4	Central Cylinder	2 Pieces	A240 Type 304	5727-E114	0.057	
				5637-E114	0.080	
5	Central Cylinder	2 Piece	A240 - Type 304	2170-E212	0.057	
				2818-E15	0.080	
6	Lower Ring	1 Piece	A182-F304	F1400-66.159	0.035	
7	Lower Cylinder	2 Pieces	A240 Type 304	3586-E40	0.059	
				2784-E11	0.059	

NOTES:

1. CORE SPRAY SPARGER ASSEMBLY, INTERNAL AND EXTERNAL BRACKETS/PADS ARE REMOVED FOR CLARITY.

Table 2-1



NOTES:

1. AZIMUTHAL LOCATIONS OF LONGITUDINAL WELDS ARE NOT DEFINED ON THE EXISTING DOCUMENTATION.
2. THE AZIMUTHAL LOCATION OF THE LONGITUDINAL WELDS, V3, V4, V5 AND V6 WERE IDENTIFIED DURING A VISUAL INSPECTION BY PEACHBOTTOM PERSONNEL.

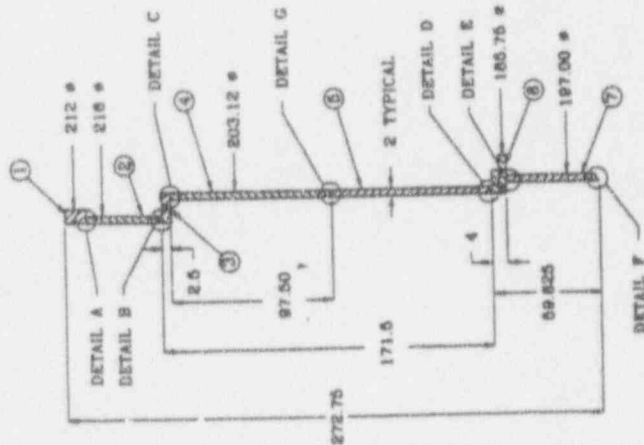


Figure 2-1

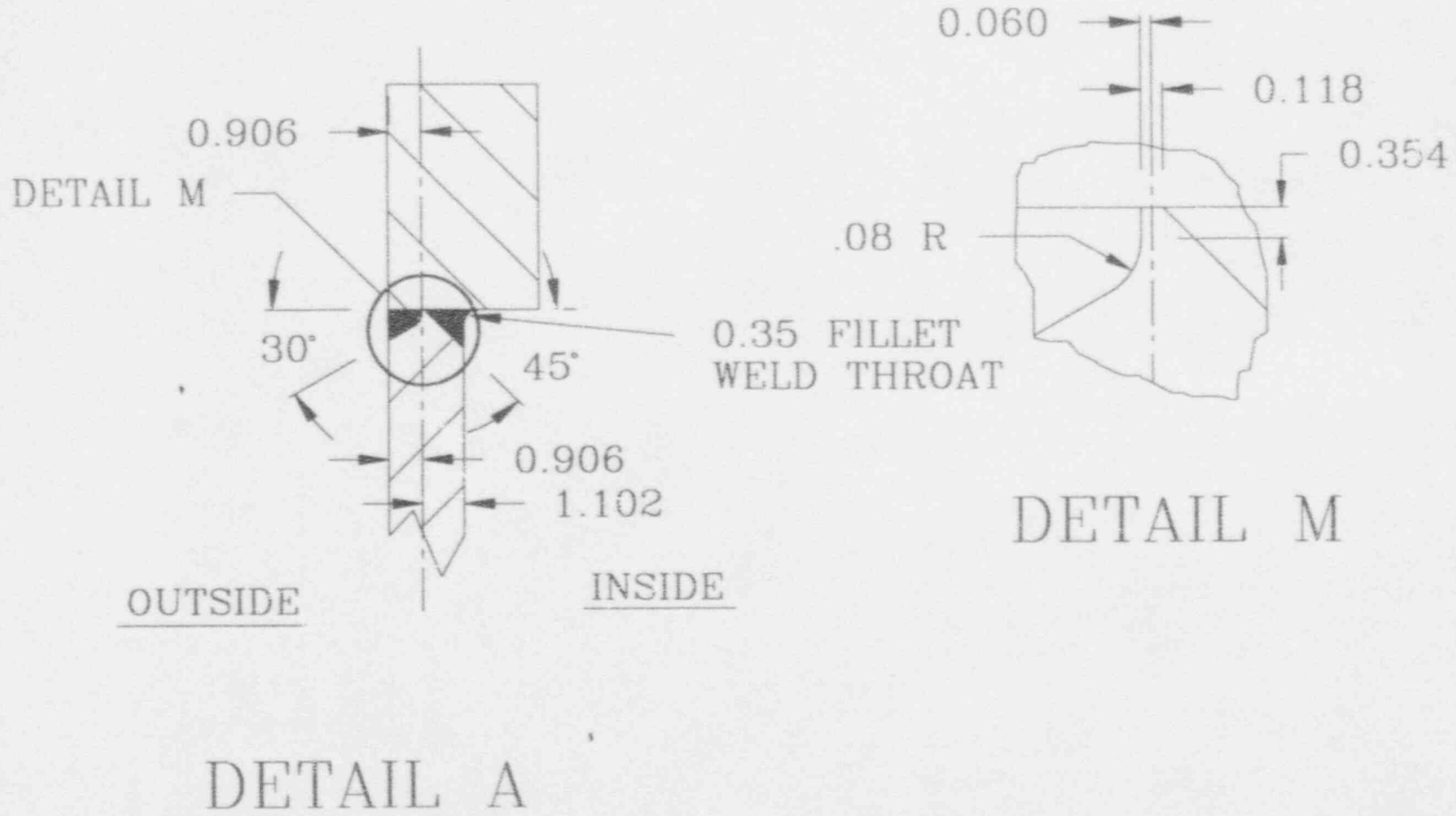


Figure 2-2

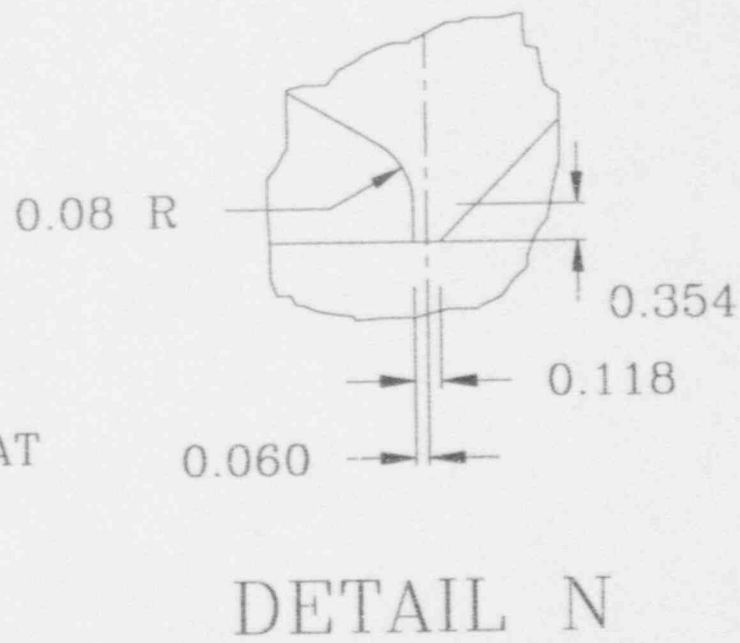
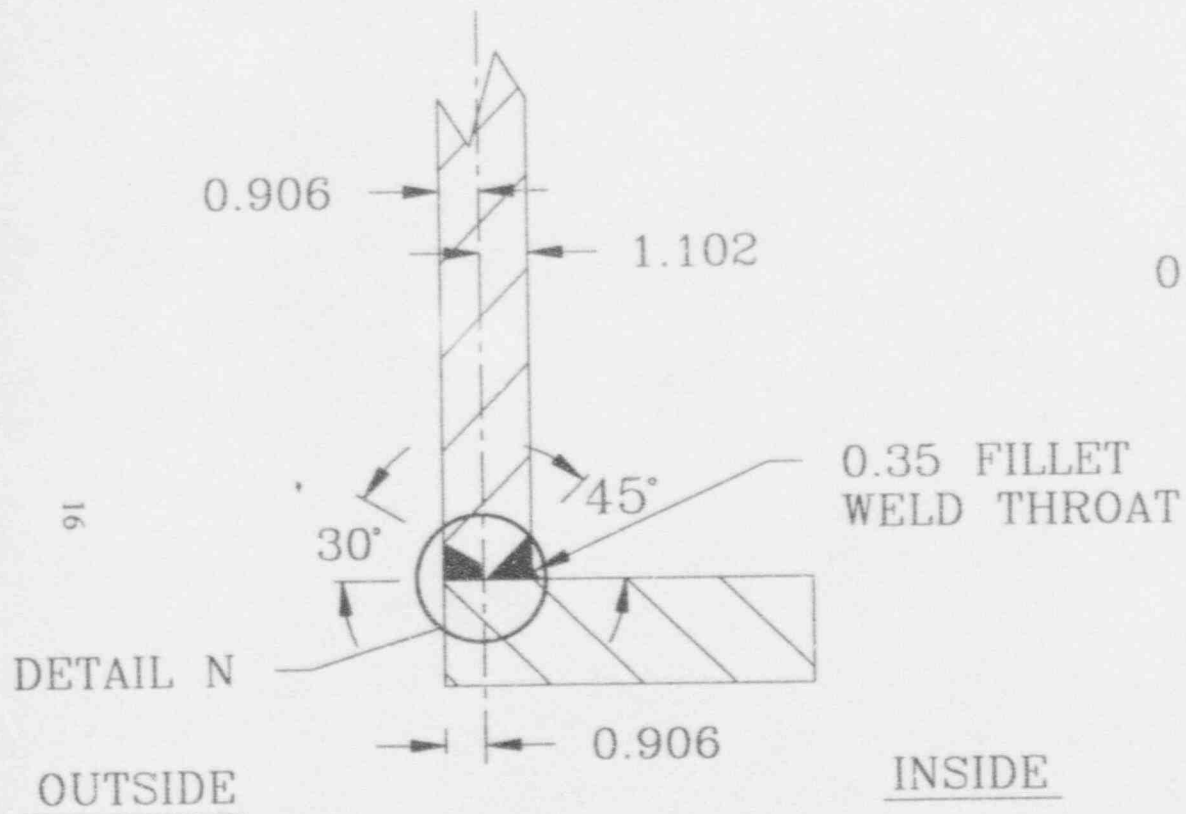


Figure 2-3

17

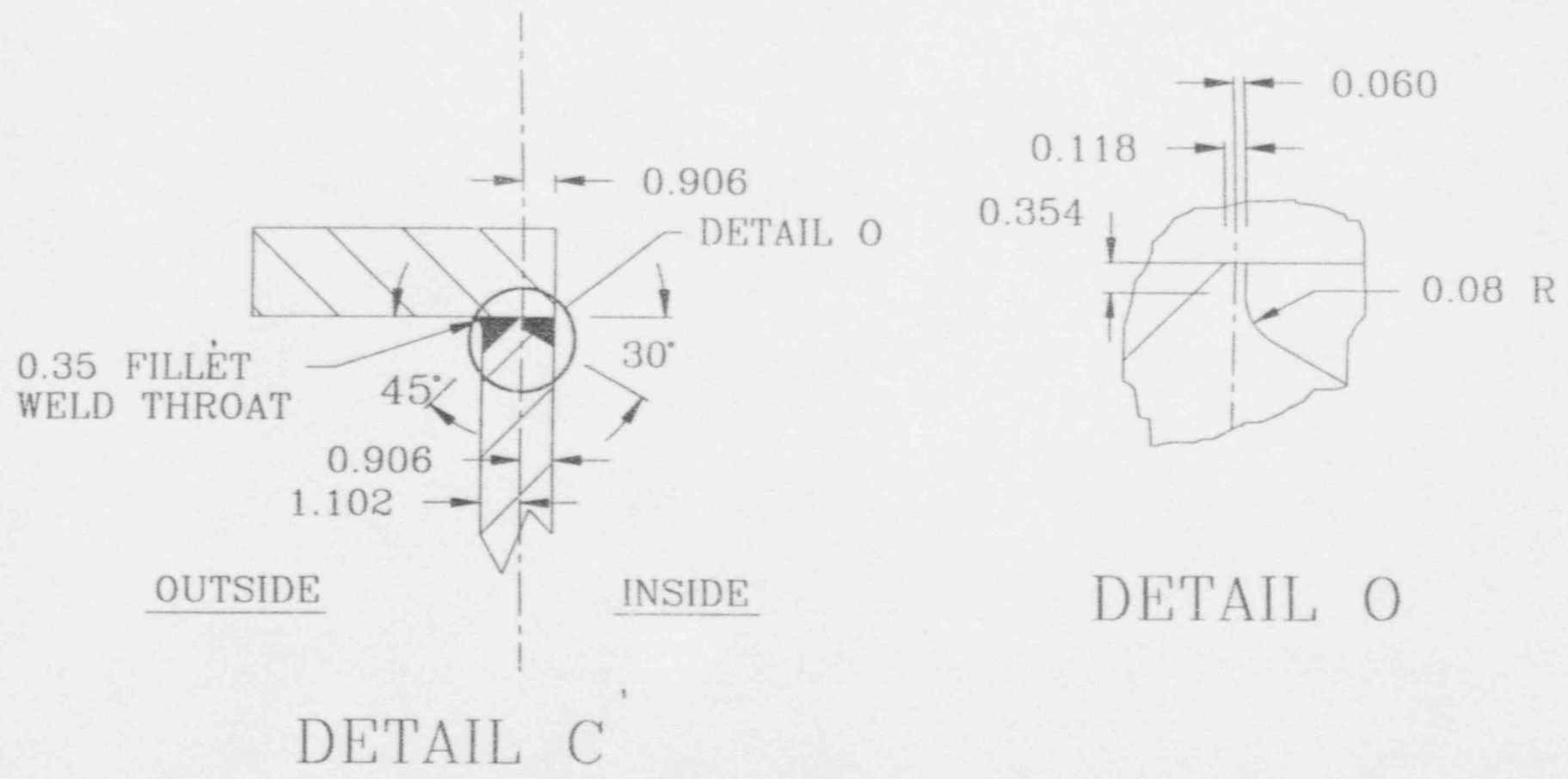
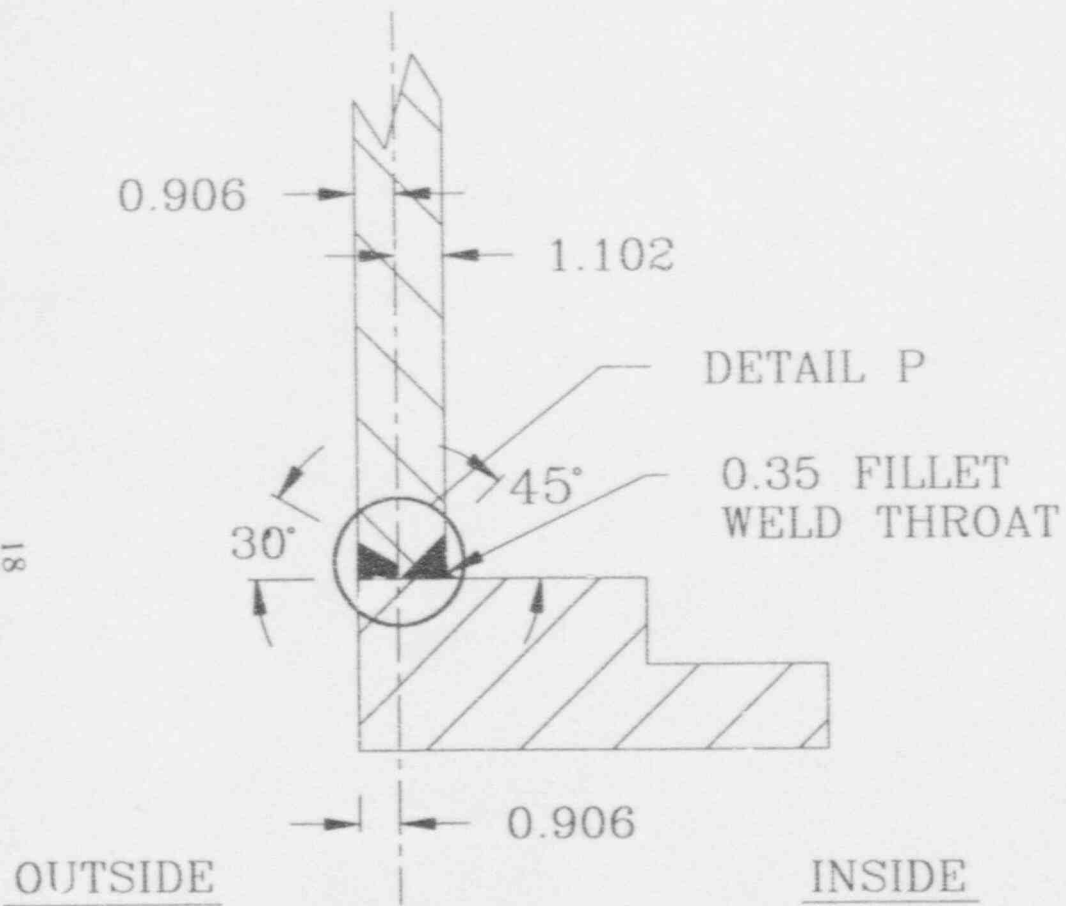


Figure 2-4



DETAIL D

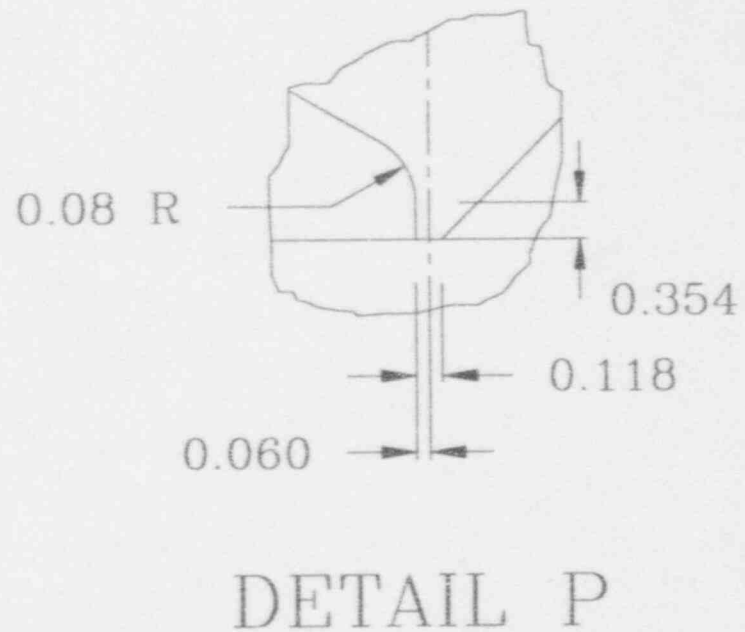
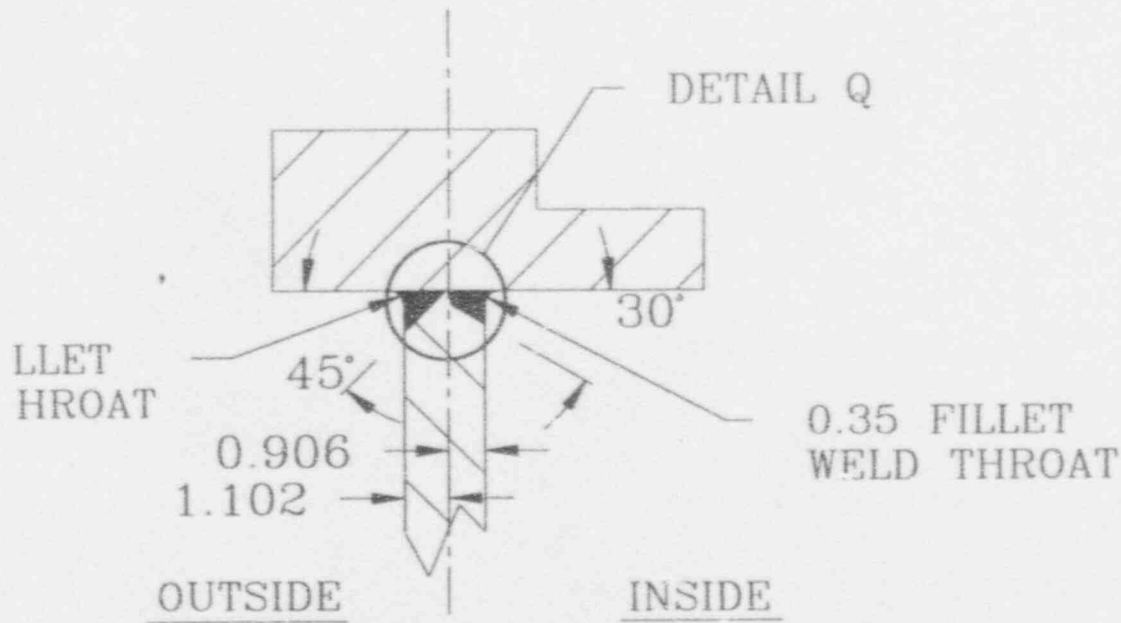
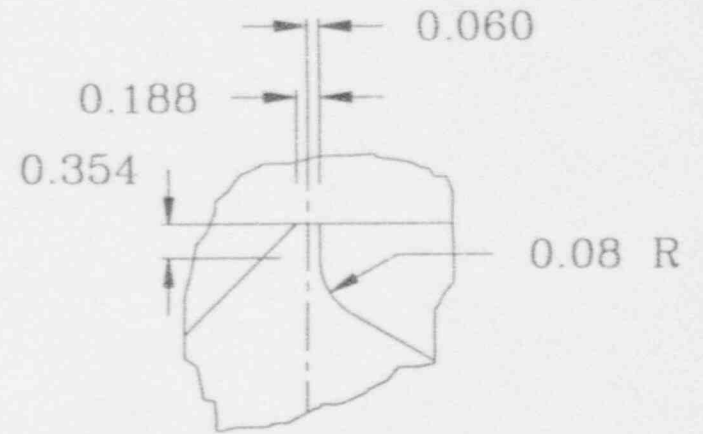


Figure 2-5

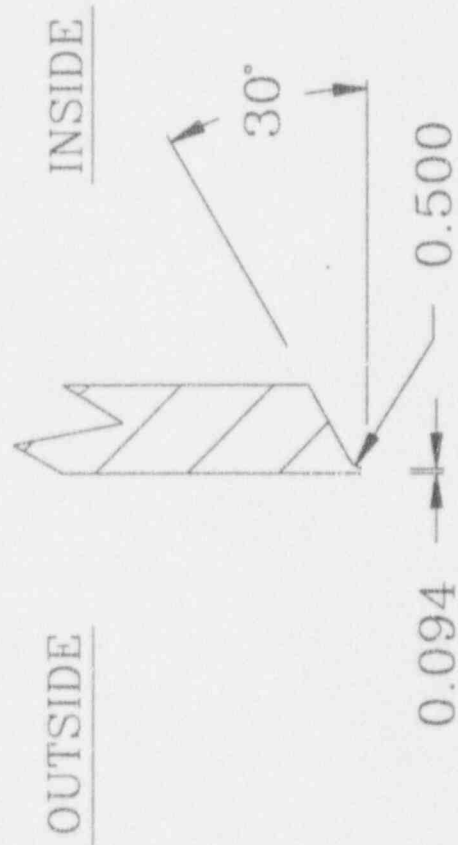


DETAIL E



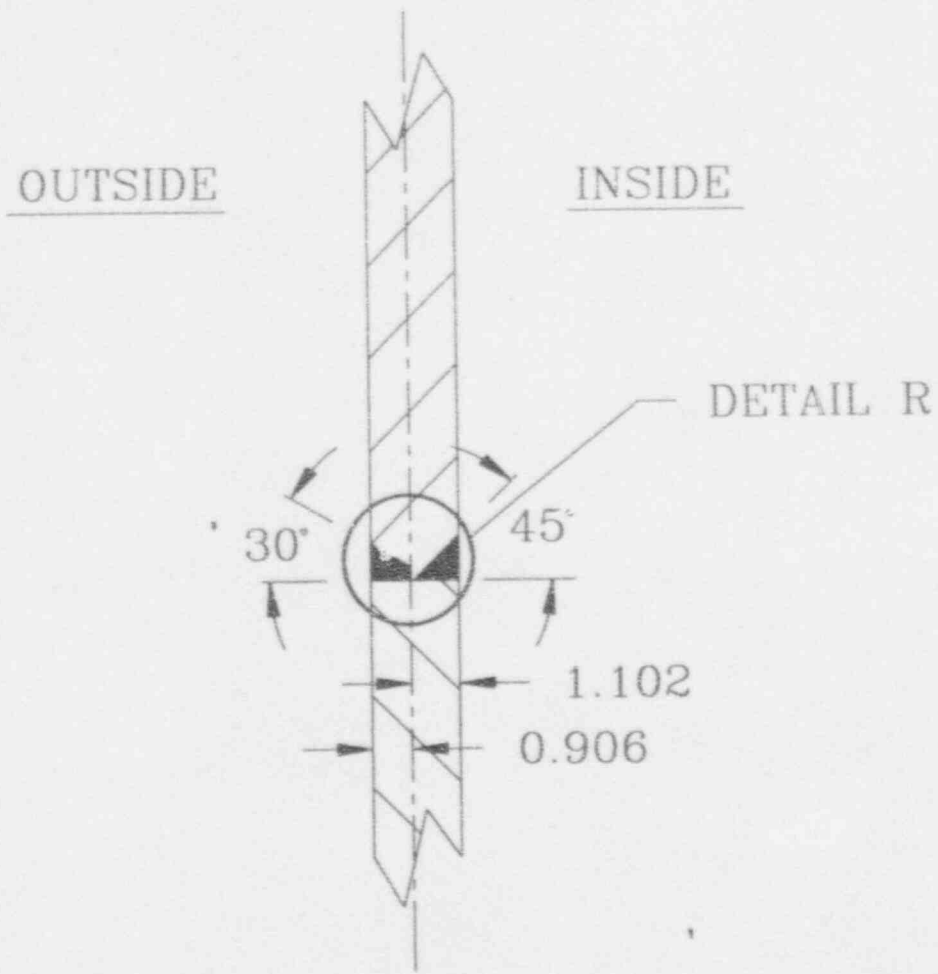
DETAIL Q

Figure 2-6

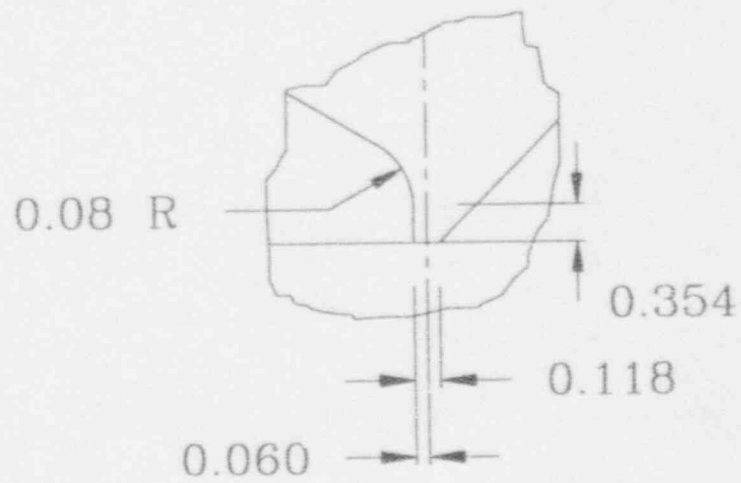


DETAIL F

Figure 2-7



DETAIL G

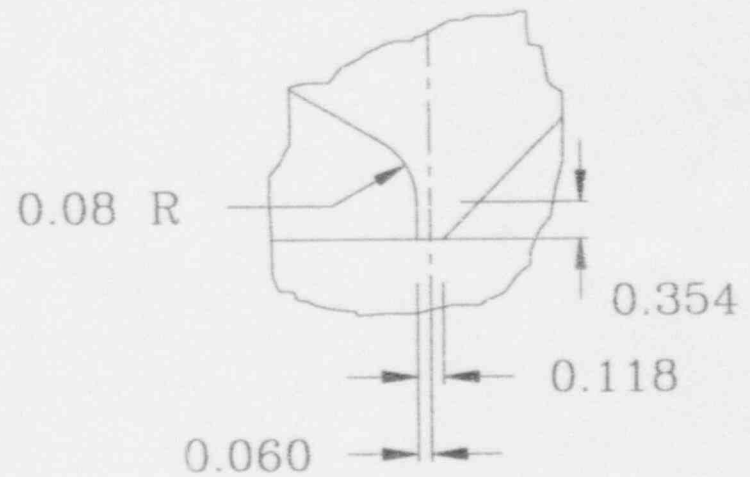
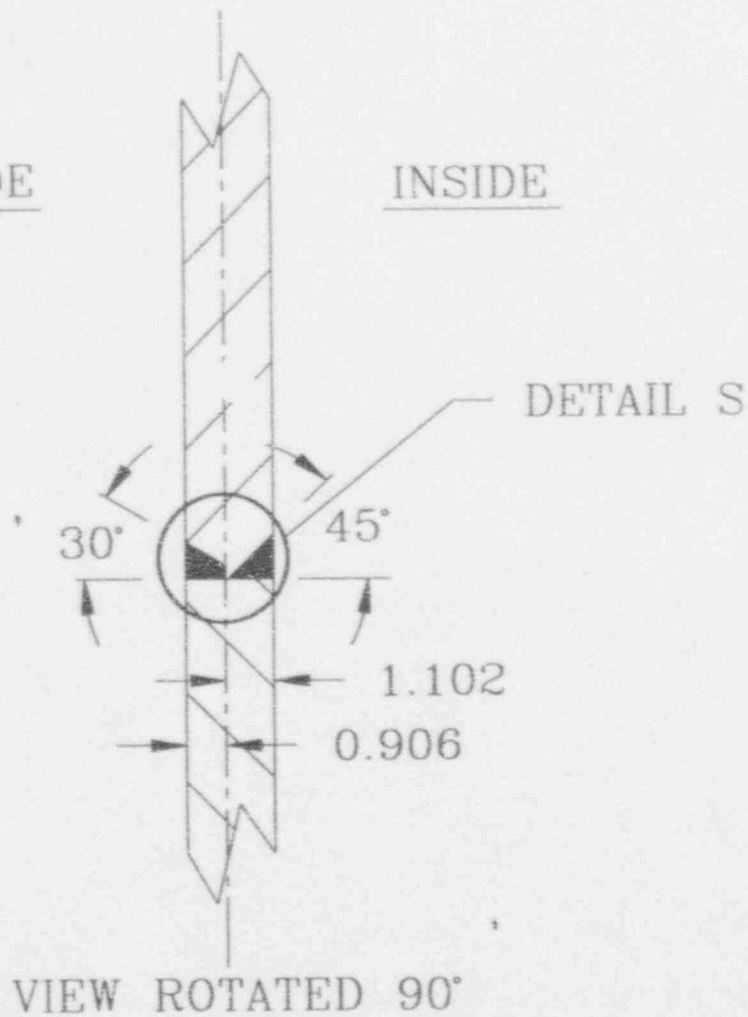


DETAIL R

Figure 2-8

OUTSIDE

INSIDE



DETAIL S

DETAILS H/I/J/K

Figure 2-9

3.0 CHEMISTRY AND FLUENCE CONSIDERATIONS

3.1 Water Chemistry History

For the first decade of hot operation, Peach Bottom Unit-3 operated with relatively high primary water conductivity. As can be seen in Figure 3-1, Unit-3's arithmetic mean conductivity actually exceeded $1.0 \mu\text{S}/\text{cm}$ in 1976 and 1977. The arithmetic mean conductivity was very high and exceeded $0.4 \mu\text{S}/\text{cm}$ through 1986. Subsequently, conductivity values steadily decreased, and was $<0.1 \mu\text{S}/\text{cm}$ ($0.089 \mu\text{S}/\text{cm}$) during 1992 and 1993. These last two year's conductivity values are considered world class performance.

The high conductivity during the first half of life was partly due to leaking condensers and resin change out problems. However, besides the high early life steady state conductivity, there was also one relatively severe transient experienced at Unit-3 as presented in Table 3-1, a summary of BWR fleet severe transients through about 1983. As can be seen in Table 3-1, Unit-3 suffered at least one power resin intrusion (Incident Rank 13) during which the conductivity reached $23.6 \mu\text{S}/\text{cm}$ due to possible condensate demineralizer resin intrusion. This intrusion type of incident results in the injection of sulfate into the RPV. Since IGSCC initiation and propagation in sensitized austenitic stainless steel and nickel base alloys are controlled by the rate of cathodic reduction of species such as dissolved oxygen, hydrogen peroxide and/or various oxyanions, then the additional presence of a detrimental oxyanion, such as sulfate, would increase the cathodic current and thus accelerate anodic dissolution at the crack tip, i.e., IGSCC (Reference 3-1).

3.1.1 Effects of Impurities on IGSCC

An example of the effects of sulfate/conductivity on crack initiation in uncreviced material is presented in Figure 3-2. It is clear that an increase in sulfate/conductivity results in an acceleration in crack initiation as measured by the constant extension rate test (CERT) (References 3-1 through 3-4). A specific Peach Bottom example of acceleration in crack propagation rate (creviced) with sulfate is shown in Figure 3-3. Figure 3-3 displays June 1986 (not included in Table 3-1) Unit-3 on-line crack monitoring data for sensitized Type 304 stainless steel. The results clearly illustrate the change in crack growth observed after two closely linked water chemistry transients of $4-5 \mu\text{S}/\text{cm}$, i.e., increases in water

conductivity due to intrusions of demineralizer resin material (Reference 3-5). This figure demonstrates the dramatic increase in crack growth rate (2X) with conductivity. Similar on-line crack monitoring results with sulfate have also been documented in the laboratory, Figure 3-4 (Reference 3-6). Other anions such as chloride, carbonate, etc. have similar kinetic effects on IGSCC initiation and propagation (References 3-7 and 3-8).

This high conductivity crack initiation and propagation acceleration factor is consistent with the relatively high incidence of IGSCC observed at Unit-3 in creviced Alloy 600 shroud head bolts (15 of 25 bolts examined cracked) and access hole covers. No cracking of these two components has been identified in Unit-2. Both units have suffered IGSCC of creviced safe ends. Additional documentation on the strong correlation of IGSCC susceptibility with actual BWR plant water chemistry history for creviced BWR components has been published (Reference 3-9).

3.1.2 IGSCC Modeling

Finally, the effect of conductivity on crack propagation has also been quantified at the GE Research and Development Center based on a "first principles" model of crack advance known as the film rupture/slip dissolution model (Reference 3-10). Predictions from the film rupture/slip dissolution model, PLEDGE (Plant Life Extension Diagnosis by GE), have been extensively compared with laboratory and field data and has provided validation of the technique. For example, PLEDGE predicts the crack growth rate in stainless steel and low alloy steel within a factor of approximately two for a 70% statistical confidence over a range in observed crack growth rate of more than six orders of magnitude. Likewise, it provides a very reasonable mean value and can accurately bound the observed crack growth rate in stainless steel piping and other components. Aside from piping predictions, PLEDGE has been successfully used for on-line crack growth monitoring data, safe ends (avoiding mid-cycle plant shutdowns), non-sensitized (stabilized) stainless steels and reactor internals such as the core shroud, top guide, access hole cover and in-core monitor housing. The PLEDGE model of IGSCC and more recently IASCC (Reference 3-11) indicates the strong effect of conductivity on crack growth rate and by inference crack initiation.

Figure 3-5 presents a schematic estimation of Unit-3 crack growth rates as a function of conductivity using PLEDGE. Crack growth rates based on actual conductivity averages for the first ten years (0.752 $\mu\text{S}/\text{cm}$) were compared to those averages for the last two

years. A value of 200 mV[SHE] was used for the electrochemical potential (ECP) in these calculations. As noted in Figure 3-5, a factor of approximately nine decrease in crack growth rate is obtained with the unit's decrease in conductivity. Thus, crack growth over the past few years has been significantly reduced by proper control of water chemistry.

3.2 Fluence Considerations

An important parameter which helps in the evaluation of the cracking mechanism is fluence. The fluence is the time integrated flux at a particular location. Shroud peak fluence was calculated by multiplying peak flux at the shroud location by the effective full power seconds of operation. The peak fluence in the Unit-3 shroud at the end of the next fuel cycle will be approximately 7.9×10^{20} n/cm² (E>1Mev). Typically, the fluence varies with shroud azimuthal location and elevation.

Although peak shroud flux may vary significantly from cycle to cycle, available flux results are generally limited to one operating cycle per plant due to substantial resource requirements for vessel flux analysis. Shroud fluence estimates were therefore calculated based on the assumption that flux remains constant throughout the life of the plant. Further evaluation would be needed to quantify the uncertainty associated with this assumption. However, the method of determining fluence is considered to be sufficient to obtain an estimate of the overall condition of the material with respect to irradiation effects. The impact of irradiation on core materials including crack growth rates has been studied and is discussed in References 3-11 and 3-12.

3.3 References

- 3-1 W.J. Shack, et al, "Environmentally Assisted Cracking in Light Water Reactors: Semiannual Report April - September 1985," NUREG/CR-4667, ANL-86-31, June 1986.
- 3-2 W.J. Shack, et al, "Environmentally Assisted Cracking in Light Water Reactors: Annual Report October 1983 - September 1984," NUREG/CR-4287, ANL-85-33, June 1985.
- 3-3 L.G. Ljungberg, D. Cubicciotti and M. Trolle, "Effects of Impurities on the IGSCC of Stainless Steel in High Temperature Water," Corrosion, Vol. 44, No. 2, February 1988.
- 3-4 W.E. Ruther, W. K. Soppet and T. F. Kassner, "Effect of Temperature and Ionic Impurities at Very Low Concentrations on Stress Corrosion Cracking of Type 304 Stainless Steel," paper 102 presented at Corrosion 85, Boston, MA, NACE, March 1985, published in Corrosion, Vol. 44, No. 11, November 1988.
- 3-5 D.A. Hale and C. G. Diehl, "Real Time Monitoring of Environmental Crack Growth in BWRs", paper 455 presented at Corrosion 88, St. Louis, MO, NACE, March 1988.
- 3-6 B.M. Gordon, Corrosion and Corrosion Control in BWRs, NEDE-30637, p. 6-22, December 1984.
- 3-7 R.B. Davis and M. E. Indig, "The Effect of Aqueous Impurities on the Stress Corrosion Cracking of Austenitic Stainless Steel in High Temperature Water," paper 128 presented at Corrosion 83, Anaheim, CA, NACE, April 1983.
- 3-8 P.L. Andresen, "A Mechanism for the Effects of Ionic Impurities on SCC of Austenitic Iron and Nickel Base Alloys in High Temperature Water," paper 101 presented at Corrosion 85, Boston, MA, NACE, March 1985
- 3-9 K.S. Brown and G. M. Gordon, "Effects of BWR Coolant Chemistry on the Propensity for IGSCC Initiation and Growth in Creviced Reactor Internals Components," paper presented at the Third Int. Symp. of Environmental Degradation of Materials in Nuclear Power Systems-Water Reactors, Traverse City, MI, August 1987, published in proceedings of same, TMS-AIME, Warrendale, PA, 1988.
- 3-10 F.P. Ford et al, "Prediction and Control of Stress Corrosion Cracking in the Sensitized Stainless Steel/Water System," paper 352 presented at Corrosion 85, Boston, MA, NACE, March 1985.

3.3 References (cont'd)

- 3-11 P.L. Andresen and F. P. Ford, "Modeling of Irradiation Effects on Stress Corrosion Cracking Growth Rates," paper 497 presented at Corrosion 89, New Orleans, LA, NACE, April 1989.
- 3-12 P.L. Andresen, F.P. Ford, and A.M. Murphy, "State of Knowledge of Radiation Effects on Environmental Cracking in Light Water Reactor Core Materials," Proceedings of the Fourth International Conference on Environmental Degradation of Materials in Nuclear Power Systems - Water Reactors, Jekyll Island, GA, August 1989, NACE, 1990

Table 3-1 Severe Water Chemistry Transients in BWRS

RANK	PLANT	MAX		MAX		DATE	COMMENTS	REFERENCE	DATA POINT
		COND. uS/cm	pH min	Cl ⁻ ppb	POW LEV				
1	AG	95.0	4.5	100	P	780307	COND DEMIN RESIN BLEEDTHROUGH	PC&RT 82LDA01	35
2	AG	88.0			P	800802	CONDENSATE DEMIN RESIN INTRUSION	EPRI NP 4134	46
3	AL	84.0	3.2	14500	P	720901	CONDENSER LEAK, DEMIN ODEPLETED	PC&RT 82LDA01	5
4	DZ	72.0		560	P	660820		PC&RT 82LDA01	1
5	AG	70.0	4.6	198	P	771116	CRUD & CONDENSATE DEMIN RESIN INTRUSION	PC&RT 82LDA01	30
6	N	54.0	3.8		P	740804	RESIN BEAD INTRUSION *	NEDE 13405	13
7	AB	40.5	3.9		P	740608	AIR/AIR RESIN MIXTURE INJECTED INTO Rx FROM RWCU	PC&RT 82LDA01	11
8	N	33.0	4.0		P	740426	RESIN BEAD INTRUSION *	NEDE 13405	10
9	AC	30.0			P	710903	HIGH CONDUCTIVITY WATER IN CST	PC&RT 82LDA01	3
10	DZ	28.5			P	661130		PC&RT 82LDA01	2
11	B	25.6	4.1	50	P	770601	RESIN INTRUSION	PC&RT 82LDA01	28
12	B	25.0		2500	p	810412	CONDENSER LEAK	PMET 81-688-45	52
13	PEACH BOTTOM 3	23.6			P	800205	POSSIBLE CONDENSATE DEMIN RESIN INTRUSION	EPRI NP 4134	80
14	DZ	23.0		3000	P	790407	LEAKAGE OF COOLING WATER INTO RPV VIA CORE SPRAY	PC&RT 82LDA01	42
15	W	23.0		30	P	730406	AIR INJECTED INTO Rx FROM RWCU	PC&RT 82LDA01	7
16	AG	22.0			P	771212	COND DEMIN RESIN INTRUSION	PC&RT 82LDA01	32
17	K	21.0	4.6	2500	P	820428	TRICHLOROETHANE FROM RADWASTE AND CST	PC&RT 82LDA01	53
18	AG	20.0	4.5		p	821004	POSSIBLE CONDENSATE DEMIN RESIN INTRUSION	EPRI NP 4134	94
19	F	17.0			P	801001	CONDENSER TUBE LEAKS	PC&RT 82LDA01	49
20	C	14.0			P	750605	RWCU OUT OF SERVICE	PC&RT 82LDA01	20
21	T	13.8	4.7	100	P	781110	ORGANIC INTRUSION VIA CONDENSATE, DECON DETER/OILS	PC&RT 82LDA01	39
22	AB	13.5			P	740925	HIGH COND WATER	PC&RT 82LDA01	14
23	AB	13.0		100	P	800428	UNKNOWN (LONG SHUTDOWN)	EPRI NP 4134	81
24	T	12.1			P	780225	RWCU RESIN INTRUSION	PC&RT 82LDA01	34
25	Q	12.0			P	750702	CONDENSER TUBE LEAK	PC&RT 82LDA01	21
26	O	12.0	4.8	50	P	761025	RWCU RESIN TRAP, RWCU INOPERABLE	PC&RT 82LDA01	25
27	T	11.8			P	800812	ORGANIC INTRUSION	EPRI NP 4134	82
28	Q	11.5	4.8	60	P	750127	RWCU RESIN INTRUSION	PC&RT 82LDA01	17
29	AB	11.3	4.7		p	830106	POSSIBLE CONDENSATE DEMIN RESIN INTRUSION	EPRI NP 4134	95
30	B	10.8	4.5	50	P	750601	RESIN FROM FLUFFING CONDENSATE DF/D	PC&RT 82LDA01	19
31	AG	10.6	4.5	100	P	730507	RWCU RESIN INTRUSION	PC&RT 82LDA01	8
32	Q	10.0			P	741208	CONDENSER LEAK	PC&RT 82LDA01	15
33	AG	10.0			p	820818	RWCU RESIN INTRUSION	EPRI NP 4134	92
34	H	9.2	7.4	57	P	780211	CONDENSATE DEMIN RESIN INTRUSION	EPRI NP 4134	74
35	B	8.2	4.3	50	P	751110	WASHOUT OF IMPURITIES FROM TURBINE	EPRI NP 4134	63
36	B	8.0	5.0	500	P	790516		PMET 81-688-45	44
37	B	7.5			p	810411	RWCU RESIN INTRUSION	EPRI NP 4134	86
38	C	7.1		100	P	811010	DECOMPOSITION OF RADWASTE RESINS DUE TO HOT WATER	EPRI NP 4134	89
39	C	6.5			P	810210	CAUSTIC INTRUSION VIA CONDENSATE STORAGE	EPRI NP 4134	84
40	K	6.2	4.8	20	P	741118	SUSPECTED RESIN INTRUSION	EPRI NP 4134	57
41	O	5.8	4.5	50	P	730812	SUSPECTED RESIN INTRUSION	EPRI NP 4134	54
42	AA	5.6			P	700123	RESIN INTRUSION WHEN C/D RETURNED TO SERVICE	JMS QC 930717	98
43	B	5.4	4.7	50	P	751218	PROBABLE RWCU RESIN INTRUSION	EPRI NP 4134	64
44	B	5.1			p	810220	ORGANIC INTRUSION VIA RADWASTE	EPRI NP 4134	85
45	H	5.1		68	P	770727	CONDENSATE DEMIN RESIN INTRUSION, ANION RICH	EPRI NP 4134	70
46	O	5.1	4.8	50	P	760806	CONDENSATE DEMIN RESIN INTRUSION	EPRI NP 4134	67

Table 3-1 Severe Water Chemistry Transients in BWRS

RANK	PLANT	MAX		MAX		DATE	COMMENTS	10/07/93	DATA POINT
		COND. $\mu\text{S}/\text{cm}$	pH min	Cl. ppb	POW LEV			REFERENCE	
47	C	5.0		100	P	750309	POSSIBLE CONDENSATE DEMIN RESIN INTRUSION	EPRI NP 4134	79
48	Q	4.9	4.9	50	P	760522	SUSPECTED RESIN INTRUSION	EPRI NP 4134	66
49	T	4.5	5.0	50	P	781227	ORGANIC INTRUSION VIA CONDENSATE SYSTEM	EPRI NP 4134	77
50	Q	4.3	4.9	48	P	760221	SUSPECTED RESIN INTRUSION	EPRI NP 4134	65
51	K	4.1	5.1	80	P	741015	RWCU RESIN INTRUSION	EPRI NP 4134	56
52	AL	3.3	5.4	50	P	770126	IMPROPER RINSE OF CONDENSATE DEMIN	EPRI NP 4134	68
53	C	3.3	5.2	38	P	750309	POSSIBLE RESIN INTRUSION	EPRI NP 4134	59
54	B	3.2			P	810715	RWCU RESIN INTRUSION	EPRI NP 4134	88
55	S	3.2	4.7	495	P	780131	RESIN INTRUSION	EPRI NP 4134	73
56	H	3.0	5.6	96	P	750902	SUSPECTED RESIN INTRUSION	EPRI NP 4134	61
57	B	2.9	5.4	50	P	751126	PROBABLE RWCU RESIN INTRUSION	EPRI NP 4134	62
58	T	2.8	5.2	65	P	770912	IMPROPER RINSE OF CONDENSATE DEMIN	EPRI NP 4134	71
59	B	2.7	7.6		P	750626	RESIN INTRUSION	EPRI NP 4134	60
60	T	2.3			P	800824	ORGANIC INTRUSION	EPRI NP 4134	83
61	T	2.2	5.5	50	P	790108	SUSPECTED ORGANICS IN CONDENSATE STORAGE	EPRI NP 4134	78
62	Y	1.8	5.4	355	P	781208	CONDENSATE DEMIN RESIN INTRUSION	EPRI NP 4134	76
63	AC	1.4	5.6	83	P	741125	VALVING ERROR DURING RESIN TRANSFER	EPRI NP 4134	58
64	H	1.4	8.1	38	P	780112	CONDENSATE DEMIN RESIN INTRUSION	EPRI NP 4134	72
65	AJ	1.4			P	750906	SUSPECTED FLOC/FILTER AID/SURFACT FROM RAD WASTE	JMS QC 930717	99
66	Q	1.1	5.6	30	P	770225	SUSPECTED RESIN INTRUSION	EPRI NP 4134	69
67	H	1.1	8.8	72	P	780511	CONDENSATE DEMIN RESIN INTRUSION	EPRI NP 4134	75
68	W	1.0			P	811030	GLYCOL INTRUSION VIA RADWASTE	EPRI NP 4134	90
69	PEACH BOTTOM 2	1.0			P	810622	OIL INTRUSION INTO HOTWELL	EPRI NP 4134	87
70	AS			725	P	711113	HIGH FEEDWATER CONDUCTIVITY	PC&RT 82LDA01	4
71	B			54L	P	780129		PC&RT 82LDA01	33
72	B			1200	P	760708	CONDENSATE SYSTEM MOMENTARILY BYPASSED	PC&RT 82LDA01	24
73	AR			600	P	750103	RWCU OUT OF SERVICE	PC&RT 82LDA01	16
74	B	641.0	3.5	87000	S	7904	COOLING WATER INGRESS FROM RHR, RPV H2O TO HOTWELL	PC&RT 82LDA01	43
75	B	423.0	3.2		S	740801	ACID INTO RPV FROM DEMIN STORAGE TANK	PC&RT 82LDA01	12
76	H	140.0			S	760519		PC&RT 82LDA01	22
77	T	45.9	3.8	244	S	761103	TORUS WATER PUMPED INTO RPV PRIOR TO STARTUP	PC&RT 82LDA01	26
78	B	13.3		1800	S	760520		PC&RT 82LDA01	23
79	A	13.0			S	780801	LEAK IN RHR HEAT EXCHANGER	PC&RT 82LDA01	36
80	B	12.9			S	770917	RWCU OUT OF SERVICE	PC&RT 82LDA01	29
81	T	12.1			S	800815		PC&RT 82LDA01	47
82	AL	11.6			S	730603	RWCU OUT OF SERVICE	PC&RT 82LDA01	9
83	B	11.2			S	800822		PC&RT 82LDA01	48
84	O	11.2			S	801219		PC&RT 82LDA01	51
85	F	10.5			S	820427	POSSIBLE ORGANIC INTRUSION	EPRI NP 4134	91
86	B	10.5	5.6	140	S	780923	RWCU RESIN INTRUSION	EPRI NP 4134	37
87	H	10.3			S	750405	RWCU OUT OF SERVICE	PC&RT 82LDA01	18
88	AS	10.0		730	S	720804	DEPLETED RWCU DEMIN	PC&RT 82LDA01	5
89	Q	5.0	5.5	60	S	740829	CONDENSATE DEMIN RESIN INTRUSION	EPRI NP 4134	55
90	AX	4.5	5.2	220	S	830505	ORGANIC INTRUSION VIA RADWASTE	EPRI NP 4134	97
91	B	4.2	5.3	600	S	781110	ORGANIC INTRUSION VIA CONDENSATE, DECOM DETER/OILS	PC&RT 82LDA01	38
92	AP	1.0			S	820900	GLYCOL INTRUSION VIA RADWASTE	EPRI NP 4134	93

Table 3-1 Severe Water Chemistry Transients in BWRS

RANK	PLANT	MAX		MAX		POW	DATE	COMMENTS	10/07/93	DATA
		COND.	pH.	Cl.	ppb				LEV	
		uS/cm	min							
93	F			700	S	800305				
94	T			1300	S	790329	CONDENSER LEAK, CONDENSATE BYPASSED, RWCU OUT	PC&RT 82LDA01	45	
95	O			500	S	801017		PC&RT 82LDA01	41	
96	AC			683	S	770309		PC&RT 82LDA01	50	
97	K				S	830213	GLYCOL INTO RADWASTE, DETECTED PRIOR TO COND STOR	PC&RT 82LDA01	27	
98	T			1200	S	790316	CONDENSER LEAK, CONDENSATE DEPLETED, Cl INTO CST	EPRI NP 4134	96	
99	B			800	S	771206	RWCU OUT OF SERVICE	PC&RT 82LDA01	40	
								PC&RT 82LDA01	31	

NOTE: BWRS RANKED IN THE FOLLOWING ORDER:

1. POWER (P) OR SHUTDOWN (S)
2. CONDUCTIVITY

OTHER NOTES: * = RESIN BEADS PROVIDE LONG TERM LOW pH

Arithmetic Mean Conductivity Peach Bottom 3

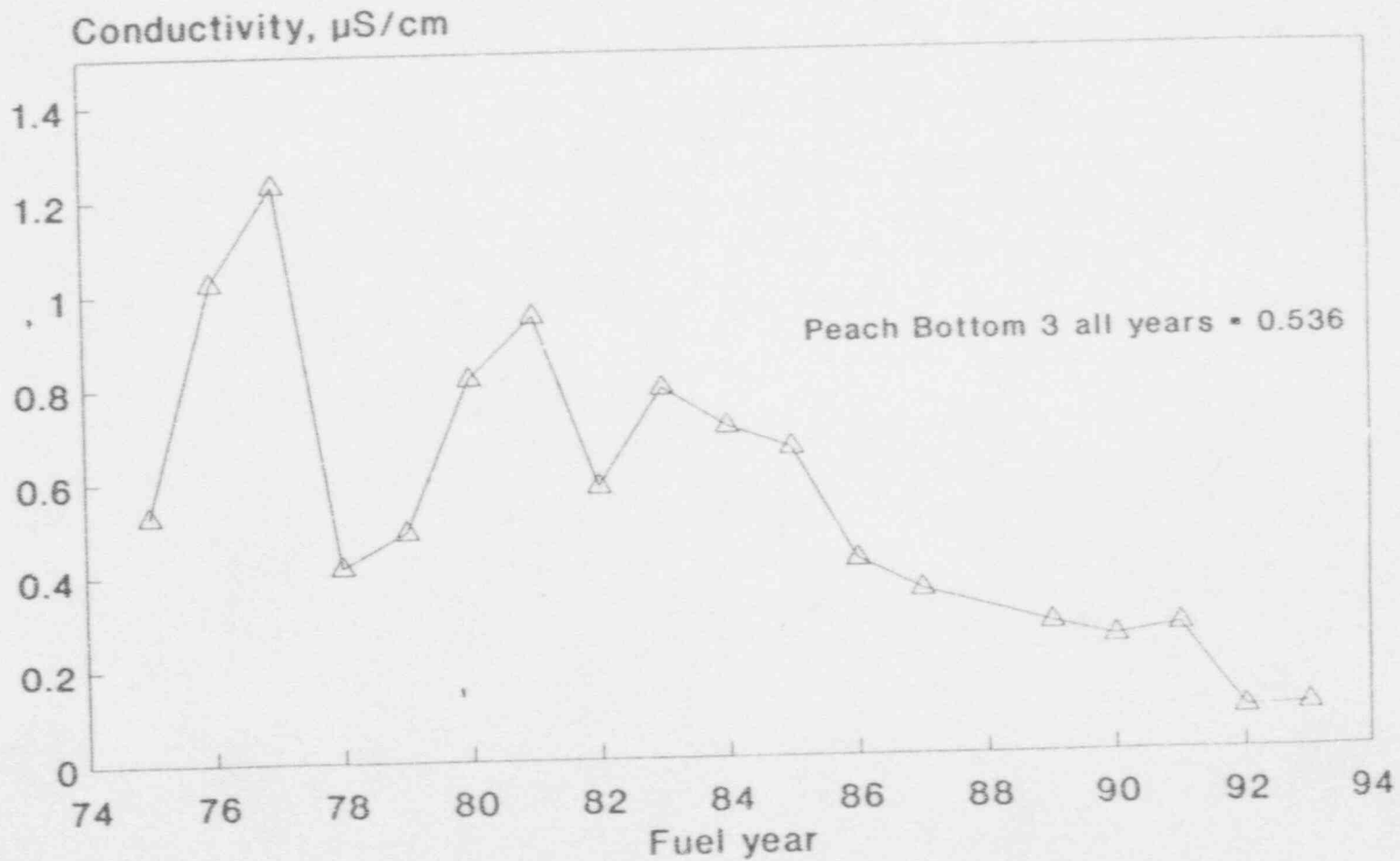
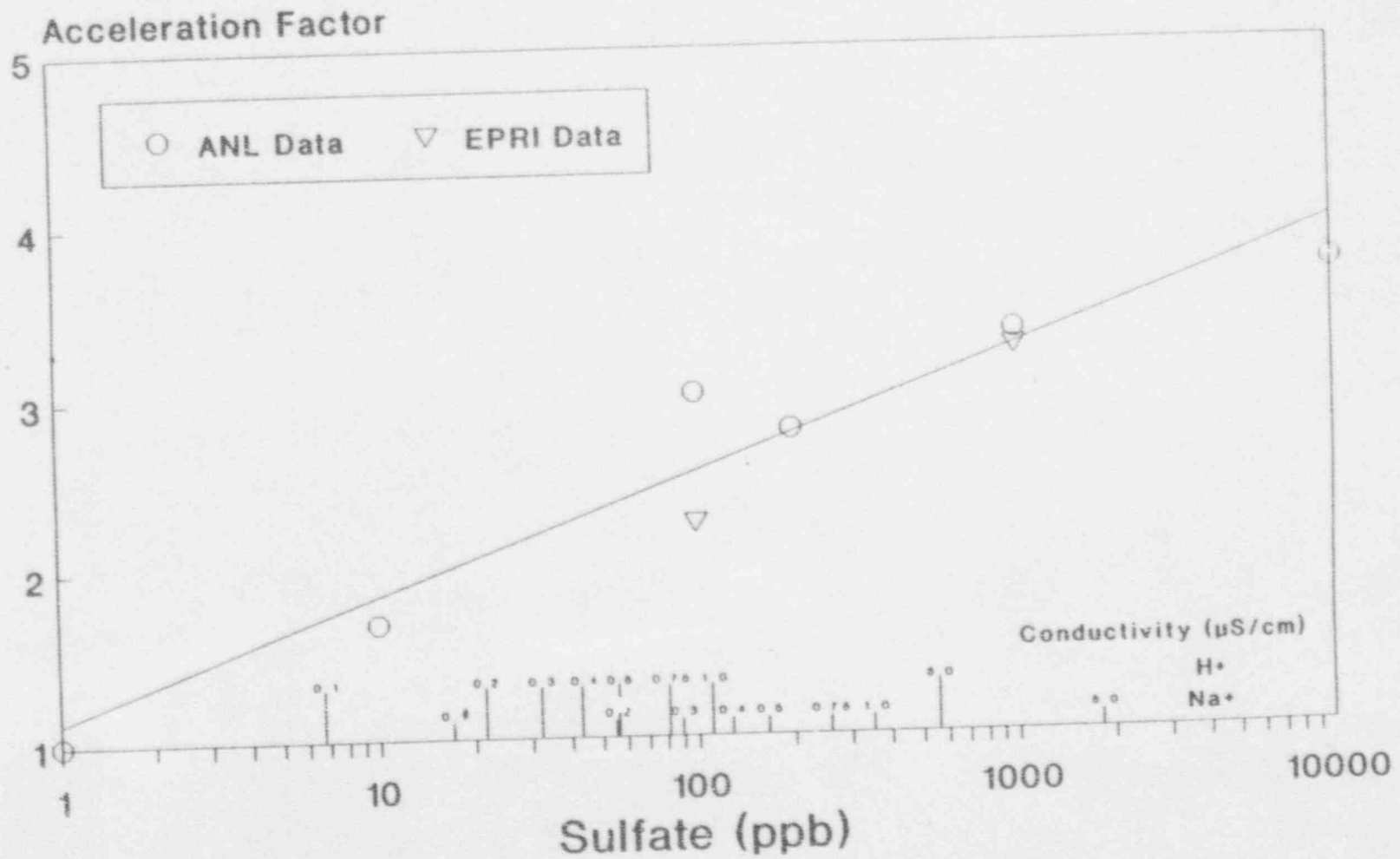


Figure 3-1 Peach Bottom 3 Arithmetic Mean Conductivity

Effect of Concentration and Conductivity on IGSCC Initiation - FS Type 304



Crack initiation data based on CERT

Figure 3-2 Effect of Concentration and Conductivity on IGSCC Initiation FS Type 304

Peach Bottom 3 Response to June 1986 Water Chemistry Transient

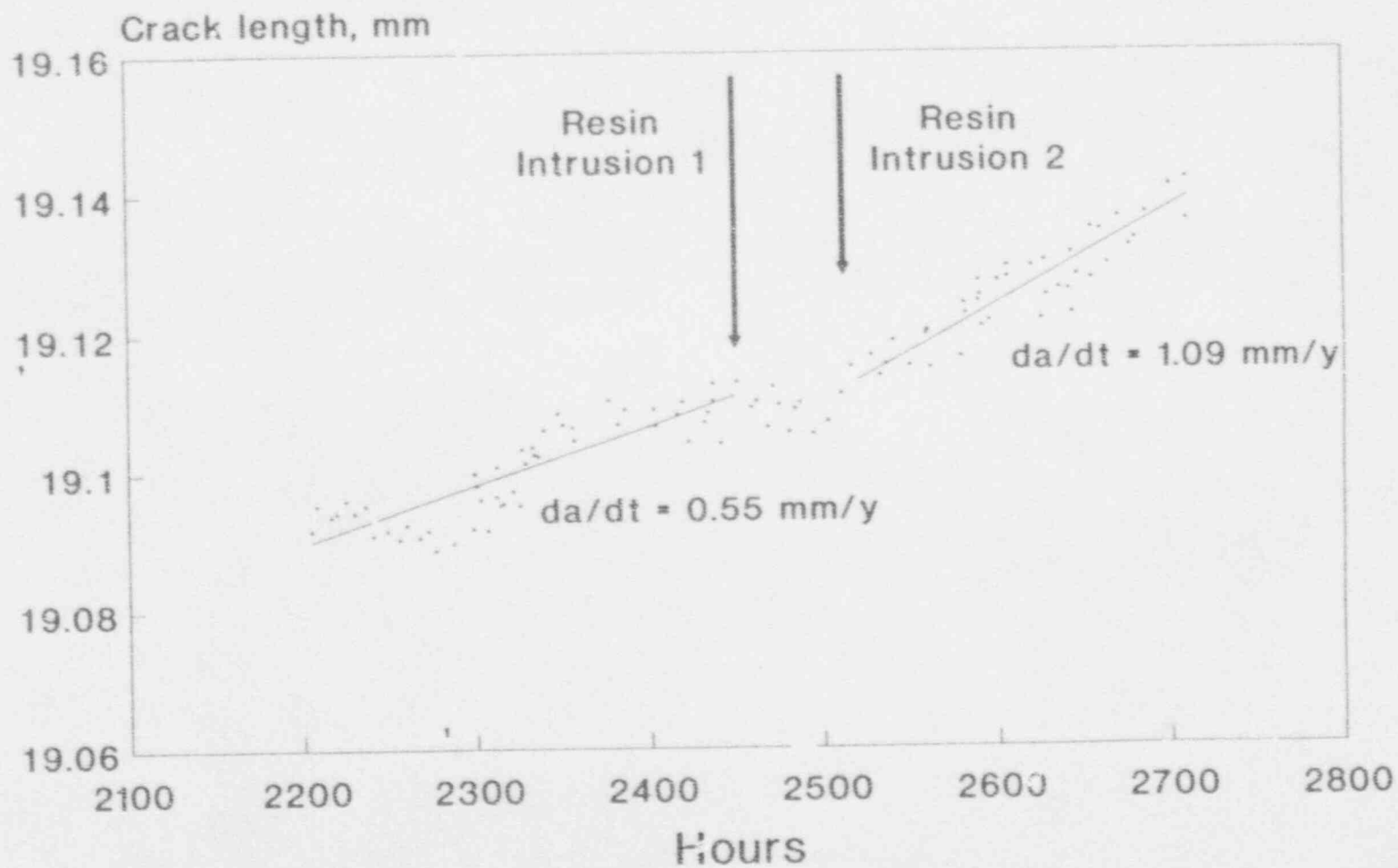


Figure 3-3 Peach Bottom 3 Response to June 1986 Water Chemistry Transient

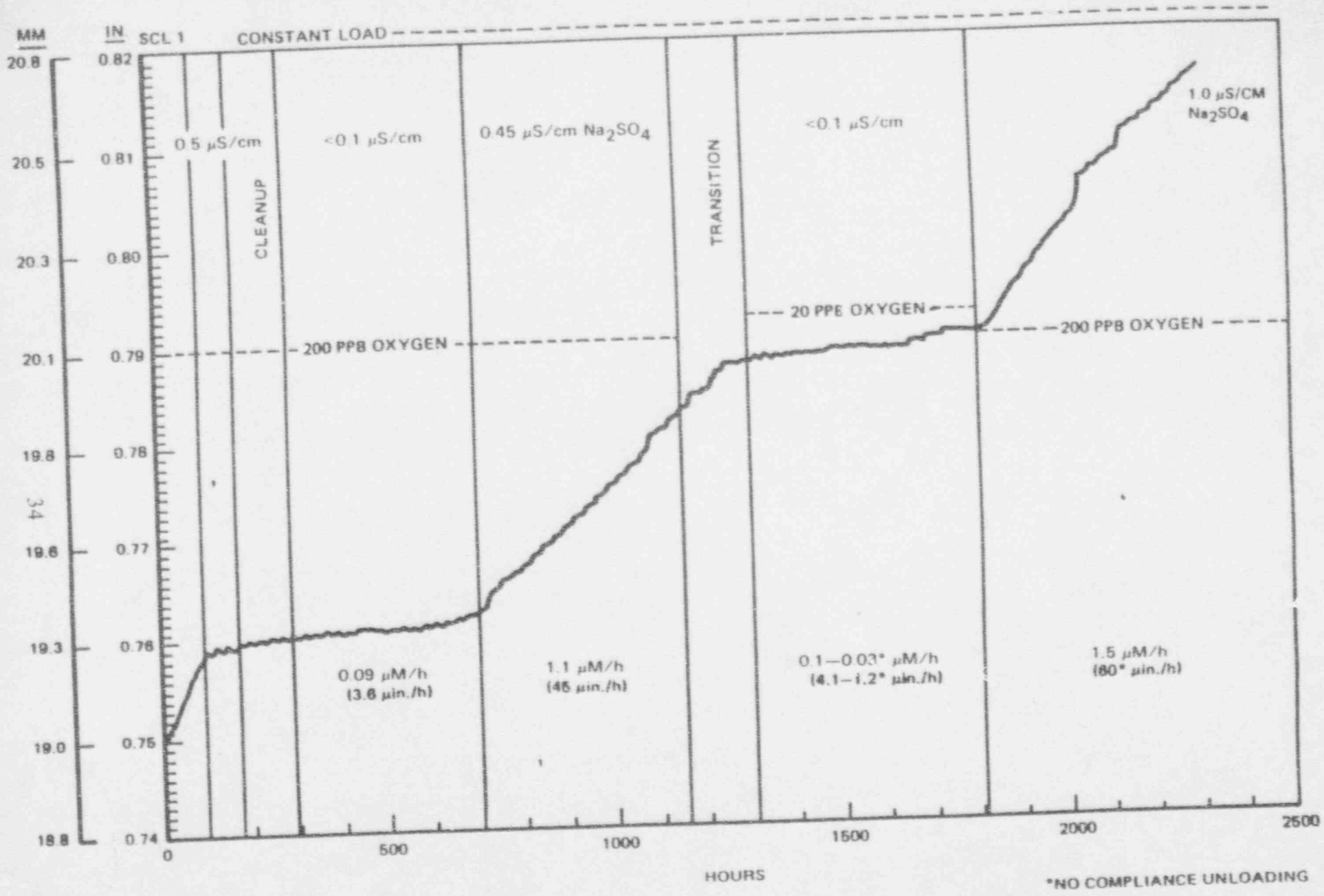
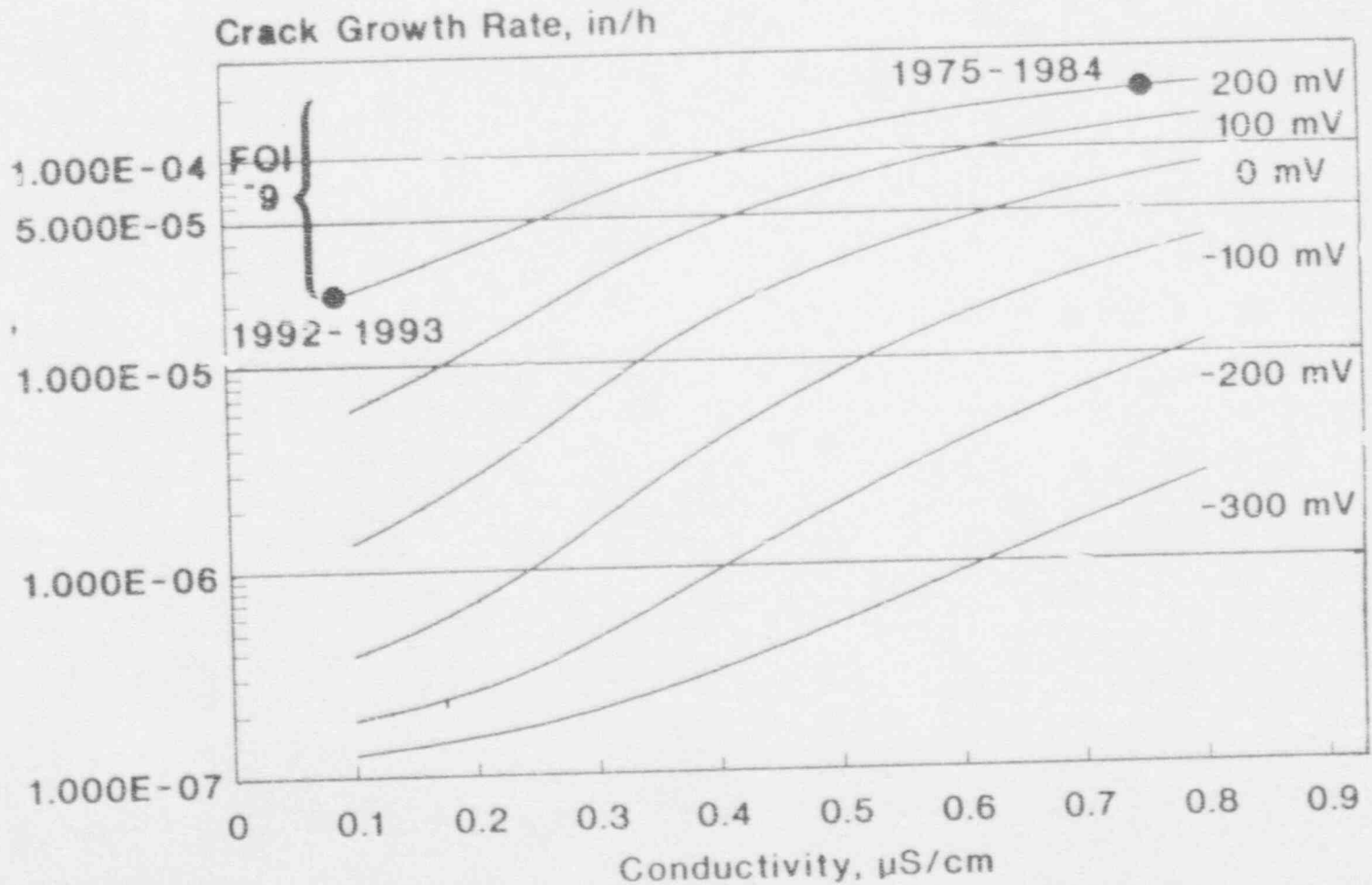


Figure 3-4 Crack Length Versus Time, Sensitized Type-304 Stainless Steel 286°C Oxygenated Water Environment, $K = 28.6-30.5 \text{ MPa}\sqrt{\text{m}}$ (26-28 ksi $\sqrt{\text{in}}$)

*NO COMPLIANCE UNLOADING

GENE PLEDGE Model Prediction for PB-3 Sensitized Type 304 Crack Growth Rate



PLEDGE: 15 C/cm², 20ksi $\sqrt{\text{in}}$

Figure 3-5 GENE Pledge Model Prediction for Peach Bottom 3 Type 304 Crack Growth

35

4.0 IN-VESSEL VISUAL INSPECTION

This section summarizes the IVVI results of the Peach Bottom Unit-3 core shroud. IVVI of welds H1 through H8 were performed during this outage. The IVVI included both inside surface and outside surface examination. Figures 1-2 shows the indications associated with the H3 and H4 welds. Only a few short indications were observed on the outside surface of H1 and H4. Circumferential indications were observed on the inside surface associated with vertical weld V3 (See Figure 1-2). It should also be noted that the area adjacent to the H9 weld was visually inspected as part of access hole cover (AHC) inspection at this outage. The inspection did not reveal any indications. The H9 weld in the vicinity of the access hole cover is considered a higher stressed location and therefore these IVVI results are considered to provide a reasonable assessment of the overall condition of the entire H9 weld.

All indications associated with the H3 weld inside surface were in the HAZ of the shroud cylinder. No indications were found in the ring. The indications near H3 were all circumferentially oriented. As can be seen in Figure 1-2, most of the indication length is located between the azimuth of 146° and 360°.

The indications observed at the H4 inside surface HAZ were a mixture of circumferential and axial indications as shown in Figure 1-2.

Circumferential indications were observed emanating from the V3 weld on the inside surface. Eight indications were observed grouped together with a spacing of approximately 2" between indications. All other IVVI vertical scans found no indications.

On the outside surface a limited number of short indications were observed associated with H1 and H4.

Table 4-1 is the IVVI plan which indicates the original planned inspections. Due to the observation of indications at H3 and H4, the inspection scope was expanded and is also described in Table 4-1. A summary of the IVVI results is shown in Table 4-2. See Figure 1-2, 1-3 and 1-4 for further details.

Table 4-1

Peach Bottom Unit 3 Core Shroud Exam Plan (3R09)

ORIGINAL PLAN (Prior to issuance of SIL 572)

1. Perform sample examination "ID" at (8) cell locations of the "H3" and "H4" welds.
2. Perform sample examination "OD" at (8) locations in the high flux areas at welds "H1", "H2", and "H5"

EXPANDED PLAN (Following identification of indications on the "H3" and "H4")

1. Perform 100% examination of the "H3" and "H4" welds from the ID.
2. Perform 100% examination of accessible areas of the "H4" weld from the OD.
3. Perform examinations of the "H3" weld, "OD", where cracks were not identified from the "ID"
4. Perform an examination of the "H3" weld "OD", including significant corresponding areas of cracking identified on "ID".
5. Perform a sample examination on the "OD", at (8) locations of the "H6" weld.
6. Perform a sample examination of the "OD" at (2) locations of the "H7" and "H8" welds
7. Perform an examination of (1) vertical weld between the "H3" and "H4" weld.
8. Perform a sample examination of the plate to include:
 - (1) 8" area at the vertical weld.
 - (1) 8" area between "H3" and "H4" welds.
 - (1) 2" area between "H3" and "H4" welds.

NOTE: Consideration was given to high neutron flux, stress, and repair areas for selection of the sample locations

Table 4-2
Summary of IVVI Indications

Weld	Inside Surface Indications	Outside Surface Indications
H1	N/A	1 short vertical
H2	N/A	None
H3	Circumferential in Shroud Cylinder HAZ	None
H4	Circumferential and Axial	2 short vertical
H5	N/A	None
H6	N/A	None
H7	N/A	None
H8	N/A	None
V3	8 short circumferential	N/A
PLATE	None	N/A

5.0 FLAW EVALUATION

This section provides the flaw evaluation and application of the screening criteria to the Peach Bottom Unit-3 indications. Included in this section is the structural analysis, allowable flaw size determination, and screening criteria.

5.1 Structural Analysis

This section describes the details and the results of the structural analysis performed to determine the allowable flaw lengths. The structural analysis consists of two steps: the determination of axial and circumferential stress magnitudes in the shroud, and the calculation of the allowable flaw lengths. Both the fracture mechanics (LEFM) and limit load methods are used in the calculation of allowable flaw lengths.

5.1.1 Applied Loads and Calculated Stresses

The applied loads on the shroud consist of internal differential pressure, weight and seismic. The seismic loads consist of a horizontal shear force at the top of the shroud and an overturning bending moment. The shear force produces a shear stress of insignificant magnitude, and is not considered. The bending moment stress at a shroud cross-section varies as a function of its vertical distance from the top of the shroud. Because of the inherent ductility of the material, residual stresses and other secondary stresses do not affect structural margin. Thus, they need not be considered in the analysis.

The magnitudes of the applied loads were obtained from the seismic stress analysis and system information reports. The nominal shroud radius and thickness (2.0 in.) were used to calculate the stresses from the applied loads. The stresses are essentially based on the strength of materials formulas. Since the bending stress due to seismic shear force varies with the elevation of a location, two conservative values of this stress were calculated: one applicable to shroud sections above the core plate (H1, H2, H3, H4, and H5) and the other for sections below the core plate (H6, H7 and H8). Figure 5-1 shows the weld designation and relative locations in the shroud.

Table 5-1 shows the calculated seismic stress magnitudes for both the upset (Design Earthquake - DE) and faulted conditions (Maximum Credible Earthquake - MCE). The appropriate pressure differences for the upset and faulted conditions are shown in Table 5-2.

Table 5-1 Seismic Axial Stresses at Shroud Welds

Weld Designation	MCE Moment (ft-kips)	Stress (ksi)	
		MCE	DE
H1	1104.7	0.18	0.08
H2	1438.6	0.23	0.11
H3	1479.1	0.27	0.13
H4	2995.8	0.54	0.24
H5	4583.8	0.83	0.37
H6	4679.7	0.90	0.40
H7	5697.6	1.10	0.49
H8	6749.7	1.30	0.58

Table 5-2 Pressure Differences

Component	Pressure Differences (psi)	
	Faulted Condition	Upset Condition
Shroud Head and Upper Shroud	32.9	14.12
Core Plate Support Ring and Lower Shroud	54.8	35.68

The structural analysis for the indications uses two methods; linear elastic fracture mechanics (LEFM) and limit load analysis. Both the limit load and the LEFM methods were used in determining the allowable flaw sizes in the shroud. Since the limit load is concerned with the gross failure of the section, the allowable flaw length based on this approach may be used for comparison with the sum of the lengths of all the flaws at a cross-section. On the other hand, the LEFM approach considers the flaw tip fracture toughness and thus, the allowable flaw length based on this approach may be used for comparison with the largest effective flaw length at a cross-section. The technical approach for the two methods is described below.

5.1.2 Fracture Mechanics Analysis

The shroud material (austenitic stainless steel) is inherently ductile and it can be argued that the structural integrity analysis can be performed entirely on the basis of limit load. In fact, J-R curve measurements (Figure 5-2) made on a core shroud sample taken from an overseas plant having higher fluence (8×10^{20} n/cm²) showed stable crack extension and ductile failure. The ASME Code recognizes this fact in using only limit load techniques in Section XI, Subsubarticle IWB-3640 analysis. Nevertheless, a conservative fracture mechanics evaluation was performed using an equivalent K_{jC} corresponding to the material J_{IC} . The K_{jC} for the overseas plant shroud was approximately 150 ksi $\sqrt{\text{in}}$. Use of this equivalence is conservative since:

- i) The calculated fluence for Peach Bottom Unit-3 is lower than that for the overseas plant from which J-R curves were obtained.
- ii) The J-R curves show J_{max} values well above the J_{IC} , confirming that there is load capability well beyond crack initiation (See Figure 5-2).

Using the ASME Code safety factor of 3, which is applicable for normal and upset conditions of pressure boundary components, the allowable K_{IC} value becomes 50 ksi $\sqrt{\text{in}}$. For faulted conditions the allowable K_{IC} is 107 ksi $\sqrt{\text{in}}$ using the ASME Code safety factor of $\sqrt{2}$. For the analysis presented here, the LFM analysis is confined to the H4 weld and above. The fluence corresponding to welds at and below the core plate elevation is an order of magnitude lower and the associated fracture toughness is comparable to that of the unirradiated material. For those locations, limit load analysis is used.

An additional consideration that applies only to the fracture mechanics analysis is the question, "When is a flaw independent of an adjacent flaw?". The ASME Code proximity rule considers how flaws can link up and become a single flaw as a result of proximity. However, even when two flaws are separated by a ligament that exceeds the criterion, they may not be considered totally independent of each other. That is, the flaw tip stress intensity factor may be affected by the presence of the adjacent flaw. This can be accounted for by using the finite width correction factor for a flaw in a finite plate. For a through-wall flaw in an "infinite" plate, the stress intensity factor is:

$$K = \sigma\sqrt{\pi a}$$

For a finite plate, the K value is higher as determined by the finite width correction factor, F. In this screening evaluation it is assumed that the plate is "infinite" if the correction factor F is less than 1.1. As seen in Figure 5-3, if the width of the plate exceeds 2.5L (or a/b less than 0.4), then there would be no interaction due to plate end edge effects. If this same condition is applied to two neighboring flaws, then there will be no interaction between the two indications if the tips are at least $0.75(L_1+L_2)$ apart. If the distance between indications is greater than $0.75(L_1+L_2)$, then they are considered as two separate flaws. However, if they are closer, for the purpose of fracture analysis, the equivalent flaw length is the sum of the two individual flaws.

5.1.3 Limit Load Analysis

A through-wall circumferential flaw was assumed in this calculation. Limit load calculations were conducted using the approach outlined in Subsubarticle IWB-3640 and Appendix C of Section XI of the ASME Code. The flow stress was taken as $3S_m$. The S_m value for the shroud material (Type 304 stainless steel) is 16.9 ksi at the normal operating temperature of 550°F.

Safety factors similar to that used in the ASME Code (2.8 for normal and upset and 1.4 for emergency and faulted) were used in the analysis. The highest seismic stress was used for the limit load calculations and is shown in Table 5-1. Similarly, the highest axial pressure stress corresponding to the lower shroud was used. Thus, the analytical results are applicable for all welds since limiting values are used.

5.2 Allowable Through-Wall Flaws

Allowable through-wall flaw sizes were determined using both fracture mechanics and limit load techniques for both circumferential and axial flaws. It should be emphasized that the allowable through-wall flaws are based on many conservative assumptions and are intended for use only in the screening criteria. More detailed analysis can be performed to justify larger flaws (both through-wall or part through when measured flaw depths are available). However, since the intent of the screening criteria is to determine when additional evaluation or NDE characterization is needed, a conservative bounding approach is utilized.

5.2.1 Allowable Through-Wall Circumferential Flaw Size

Both the LEFM and limit load methods were used to evaluate the allowable through-wall flaws. Above the core plate, LEFM and limit load analysis methods were used. Since this is a screening criteria, single allowable flaw size criteria (limiting location) was used for all weld locations. It should be noted that the H7 and H8 welds involve Alloy 600 which has higher S_m values and therefore has higher limit load capability.

Fracture Mechanics Analysis

The total axial pressure and seismic stress corresponding to the upset condition is 0.61 ksi, and 1.39 ksi for the faulted condition. Using the ASME Code safety factors for fracture analysis, the faulted condition is limiting.

To determine the allowable flaw size based on LEFM methods, the conservatively estimated irradiated material fracture toughness K_{Ic} value of 150 ksi $\sqrt{\text{in}}$ was used. Applying a safety factor of 1.4 for the faulted condition, the allowable K_I of 107 ksi $\sqrt{\text{in}}$ was obtained. The allowable flaw size was calculated using the following equation:

$$K_I = G_m * \sigma * \sqrt{(\pi a)}$$

where G_m is a curvature correction factor as defined in Figure 5-4 (Reference 5-1), σ is the axial stress, and 'a' is the half flaw length. The allowable through-wall circumferential flaw length (2a) was determined as \cong 344 inches.

Limit Load Analysis

A through-wall circumferential flaw was assumed in this calculation. The limit load calculations were conducted using the approach outlined in Subsubarticle IWB-3640 and Appendix C of Section XI of the ASME Code. The flow stress was taken as $3S_m$. The S_m value for the shroud material is 16.9 ksi at the normal operating temperature of 550°F.

The stresses for the limit load analysis for the upset condition consisted of an axial force stress of 0.71 ksi, and a bending moment stress of 0.49 ksi.

Similarly for the faulted condition, the axial force stress was 1.21 ksi, and the bending moment stress was 1.1 ksi. The allowable flaw length was approximately 430 in. including the ASME Code, Section XI safety factors.

5.2.2 Allowable Through-Wall Axial Flaw Size

Fracture Mechanics Analysis

The allowable axial flaw size is governed entirely by the pressure hoop stress. Similar to the circumferential flaw case, the allowable axial flaw size was determined assuming a through-wall flaw. For a through-wall flaw of length $2a$ in the shroud, the applied stress intensity factor is given by:

$$K = M * \sigma_h * \sqrt{(\pi a)}$$

where M is the curvature correction factor. M is given by:

$$M = G_m + G_b \quad (\text{Figure 5-5, from Reference 5-1})$$

In the above expression, the allowable flaw length, $2a$, can be determined by equating the calculated K to the fracture toughness divided by the safety factor of 3. The hoop stress is 1.85 ksi and the allowable $K = 150/3$ (where 150 ksi $\sqrt{\text{in}}$ represents a conservative estimate of the material toughness and 3 is the safety factor).

The allowable flaw length was conservatively determined to be $2a = 59$ in.



Limit Load

An alternate approach to determining the allowable flaw size is to use limit load techniques. The allowable flaw length is given by the equation:

$$\sigma_h = \sigma_f / (M_1 * SF)$$

where M_1 is a curvature correction factor (which is a function of the flaw length (Reference 5-2)), $\sigma_f = 3S_m$ is the flow stress, SF is the safety factor of 2.8 for upset conditions, and σ_h = the hoop stress corresponding to the upset ΔP of 35.68 psi. The allowable flaw length based on the limit analysis is 200 in. which exceeds that determined by LEFM. Thus, the allowable axial through-wall flaw length is 59 in.

5.3 Screening Criteria

The determination of the allowable through-wall flaws has been described in Section 5.2. The objective was to use the allowable flaw size as the basis for the screening criteria. Since the screening rules represent the first step in the evaluation, they are by definition conservative. If the criteria are exceeded, the option of doing further detailed evaluation or performing additional NDE remains. The effective flaw lengths ($L_{1\text{eff}}$, $L_{2\text{eff}}$, etc.) determined by combining indications using the proximity and interaction rules, are used in the comparison with the allowable flaw sizes. The determination of effective flaw sizes are discussed in detail in Appendix A. The allowable through-wall flaws were:

- Circumferential Flaws
 - 344 in. using LEFM
 - 430 in. using limit load

- Axial Flaws
 - 59 in. using LEFM
 - 200 in. using limit load

A conservative approach in developing the screening rule is to include both the LEFM and limit load analysis. For axial flaws, the allowable flaw length based on the LEFM controls, and the screening limit is 59 in.

For circumferential flaws the fracture mechanics based limit for a single flaw is 344 in. This in itself is not sufficient since there could be several flaws (each less than 344 in.) in a circumferential plane that cumulatively add up to greater than 430 in. (the allowable circumferential flaw size based on limit load analysis). Thus, the cumulative flaw length should be less than 430 inches. While this fully assures the ASME Code margins, an additional conservatism is included in the screening. **This states that the cumulative flaw length cannot be more than $430/4 = 107.5$ in. in any 90 degree sector of the shroud.** This is a conservative restriction that assures that long continuous flaws are not admissible. With the provision that the cumulative flaw length cannot exceed 107.5 in. in any 90° sector of the shroud, this criterion becomes more limiting than the fracture mechanics limit of 344 in. The approach used here for the 107.5 inch limit for circumferential flaws is to assume a template with a moving window equal to the 90° sector. The cumulative length of flaws that appear in the window should be less than

107.5 in. A similar restriction based on limit loads is not needed for axial flaws since they are associated only with circumferential welds and are unlikely to be aligned in the same plane.

The removal or reduction of the factor of 4 is justified if the IVVI results indicate that the remaining ligament is spread around the circumference of the shroud circumference. Evaluation of the IVVI results indicate that this is the case for the Peach Bottom Unit 3 shroud (See Figure 1-2 and 1-3).

It should be noted that when considering LEFM based evaluations, the crack interaction criteria described in Appendix A, must be applied in comparing against the allowable lengths. For example, the adjacent flaws where the spacing S is less than $0.75 (L_{1\text{eff}} + L_{2\text{eff}})$, the length $L = L_{1\text{eff}} + L_{2\text{eff}}$ is used for comparison with the LEFM based allowable flaw length.



5.4 Summary of Screening Criteria

The screening criteria is schematically shown in Figure 5-6. The first step is to map the flaw indications observed by IVVI. Next the proximity rules are applied to the flaw map to develop effective flaw lengths (Appendix A provides the details for determining effective lengths). The results of the effective flaw lengths are also mapped.

For axial flaws located in a vertical plane, two neighboring flaws must be summed if $S < 0.75(L1_{eff} + L2_{eff})$. If the longest resulting flaw is less than 59 inches, then the screening limit is met for axial flaws.

For circumferential flaws, all flaws are summed in any 90° sector using a template. The total flaw length in the 90° window must be less than 107.5 inches to meet the screening criteria. The next step is the LEFM based comparison using the interaction criteria. If $S < 0.75(L1_{eff} + L2_{eff})$, then the length $L = L1_{eff} + L2_{eff}$ should be compared with the LEFM limit of 344 in for circumferential flaws.

If significant ligament remains around the shroud circumference, the factor of 4 may be removed or reduced. The application of this factor would be considered conservative since the presence of the ligament around the circumference assures that extremely long indications are not present. The removal or reduction of the factor of 4 would be considered as part of the "Further Evaluation" box in Figure 5-6.



5.5 Application of Screening Criteria

The screening criteria was used to evaluate the indications found by IVVI. The structural integrity of the core shroud is assured if the screening criteria are met for all of the indications.

All axial effective indication lengths are significantly less than the allowable flaw size based either on LEFM or limit load methods. Thus the axial indications seen by IVVI are acceptable per the screening criteria developed for Unit-3.

The effective indication lengths were determined for all of the circumferential indications as shown in Figure 1-2. The calculation took into consideration the detailed geometric information such as each indications length, the azimuth of each crack tip and the spacing between indication planes in order to properly determine the effective length.

The resulting effective indication lengths were then compared against the allowable indication length. Since all effective indication lengths satisfy the screening criteria, the structural integrity of the Unit-3 shroud is assured for the next two year cycle with power rerate conditions.

As mentioned in Section 5.3, for the indications observed in the Peach Bottom Unit 3 shroud, it is justified to remove or reduce the factor of 4 when determining the allowable throughwall circumferential flaw length. Again, this is justified since there was remaining ligament spread around the entire shroud circumference. If this is done, the observed indications, and resulting effective flaw lengths are well below the allowable throughwall circumferential flaw lengths. It should be noted that the limiting allowable throughwall circumferential flaw is now governed by the LEFM method and not the limit load method.



5.6 References

- 5-1. Rooke, D.P. and Cartwright, D.J., "Compendium of Stress Intensity Factors," The Hillingdon Press (1976).
- 5-2. Ranganath, S., Mehta, H.S. and Norris, D.M., "Structural Evaluation of Flaws in Power Plant Piping," ASME PVP Volume No. 94 (1984).

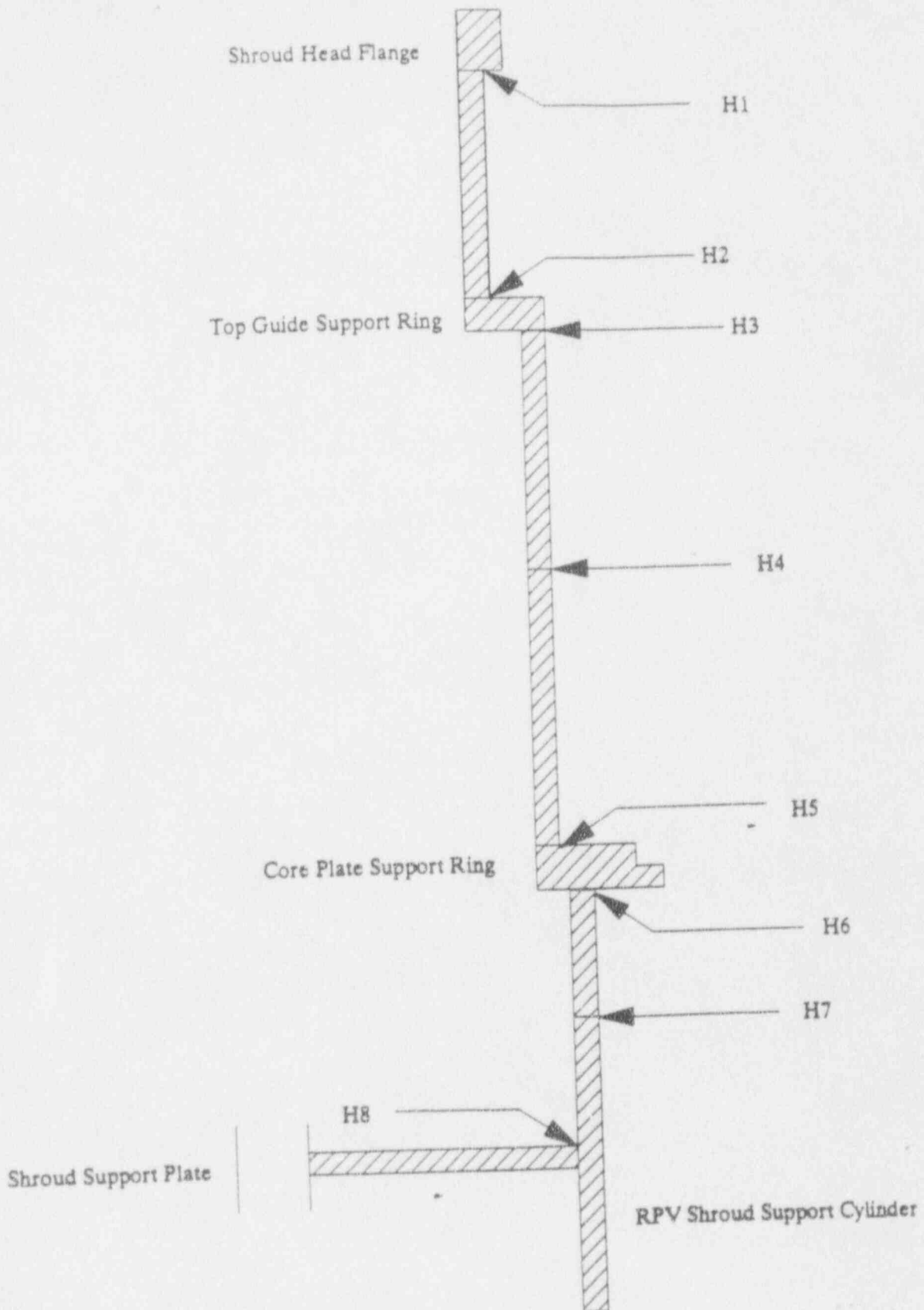


Figure 5-1

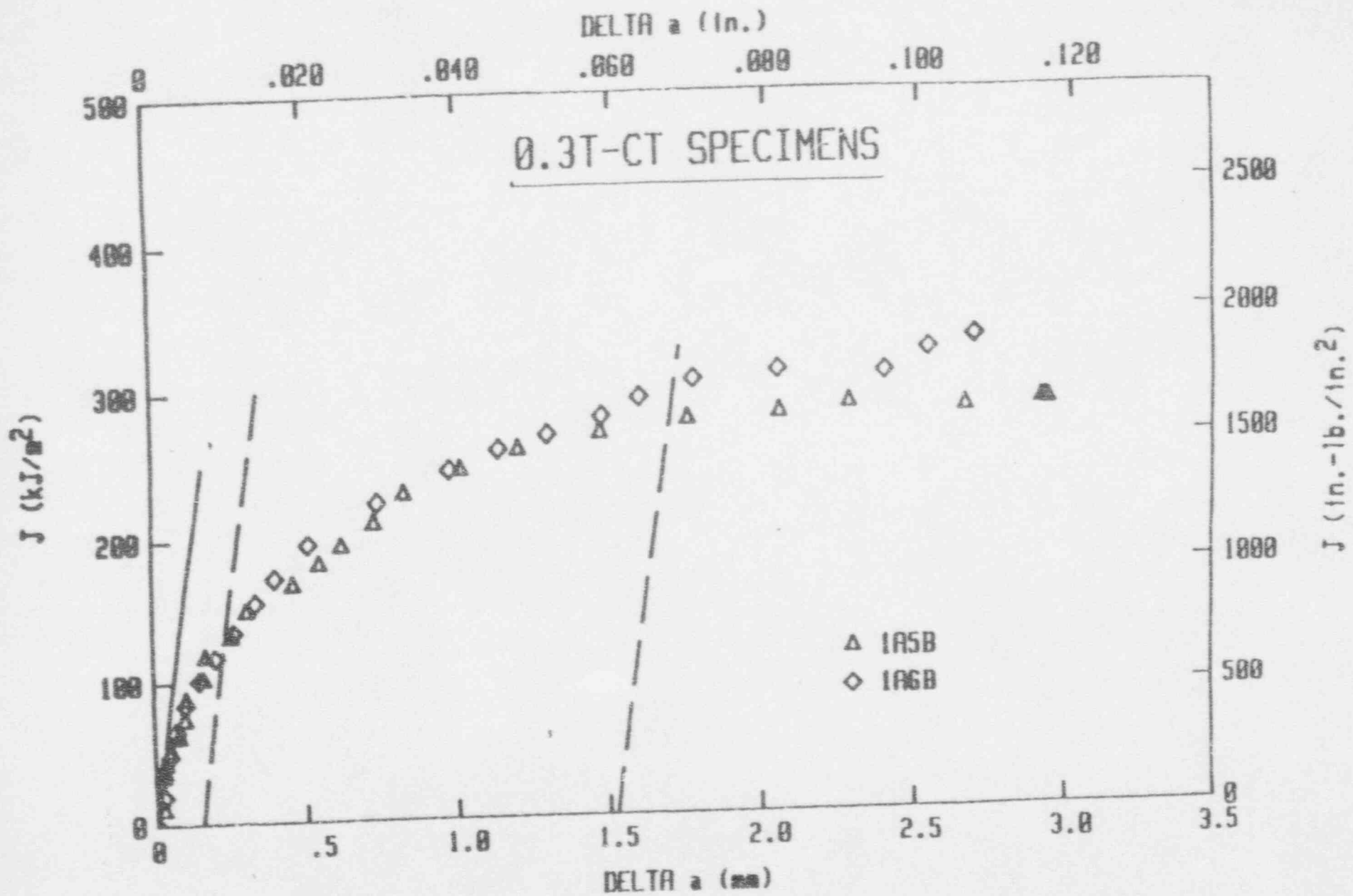


Figure 5-2 Comparison of J-R curves developed for two irradiated stainless steel specimens

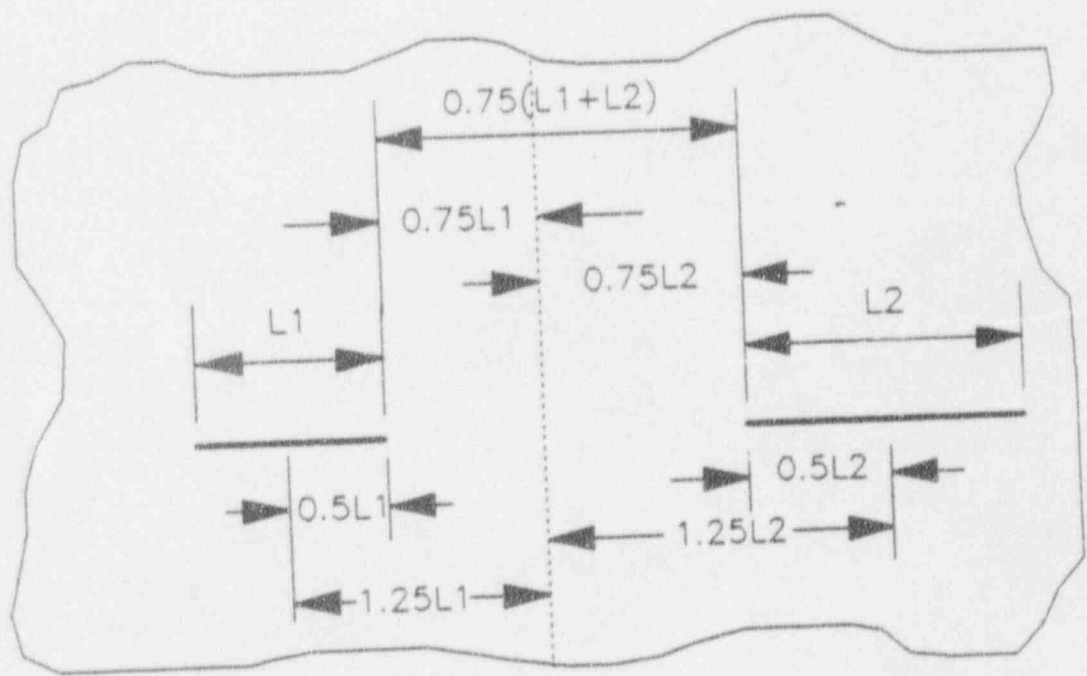
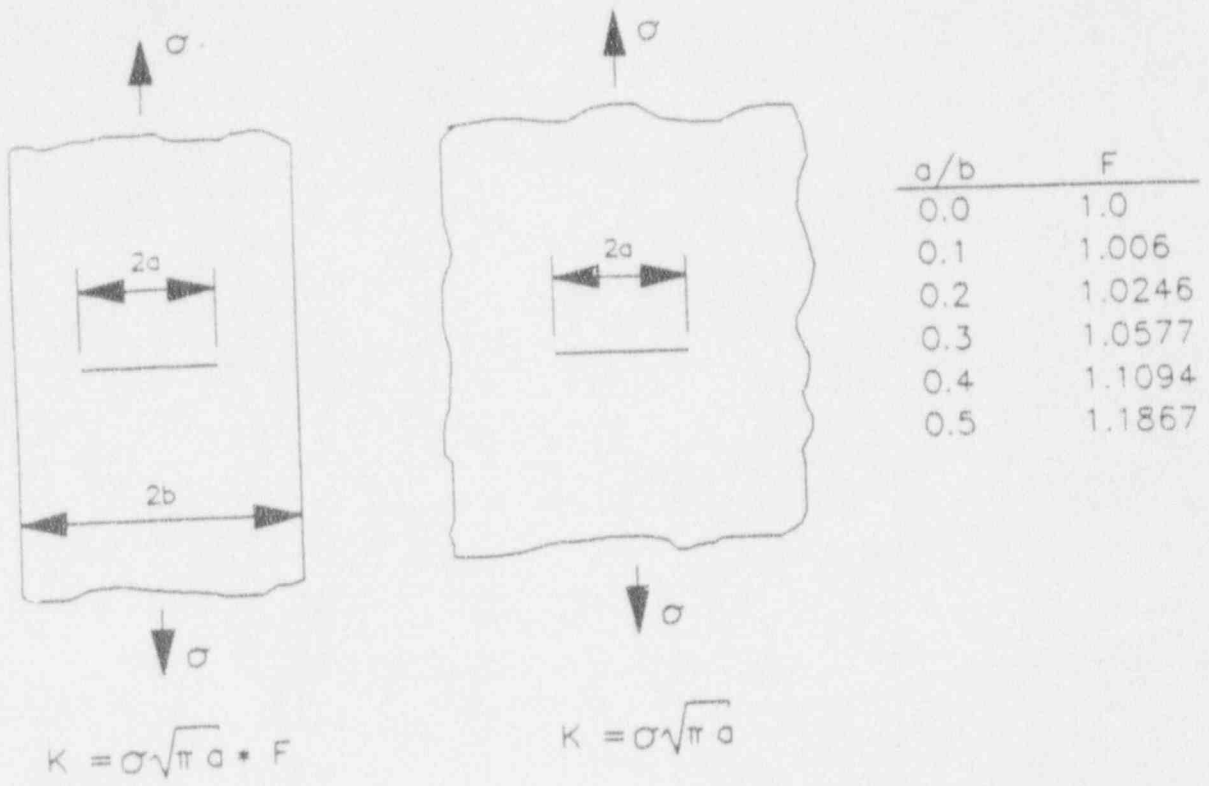


Figure 5-3 SCHEMATIC ILLUSTRATING FLAW INTERACTION

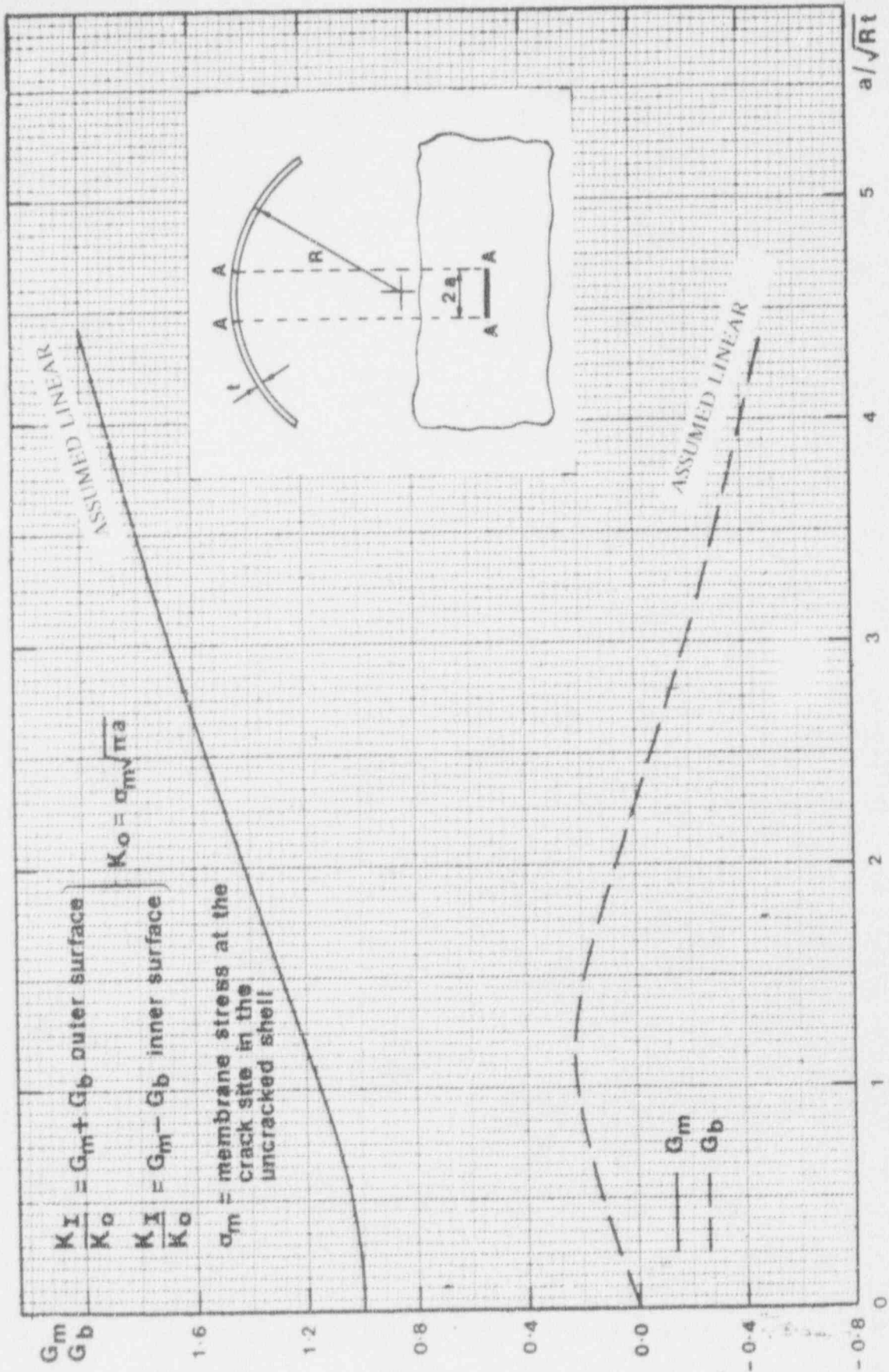


Figure 5-4 K_I for point A of a circumferential crack in a cylindrical shell subjected to a uniform membrane stress

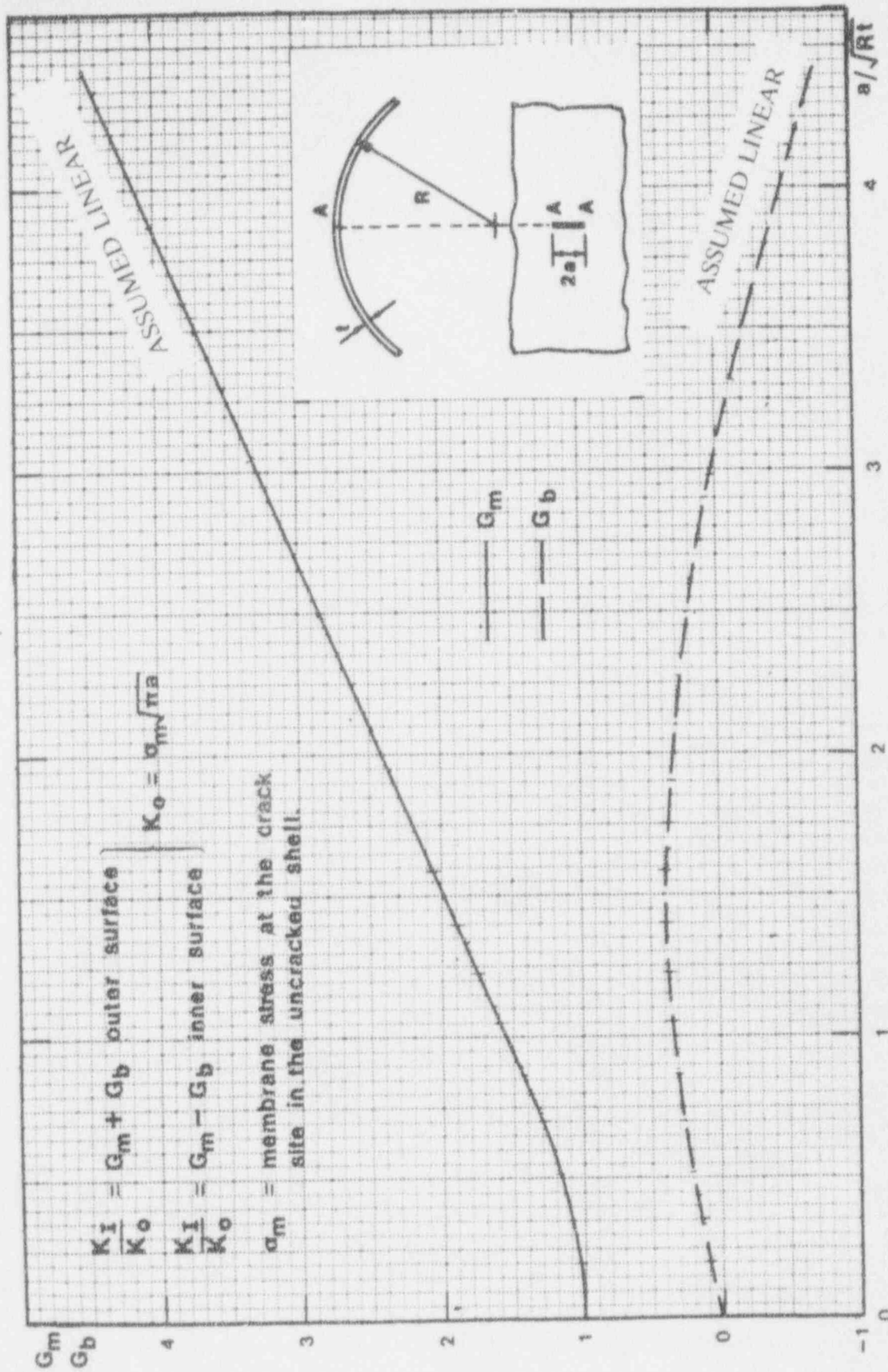


Figure 5-5 K_I for point A of a longitudinal crack in a cylindrical shell subjected to a uniform membrane stress

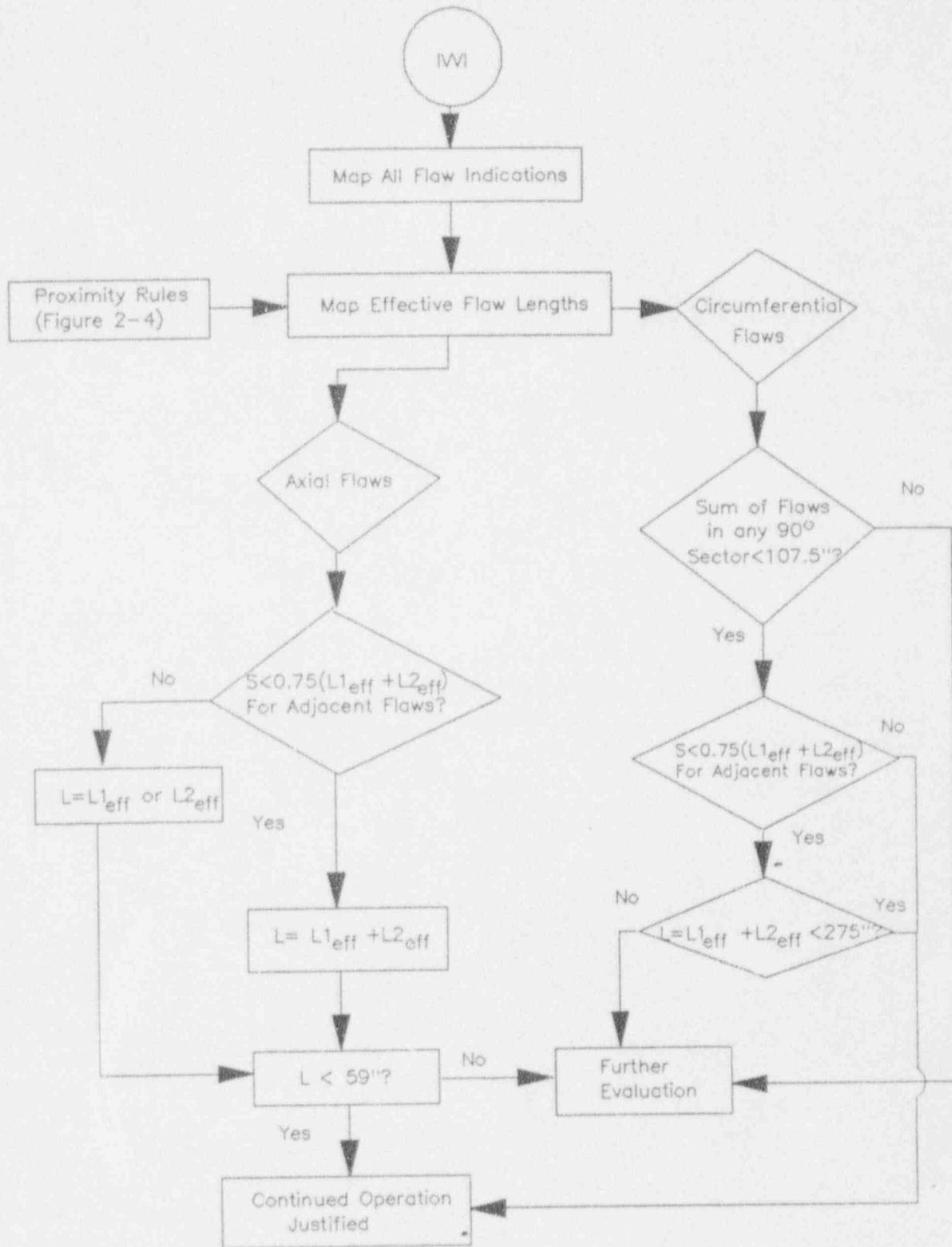


Figure 5-6 SCHEMATIC OF SCREENING CRITERIA

6.0 SUMMARY AND CONCLUSIONS

An evaluation of the indications in the Peach Bottom Unit-3 core shroud has been performed to demonstrate that the structural integrity of the shroud is assured for the next two year cycle. In addition, the report documents material, water chemistry and fluence information which provides additional insight to the shroud condition.

The primary focus of this report was to demonstrate that even with several conservatisms in the evaluation, the structural integrity of the shroud is maintained during a limiting event. This was performed by developing a screening criteria, assuming throughwall indications, which can determine the acceptability of the flaws based solely on the IVVI results. The assumption of through-wall indications removes any uncertainty regarding sizing and the need to further characterize the indications. By meeting the screening criteria, the ASME Code Section XI safety margins are satisfied.

The screening criteria uses both linear elastic fracture mechanics (LEFM) and limit load concepts to determine acceptable through-wall indication lengths. The limiting flaw length based on either LEFM or limit load was used for the screening criteria.

The screening criteria also uses the ASME Code Section XI criteria for combining flaws based on the proximity of indications. In addition, a second method for including the interaction between neighboring indication tips was considered for the LEFM allowable flaw size calculation. The resulting effective flaw lengths were compared against the screening criteria to determine if the structural integrity of the shroud was maintained.

Based on the results of the application of the screening criteria to the observed indications, it is concluded that the structural integrity of the shroud is maintained for the next fuel cycle. All effective indication lengths were shown to be less than the allowable flaw size.

APPENDIX A

DETERMINATION OF THE EFFECTIVE FLAW LENGTH

The effective flaw lengths are based on ASME Code, Section XI proximity criteria as presented in Subarticle IV A-3300. The procedure addresses both circumferential and axial flaws. Indications are considered to be in the same plane if the perpendicular distance between the planes is less than 4" (2 times the shroud thickness). All flaws are considered to be through-wall. Therefore, indications on the inside and outside surface should be treated as if they are on the same surface. When two indications are close to each other, rules are established to combine them based on proximity. These rules are described here.

A.1 Proximity Rules

The flaw combination methodology used here is similar to the ASME Code, Section XI proximity rules concerning neighboring indications. Under the rules, if two surface indications are in the same plane (perpendicular distance between flaw planes <4") and are within two times the depth of the deepest indication, then the two indications must be considered as one indication.

In Figure A-1, two adjacent flaws L1 and L2 are separated by a ligament S. Crack growth would cause the tips to be closer. Assuming a conservative crack growth rate of 5×10^{-5} in/hr, crack extension at each tip is 0.8 in. for 16,000 hours or one fuel cycle (See Appendix B for crack growth rate discussion). Therefore, combining the crack growth and proximity criteria, the flaws are assumed to be close enough to be considered as one continuous flaw if the ligament is less than $(2 \times 0.8 + 2 \times \text{shroud thickness})$. For a shroud thickness of 2.0 in., this bounding ligament is 5.6 in. Thus, if the ligament is less than 5.6 inches, the effective length is $(L1+L2+S+1.6)$ ". Note that the addition of 1.6 in. is to include crack growth at the other (non-adjacent) end of each flaw (See Figure A-2).

If the ligament is greater than 5.6 in., then the effective flaw length is determined by adding the projected tip growth to each end of the flaw. For this example, $L1_{\text{eff}} = L1 + 1.6$ ", and $L2_{\text{eff}} = L2 + 1.6$ ".

A similar approach is used to combine flaws when a circumferential flaw is close to an axial flaw (See Figure A-3). If the ligament between the flaws is less than 4.8 inches, then

the effective flaw length for the circumferential flaw is $L_{\text{eff}} = L1 + S + 0.8$ " (the bounding ligament for these cases). If the ligament is greater than 4.8 in., then the flaws are treated separately.

After the circumferential and axial flaws have been combined per the above criteria, a map of the effective flaws in the shroud can be made, and the effective flaw length can be used for subsequent fracture mechanics analysis.

In order to demonstrate the proximity criteria, three examples are shown in Table A-1 and described below.

Table A-1 Flaw Combinations Considered in Proximity Criteria

Case	Circumferential Flaw	Axial Flaw
A	Yes	No
B	Yes	Yes
C	No	Yes

A.1.1 Case A: Circumferential Flaw - No Axial Crack

This case applies when two circumferential indications are considered. Figure A-2a shows this condition. If the distance between the two surface flaw tips is less than 5.6", the indications must be combined such that the effective length is (See Figure A-2b):

$$L_{\text{eff}} = L1 + S + L2 + 1.6"$$

where: L1 = length of first circumferential indication
 L2 = length of second circumferential indication
 S = distance between two indications

If the distance between the two tips is greater than 5.6", the effective flaw lengths are (See Figure A-2c):

$$\begin{aligned}L1_{\text{eff}} &= L1 + 1.6" \\L2_{\text{eff}} &= L2 + 1.6"\end{aligned}$$

A.1.2 Case B: Circumferential Flaw - Axial Flaw

This case applies when both a circumferential and an axial flaw are being considered. Figure A-3a demonstrates this condition. For this case, only growth of the circumferential flaw is considered. If the distance between the circumferential indication tip and the axial indication is less than 4.8", then the effective circumferential flaw length is (See Figure A-3b):

$$L_{\text{eff}} = L1 + S + 0.8"$$

where: L1 = length of circumferential indication
S = distance between the circumferential tip and axial flaw.

and the effective axial length is (Figure A-3b):

$$L_{\text{eff}} = L2 + 1.6"$$

where: L2 = length of axial indication

If the distance between the circumferential indication tip to the axial indication is greater than 4.8", then the flaws are not combined (See Figure A-3c) and the effective lengths are:

$$\begin{aligned}L1_{\text{eff}} &= L1 + 1.6" \text{ (for circumferential flaw)} \\L2_{\text{eff}} &= L2 + 1.6" \text{ (for axial flaw)}\end{aligned}$$

A.1.3 Case C: No Circumferential Flaw - Axial Flaw

This case applies to when only axial flaws are being considered. The effective length is determined in a manner similar to that used for case A for circumferential flaws.

A.2 Application of Effective Flaw Length Criteria

The application of the effective length criteria is applied to two adjacent indications at a time. Figure A-4 is a schematic which illustrates the process. For example, using the 0° azimuth as the starting location for a circumferential weld or plane, the general procedure would be as follows:

- Moving in the positive azimuthal direction, the first indication encountered is indication 1.
- The next indication is indication 2.
- Apply proximity rules to the pair of indications (indications 1 and 2). Combine the flaws if necessary (L_1+L_2+S). Old indication 2 becomes new indication 1.
- Continue along positive azimuthal direction until the next indication is encountered. This becomes new indication 2.
- Apply proximity rules to new indications 1 and 2.
- Continue proximity rule evaluation until all indications along the subject weld or plane have been considered.

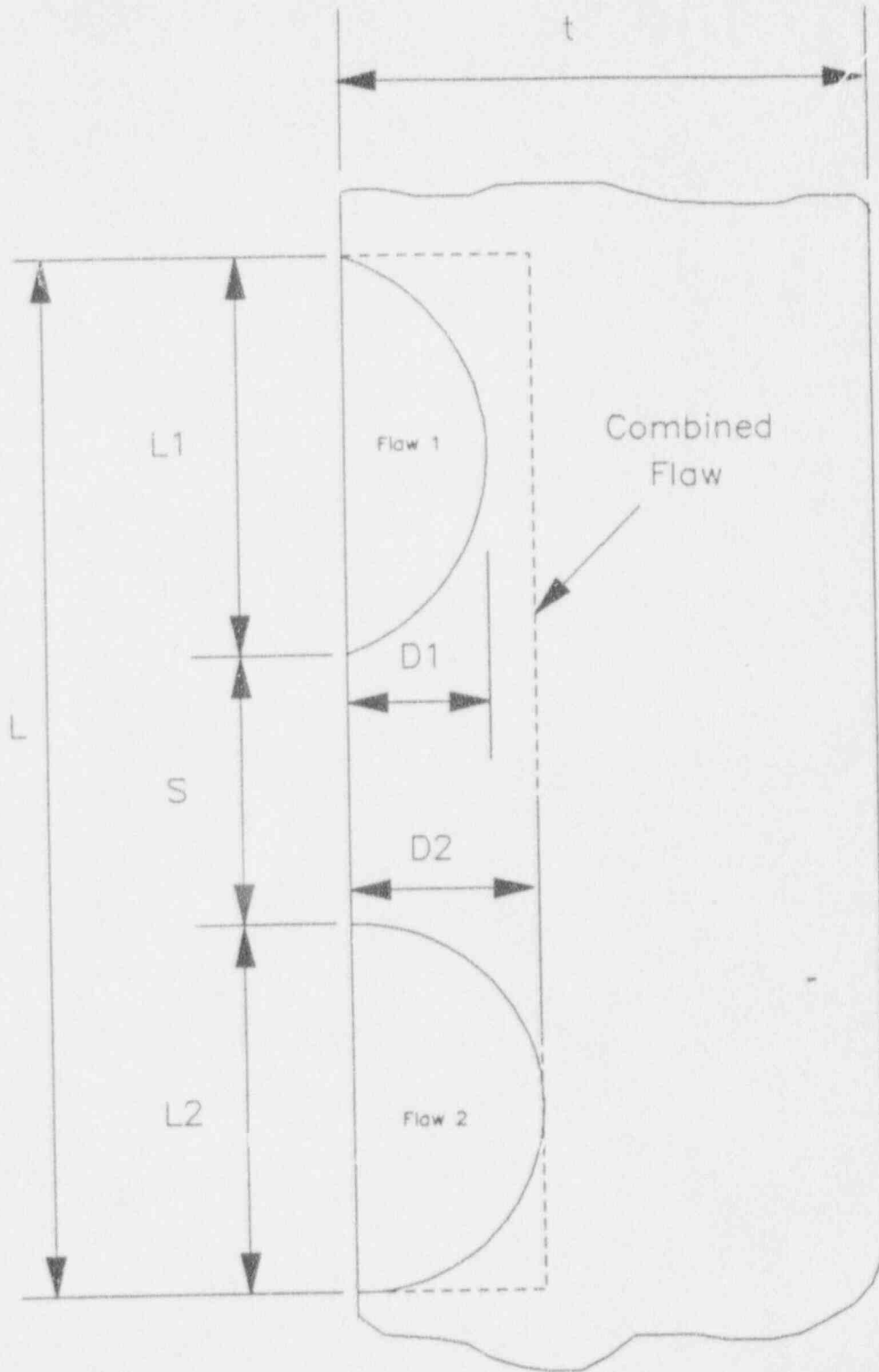


Figure A-1 - ASME Code Proximity Criteria

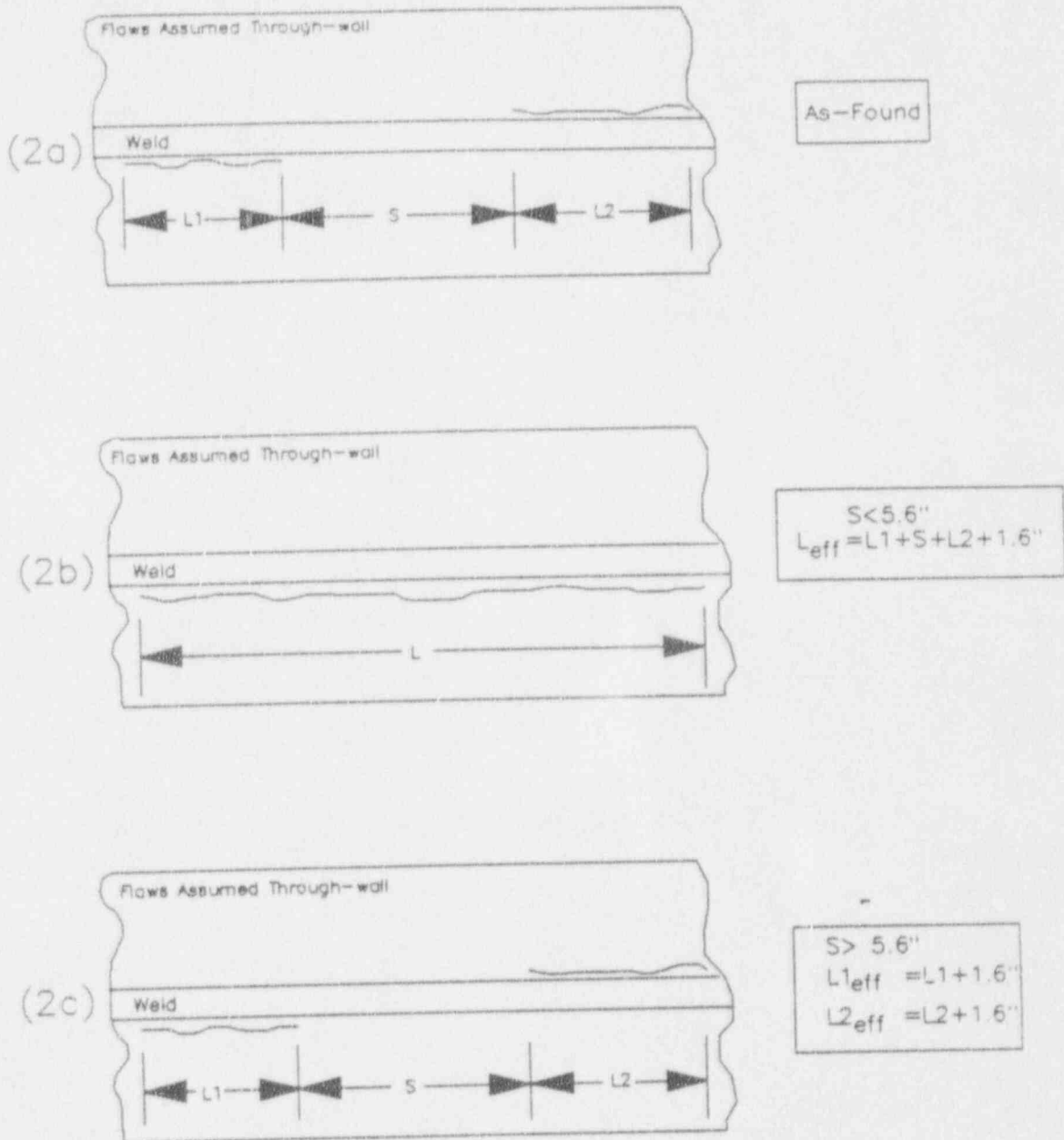


Figure A-2 — APPLICATION OF PROXIMITY PROCEDURE TO NEIGHBORING CIRCUMFERENTIAL FLAWS

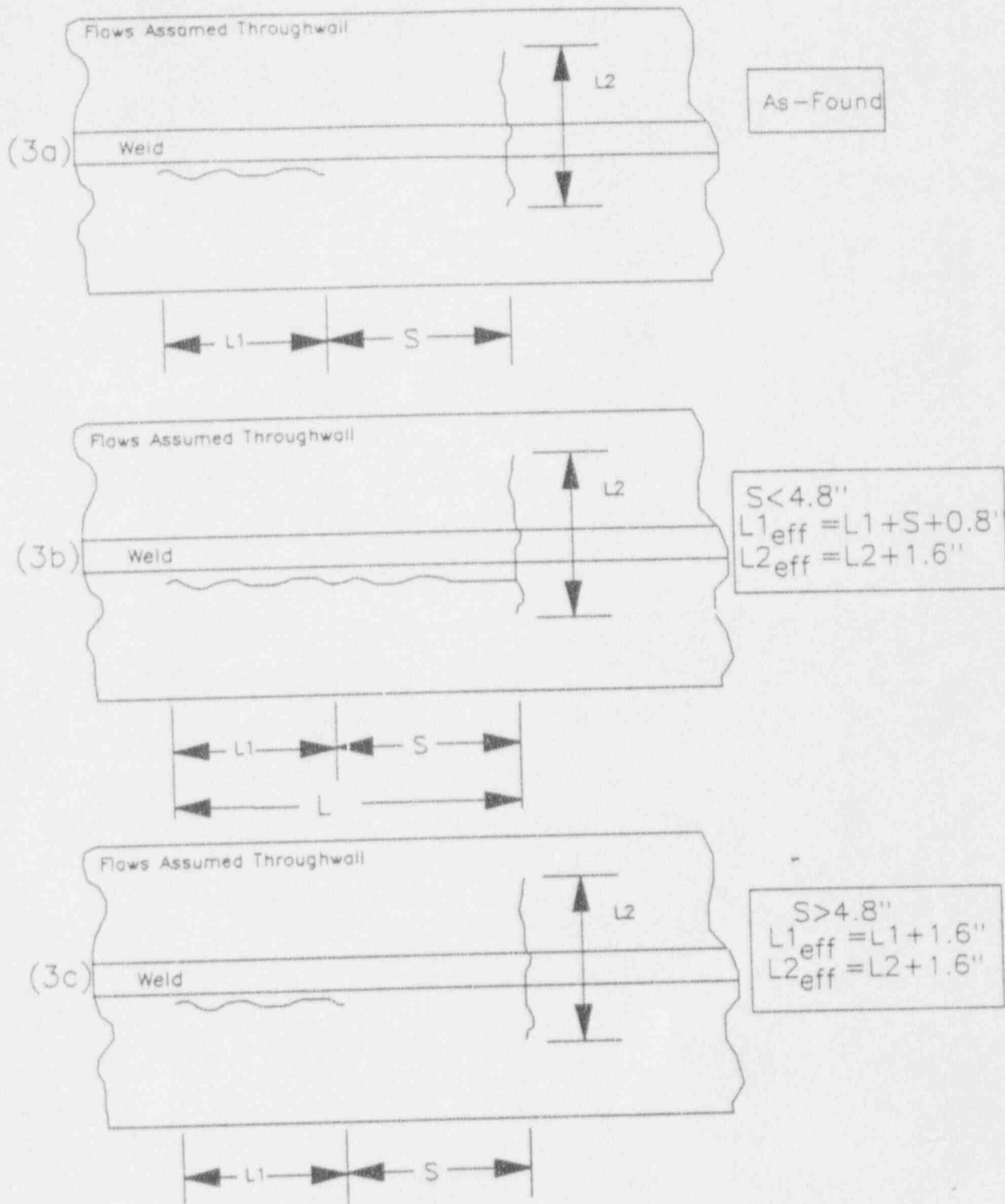


Figure A-3 - APPLICATION OF PROXIMITY PROCEDURE TO NEIGHBORING AXIAL AND CIRCUMFERENTIAL FLAWS

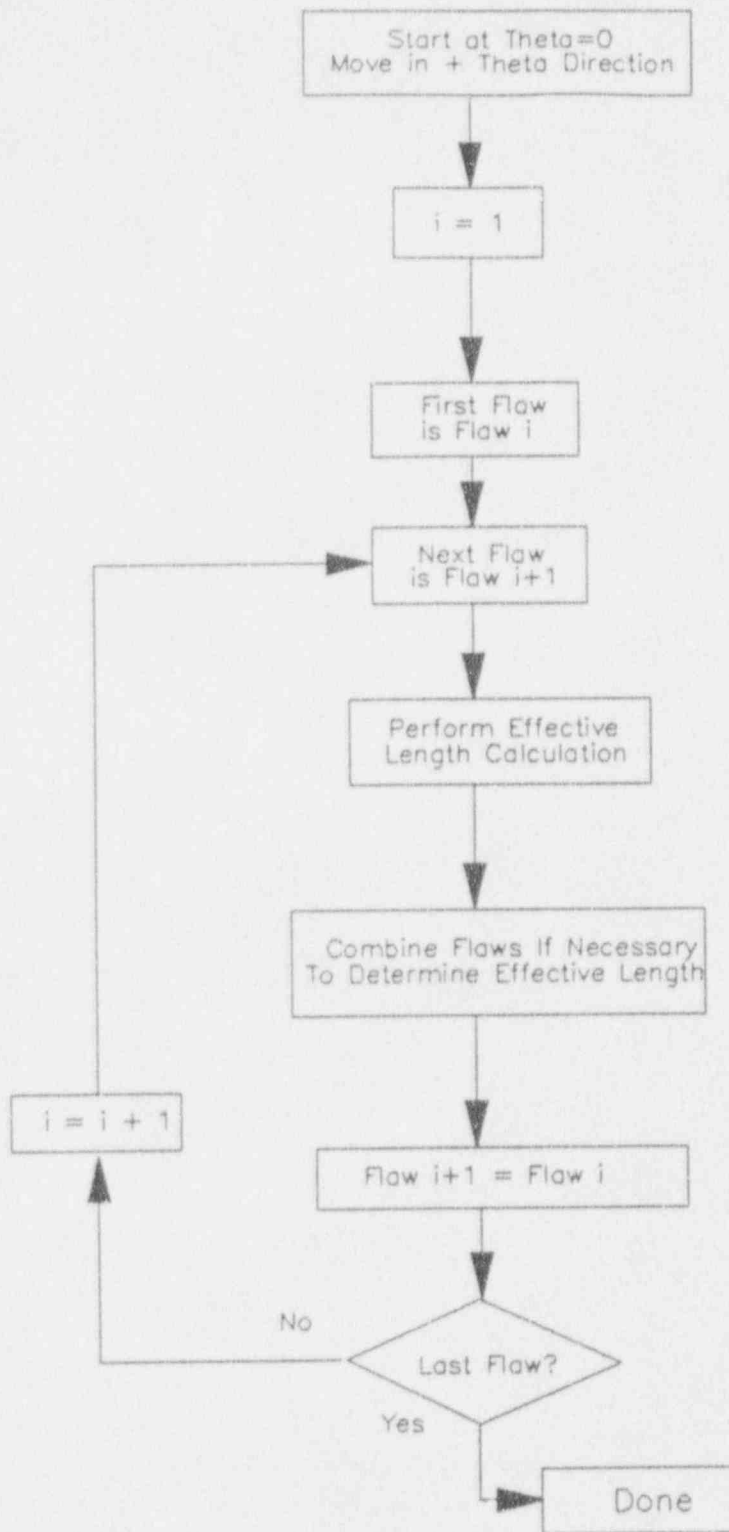


Figure A-4 - PROCESS FOR DETERMINING EFFECTIVE CIRCUMFERENTIAL FLAW LENGTH

APPENDIX B BASIS FOR THE CRACK GROWTH RATE



The basis for the crack growth rate used in the screening criteria is provided in this section. The Peach Bottom Unit 3 shroud cylinder was fabricated from roll formed Type 304 stainless steel plate. Therefore, the weld heat-affected-zone (HAZ) is likely sensitized. The shroud is also subjected to neutron fluence during the reactor operation which further increases the effective degree of sensitization. The other side-effect of neutron fluence induced irradiation is the relaxation of weld residual stresses. The slip-dissolution model developed by GE quantitatively considers the degree of sensitization, the stress state and the water environment parameters, in predicting a stress corrosion cracking (SCC) growth rate. The crack growth rate predictions of this model have shown good correlation with laboratory and field measured values. This model was used to predict a Peach Bottom Unit-3 specific crack growth rate and a conservative value was then selected based on this value.

B.1 Slip-Dissolution Model

Figure B-1 schematically shows the GE slip-dissolution film-rupture model (Reference B-1) for crack propagation. The crack propagation rate V_t is defined as a function of two constants (A and n) and the crack tip strain rate. The constants are dependent on material and environmental conditions. The crack tip strain rate is formulated in terms of stress, loading frequency, etc. When a radiation field, such as the case for the shroud, is present, there is additional interaction between the gamma field and the fundamental parameters which affect intergranular stress corrosion cracking (IGSCC) of Type 304 stainless steel (see Figures B-2 and B-3).

The increase in sensitization (i.e., Electrochemical Potentiokinetic Reactivation, EPR) and the changes in the value of constant A as a function of neutron fluence (>1Mev) is given as the following:

$$EPR = EPR_0 + 3.36 \times 10^{-24} (\text{fluence})^{1.17} \quad (\text{B-1})$$

where, EPR is in units of C/cm², fluence is in units of n/cm² and the calculated value of EPR has an upper limit of 30.

The constant A is defined as the following:

$$\text{for fluence} \leq 1.4 \times 10^{19} \text{ n/cm}^2: C = 4.1 \times 10^{-14} \quad (\text{B-2a})$$

$$\begin{aligned} \text{for fluence} > 1.4 \times 10^{19} \text{ n/cm}^2 \text{ but } \leq 3 \times 10^{21} \text{ n/cm}^2, \\ C = 1.14 \times 10^{-13} \ln(\text{fluence}) - 4.98 \times 10^{-12} \end{aligned} \quad (\text{B-2b})$$

$$\text{for fluence} \leq 1.4 \times 10^{19} \text{ n/cm}^2: C = 4.1 \times 10^{-14} \quad (\text{B-2c})$$

The units of K to be used with the above expressions is $\text{MPa}\sqrt{\text{m}}$.

B.2 Calculation of Parameters

The parameters needed for the crack growth calculation are: stress state and stress intensity factor, effective EPR, water conductivity, and electro-chemical corrosion potential (ECP).

The stress state relevant to IGSCC growth rate is the steady state stress which consists of weld residual stress and the steady applied stress. Figure B-4 shows observed through-wall weld residual stress distributions for large diameter pipes. This distribution is expected to be representative for the shroud welds also. The maximum stress at the surface was nominally assumed as 35 ksi. The steady applied stress on the shroud is due to core differential pressure and its magnitude is small compared to the weld residual stress magnitude. Figure B-5 shows the assumed total stress profile used in the evaluation. Figure B-6 shows the calculated values of stress intensity factor (K) assuming a 360° circumferential crack. It is seen that the calculated value of K reaches a maximum of approx. 25 $\text{ksi}\sqrt{\text{in}}$. The average value of K was estimated as 20 $\text{ksi}\sqrt{\text{in}}$ and was used in the crack growth rate calculations.

The weld residual stress magnitude is expected to decrease as a result of relaxation produced by irradiation-induced creep. Figure B-7 shows the stress relaxation behavior of Type 304 stainless steel due to irradiation at 550° F. Since most of the steady state stress in the shroud comes from the weld residual stress, it was assumed that the K values shown in Figure B-6 decrease in the same proportion as indicated by the stress relaxation behavior of Figure B-7.

The second parameter needed in the evaluation is the EPR. In the model, the initial EPR value is assumed as 15 for the weld sensitized condition. Using Equation (B-1), the predicted increase in EPR value as a function of fluence is shown in Figure B-8.

The third parameter used in the GE predictive model is the water conductivity. The reactor water conductivity at Peach Bottom Unit-3 has recently (1992-93) been good (approx. $0.1 \mu\text{S}/\text{cm}^2$) compared to earlier operating period (1975-84) when the average conductivity was in excess of $0.7 \mu\text{S}/\text{cm}^2$. This has a significant impact on the predicted crack growth rate by the GE model as seen in Figure B-9. To demonstrate that the GE model conservatively reflects the effect of conductivity, Figure B-10 shows a comparison of the GE model predictions with the measured crack growth rates in the crack advance verification system (CAVS) units installed at several BWRs. The comparison with CAVS data in Figure B-10 also demonstrates the conservative nature of crack growth predictions by the GE model.

The last parameter needed in the GE prediction model is the ECP. Figure B-11 shows the measured values of ECP at two locations in the core. Since Peach Bottom Unit-3 does not plan to use hydrogen injection, the ECP values at zero H_2 injection are relevant in Figure B-11. It is seen that the ECP values at zero H_2 injection rate range from 150 mV to 225 mV. Therefore, a value of 200 mV was used in the calculation.

B.3 Crack Growth Prediction

Based on the discussion in the preceding section, the crack growth rate calculations were conducted as a function of fluence assuming the following values of parameters:

Initial K	= 20 ksi $\sqrt{\text{in}}$
EPR ₀	= 15 C/cm ²
Cond.	= 0.1 $\mu\text{S}/\text{cm}^2$
ECP	= 200 mV

Figure B-12 shows the predicted crack growth rate as a function of fluence. It is seen that the predicted crack growth rate initially increases with the fluence value but decreases later as a result of significant reduction in the K value due to irradiation induced stress relaxation. The crack growth rate peaks at 4.5×10^{-5} in/hr at a fluence of 1×10^{20} n/cm². The crack growth rate for the expected fluence at the end of the next operating cycle is

approximately 2×10^{-5} in/hr. Thus, a bounding value of 5×10^{-5} in/hr can be conservatively used in the structural integrity evaluations for the shroud.

This bounding crack growth rate is quite conservative as can be shown in Figure B-13 from NUREG-0313, Rev. 2. It is seen that the crack growth rate of 5×10^{-5} in/hr at 20 ksi/in is considerably higher than what would be predicted by using the NRC curve. This further demonstrates the conservatism inherent in the assumed bounding value of crack growth rate.

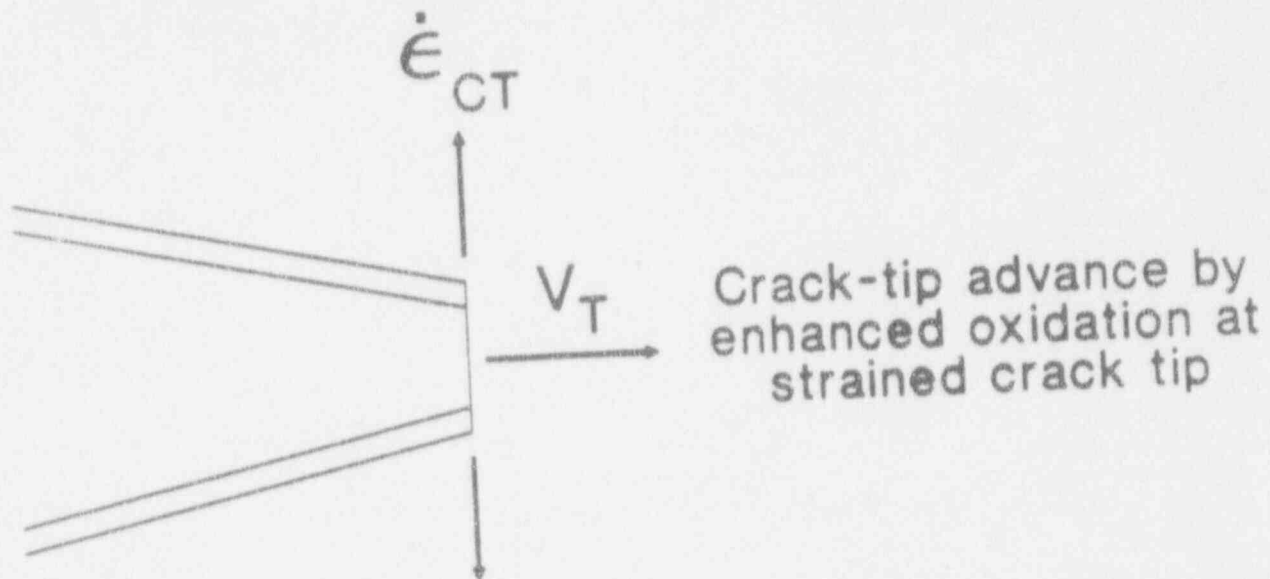
B.4 Summary

A crack growth rate calculation using the GE predictive model was conducted considering the steady state stress, EPR, conductivity and ECP values for the Peach Bottom Unit-3 shroud. The evaluation accounted for the effects of irradiation induced stress relaxation and the increase in effective EPR. The evaluation showed that a bounding crack growth rate of 5×10^{-5} in/hr may be conservatively used in the structural integrity evaluation of the Peach Bottom Unit-3 shroud.

B.5 Reference

- B-1 F.P. Ford et al, "Prediction and Control of Stress Corrosion Cracking in the Sensitized Stainless Steel/Water System," paper 352 presented at Corrosion 85, Boston, MA, NACE, March 1985.

The GE PLEDGE Slip Dissolution - Film Rupture Model of Crack Propagation



$$V_T = A \dot{\epsilon}_{CT}^n$$

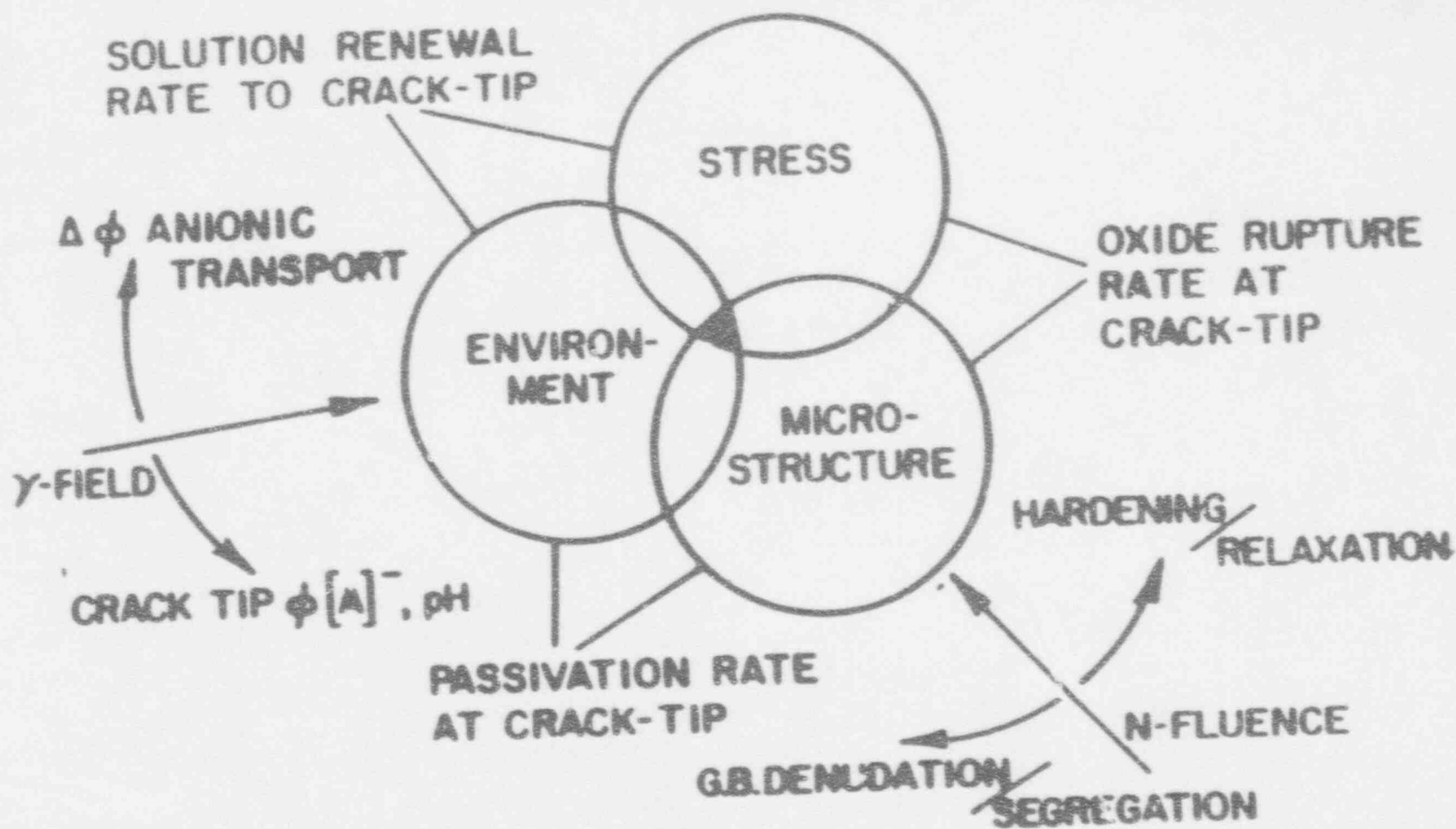
Where:

V_T = crack propagation rate

A, n = constants, dependent on material and environmental conditions

$\dot{\epsilon}_{CT}$ = crack-tip strain rate, formulated in terms of stress, loading frequency, etc.

Figure B-1



B-6

Figure B-2 Effects of Fast Fluence, flux & Gamma Field on parameters affecting IGSCC of Type 304 Stainless Steel

B-7

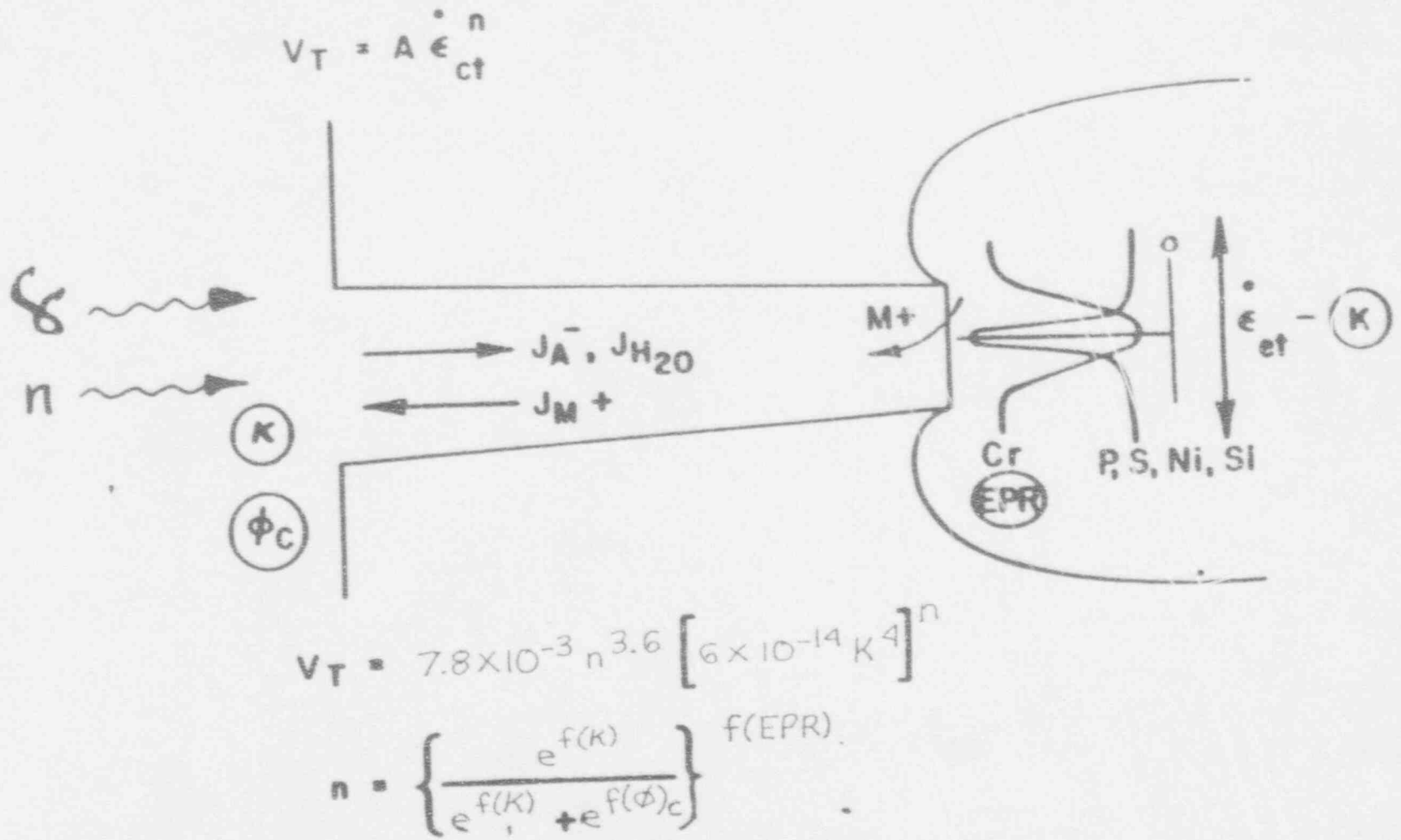


Figure B-4 Parameters of Fundamental Importance to Slip Dissolution Mechanism of IGSCC in Sensitized Austenitic Stainless Steel

OBSERVED RESIDUAL STRESS PROFILES
IN HAZ OF 24"-28" DIA. SCH. 80 PIPING

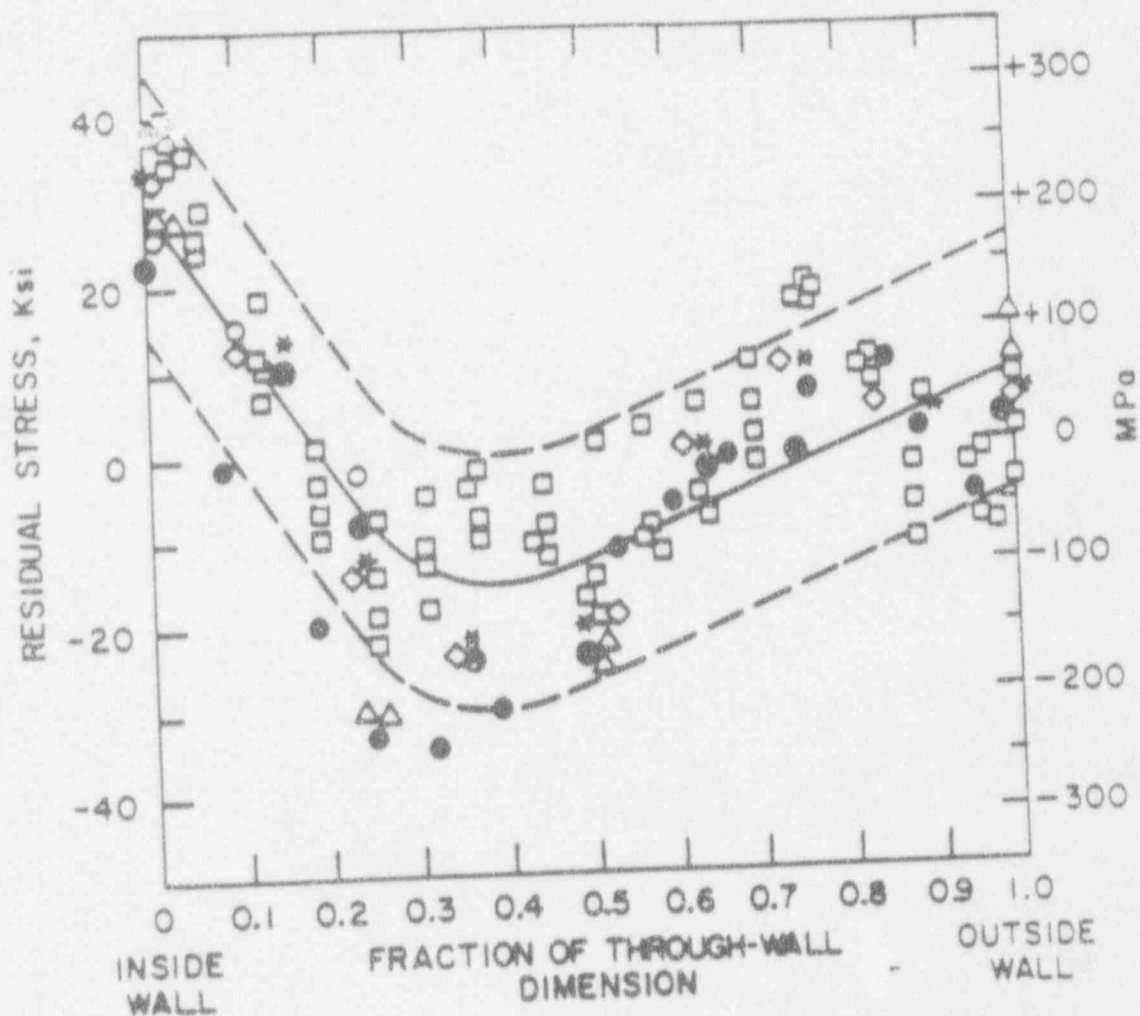


Figure B-4 Throughwall longitudinal residual stress data adjacent to welds in 12 to 28 inch diameter stainless steel piping

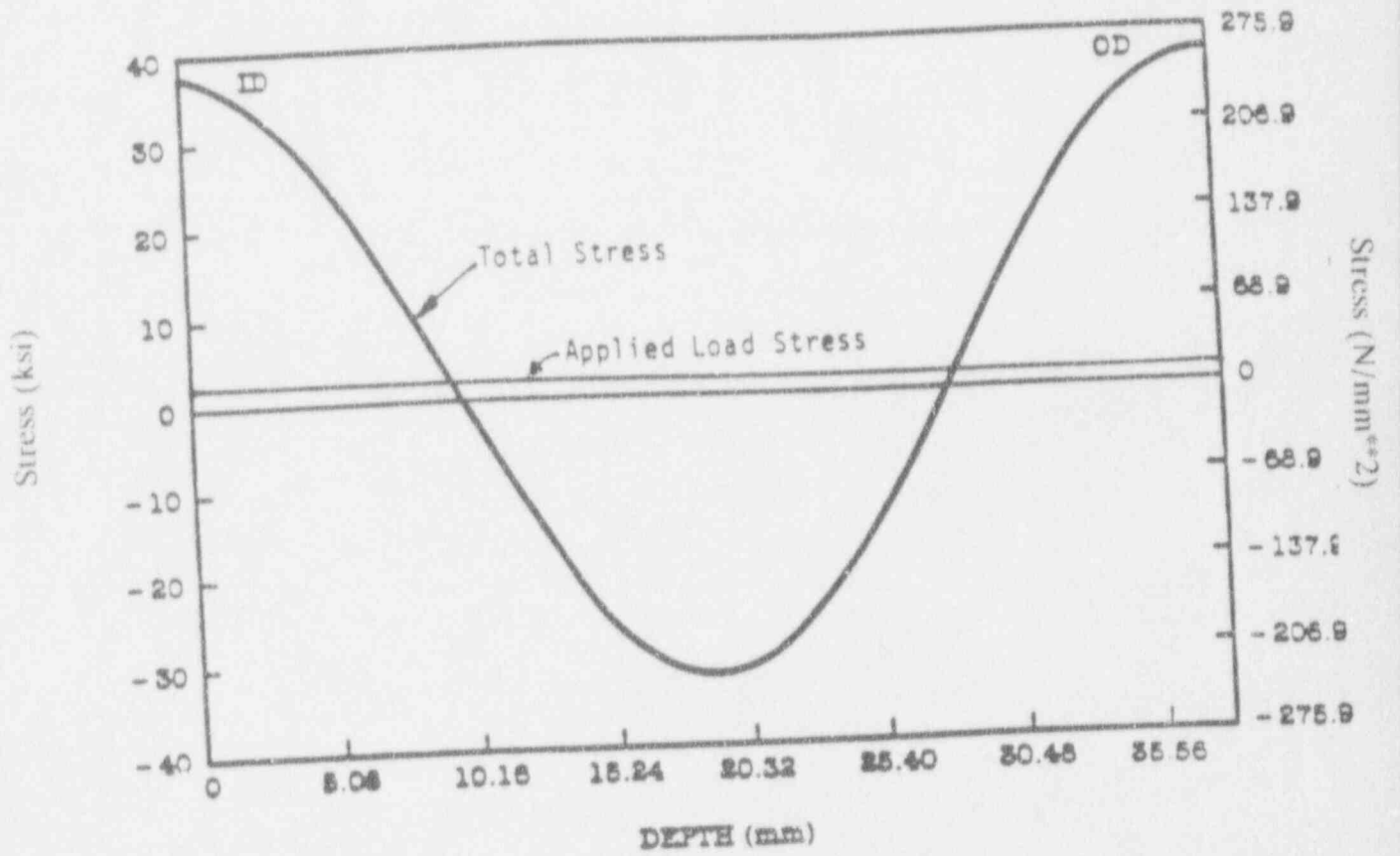


Figure B-5 Shroud Total Throughwall Stress Profile

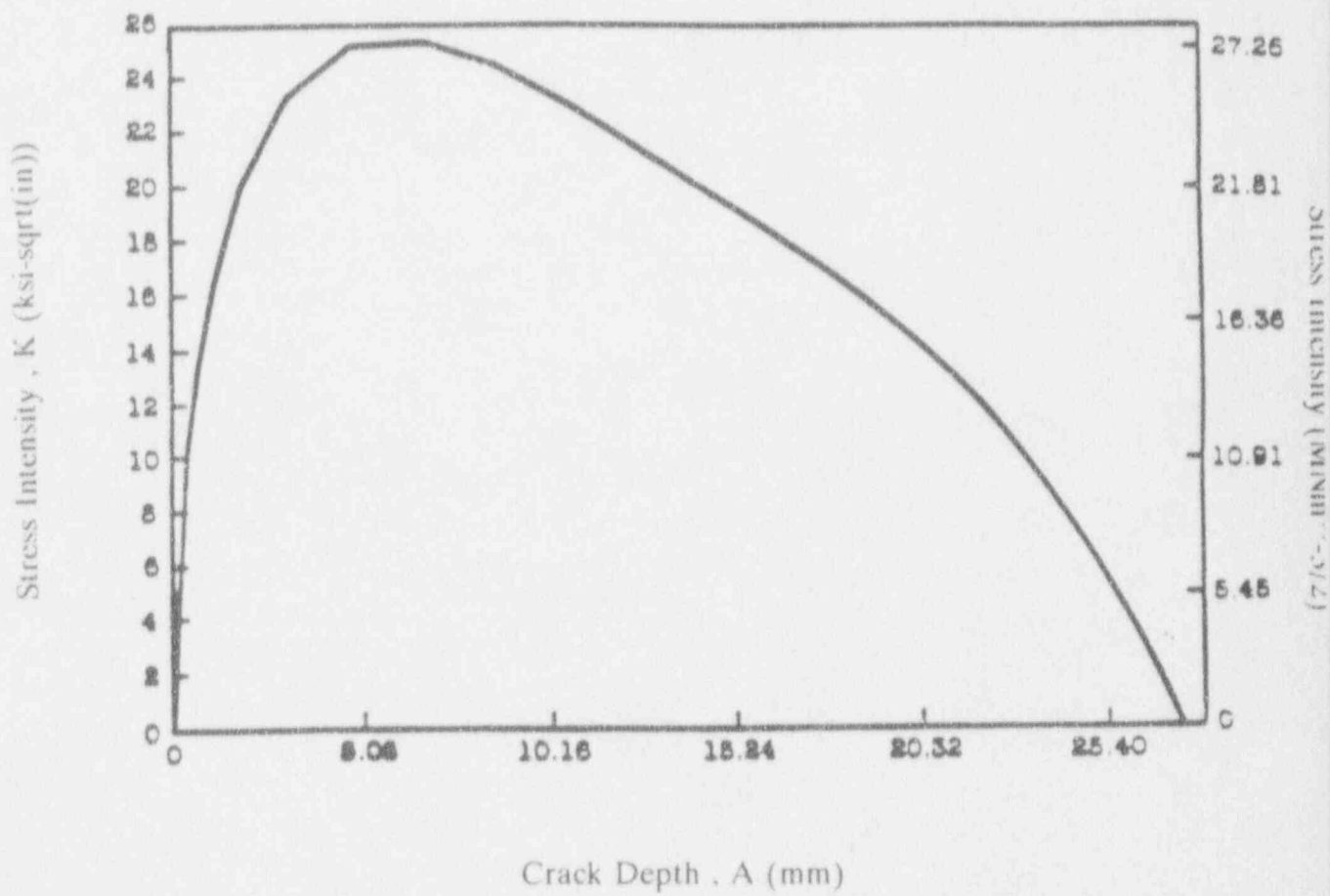


Figure B-6 Shroud Throughwall Stress Intensity Factor

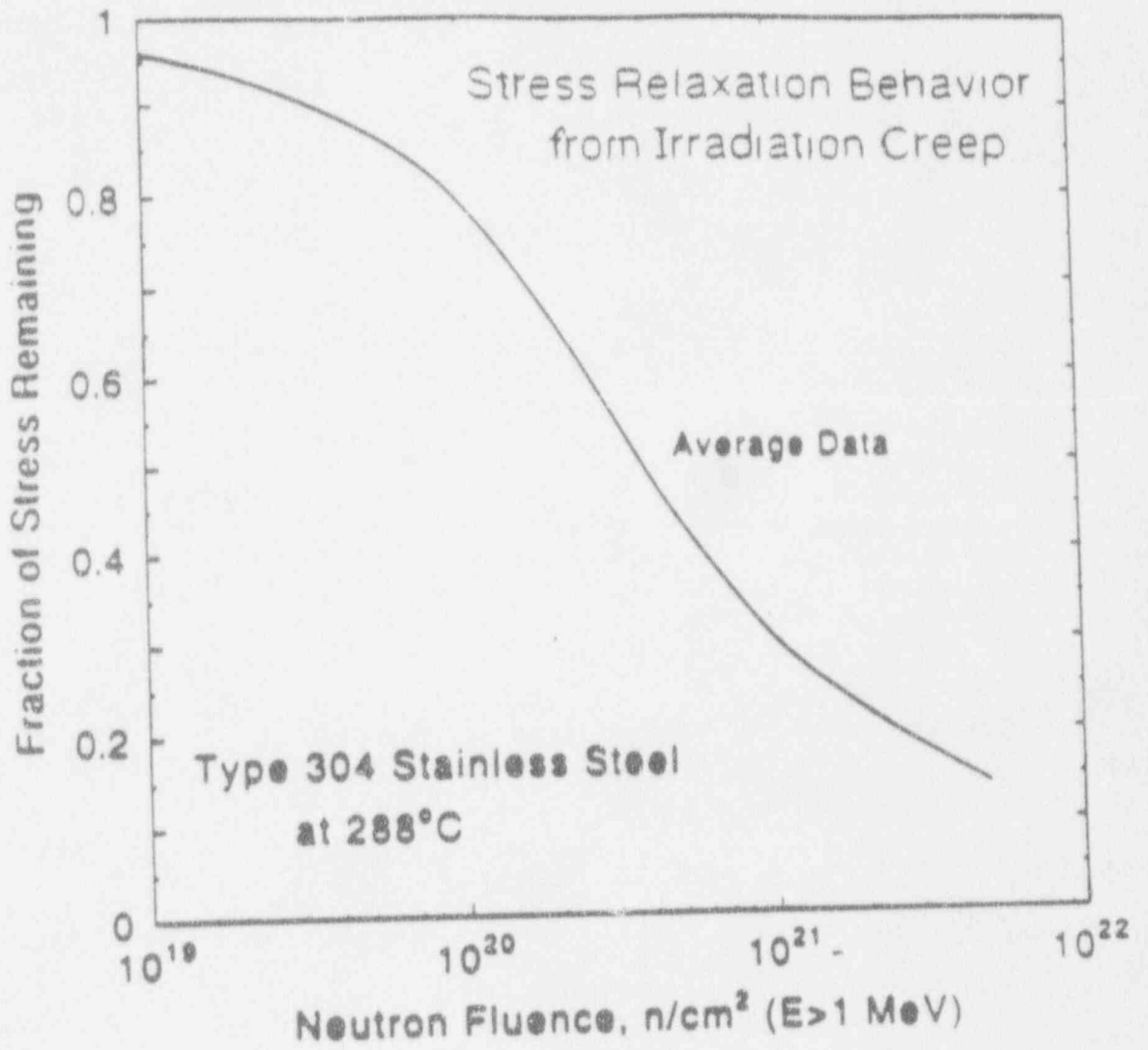


Figure B-7 Stress Relaxation Behavior of Type 304 Stainless Steel Due To Irradiation at 288C

EPR VERSUS NEUTRON FLUENCE

B-12

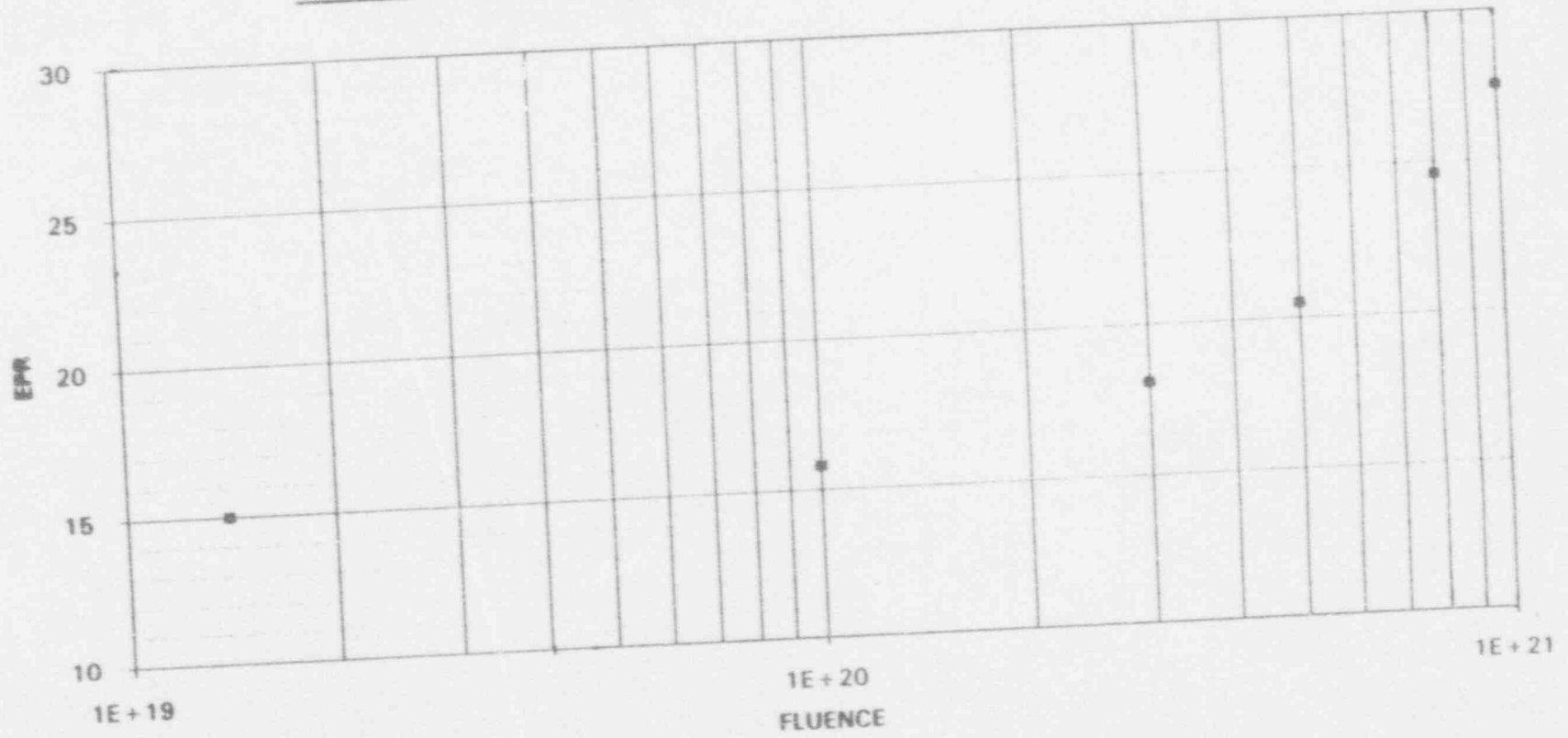
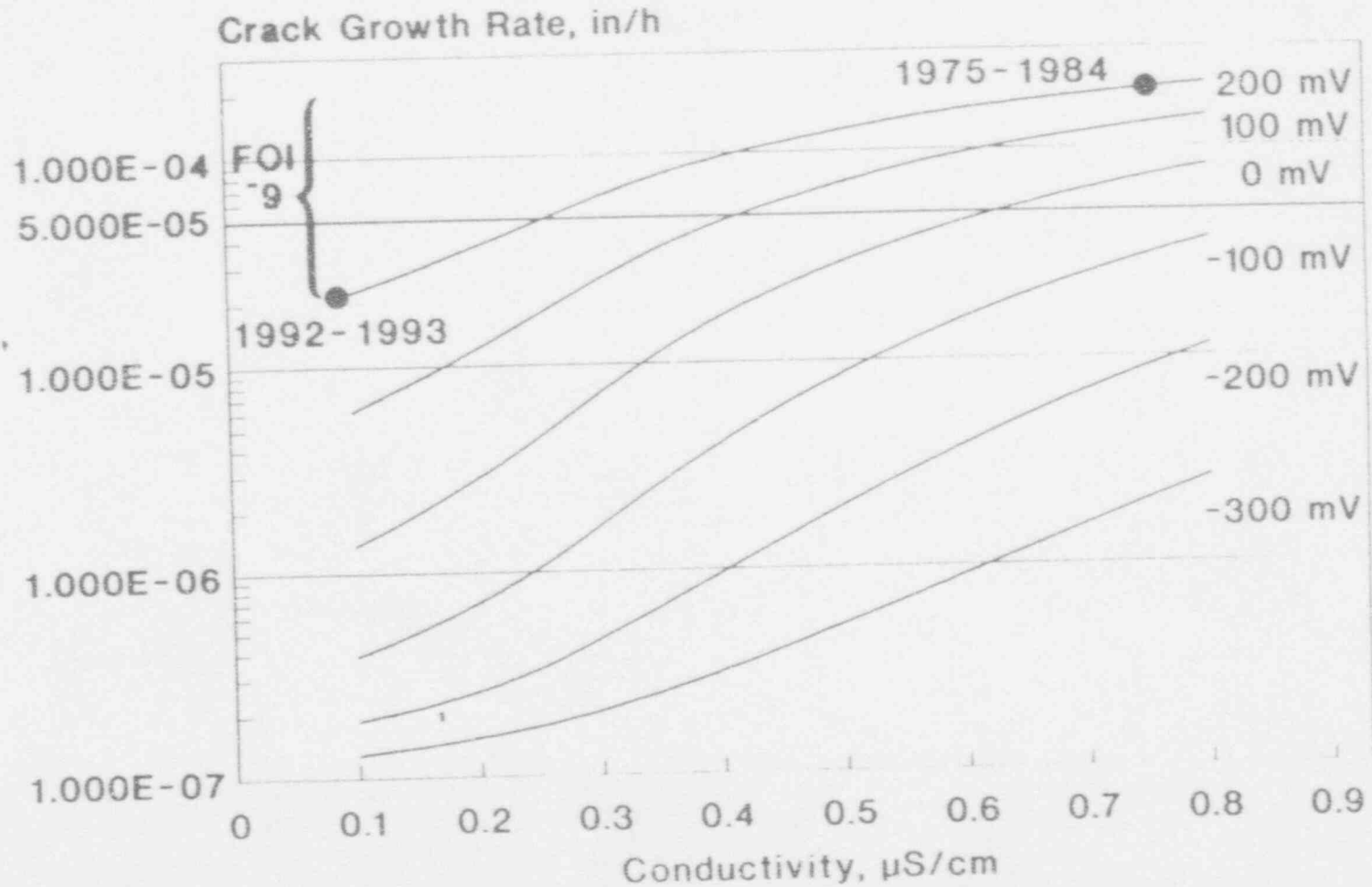


Figure B-8 EPR Versus Neutron Fluence

GENE PLEDGE Model Prediction for PB-3 Sensitized Type 304 Crack Growth Rate

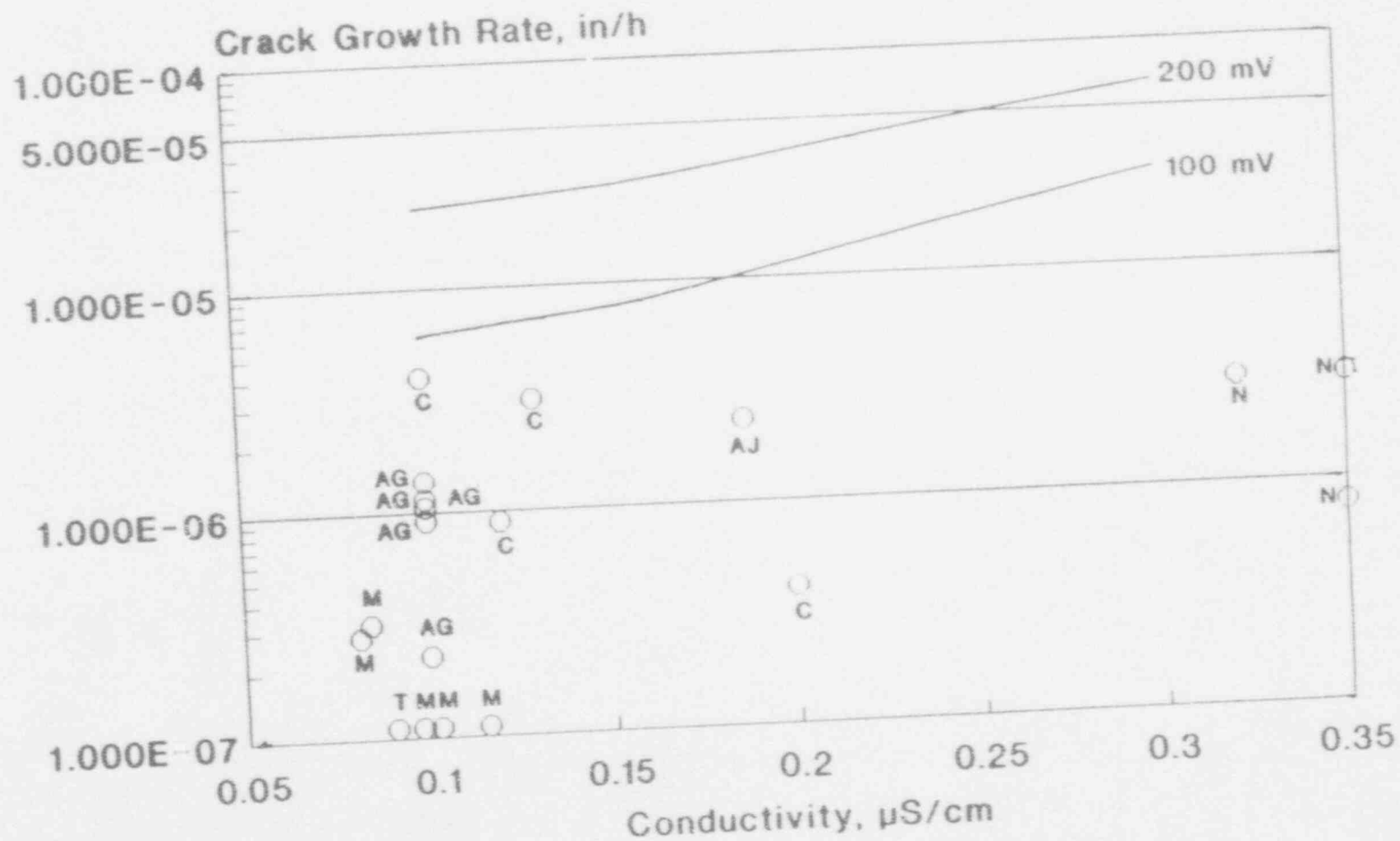


B-13

PLEDGE: 15 C/cm², 20ksi√in

Figure B-9 GENE PLEDGE Model Prediction for PB-3 Sensitized Type 304 Crack Growth Rate

Effect of Conductivity on Sensitized 304 Crack Growth Rate



B-14

PLEDGE: 20 ksi $\sqrt{\text{in}}$, 15 C/cm²
 CAV: 20-25 ksi $\sqrt{\text{in}}$, 13 C/cm², 100-160 mV

Figure B-10 Effect of Conductivity on Sensitized Type 304 Crack Growth Rate

In-Core Bypass ECP vs Feedwater Hydrogen for a BWR-4

B-15

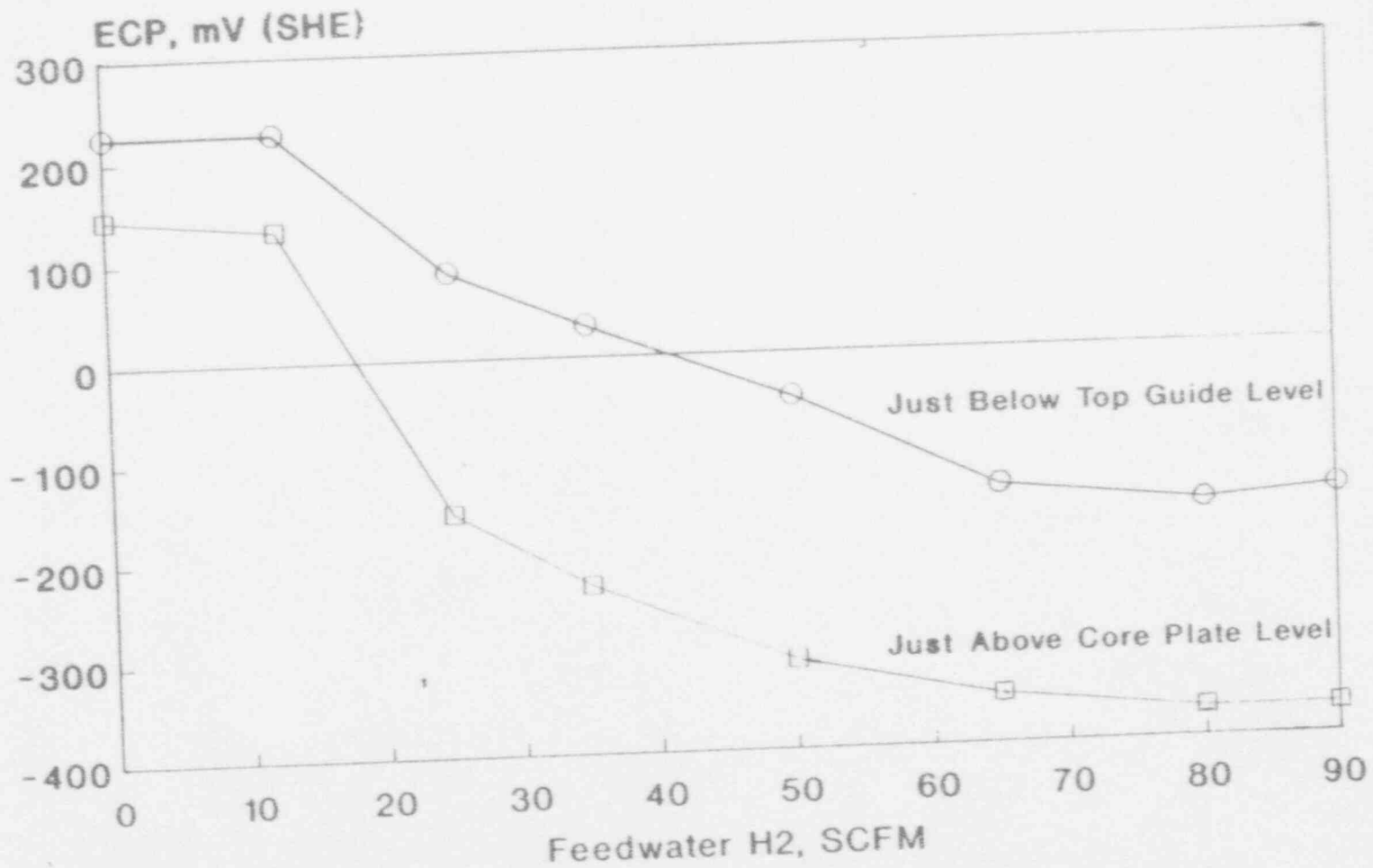
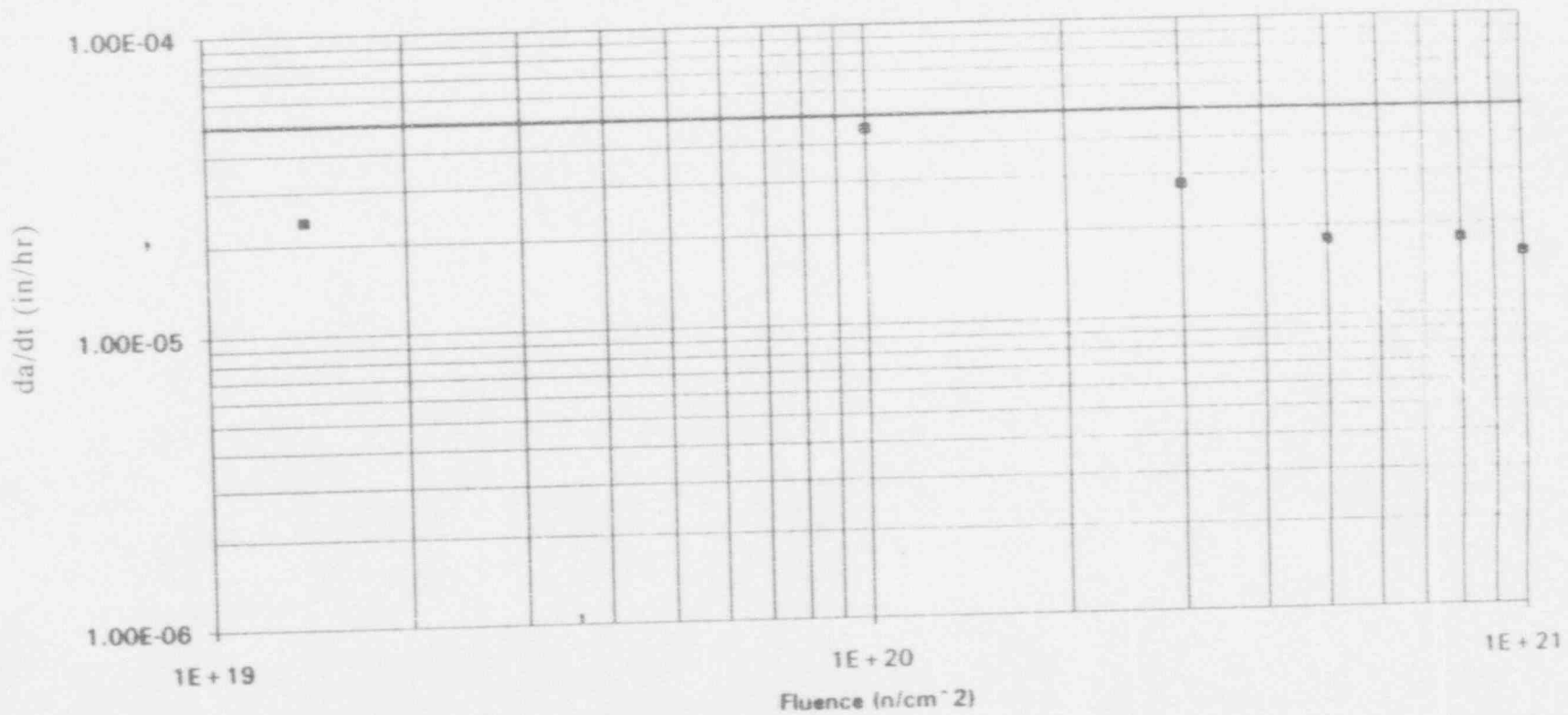


Figure B-11 In-Core Bypass ECP vs Feedwater Hydrogen for a BWR-4

Figure B-12

GROWTH RATE VERSUS FLUENCE



B-16

Stress Intensity = 20 Ksi/in, Initial EPR = 15 C/cm²

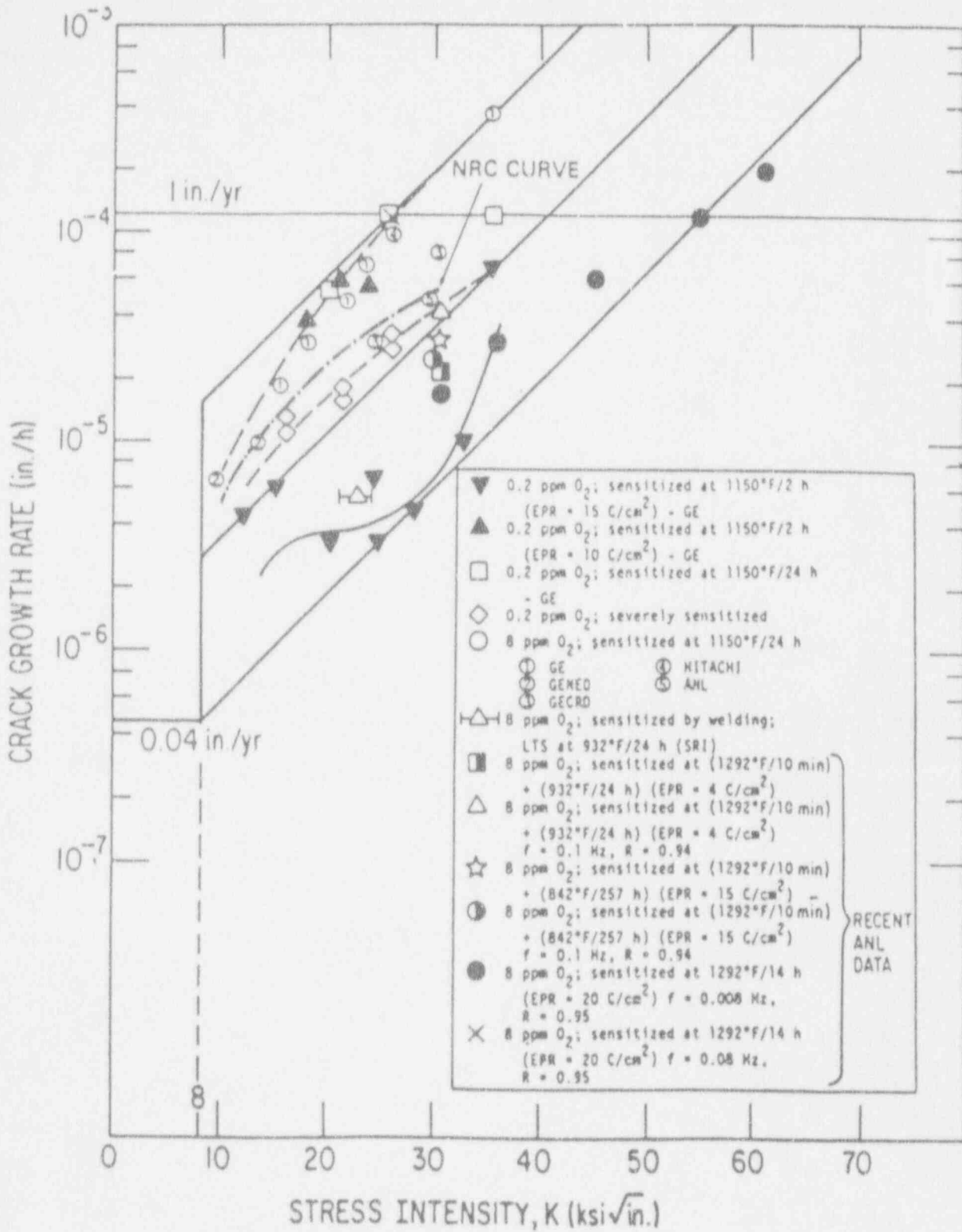


Figure B-13 Nureg 0313 Crack Growth Rate Data